THE EFFECTS OF OZONE ADDITION ON FLAME

PROPAGATION AND STABILIZATION

A Dissertation
Presented to
The Academic Faculty

by

Xiang Gao

In Partial Fulfillment
of the Requirements for the Degree
of Doctor of Philosophy in the
School of Aerospace Engineering

Georgia Institute of Technology
December 2017

THE EFFECTS OF OZONE ADDITION ON FLAME

PROPAGATION AND STABILIZATION

Approved by:

Dr. Wenting Sun, Advisor
School of Aerospace Engineering
Georgia Institute of Technology

Dr. Jerry Seitzman
School of Aerospace Engineering
Georgia Institute of Technology

Dr. Jechiel Jagoda
School of Aerospace Engineering
Georgia Institute of Technology

Dr. Timothy Ombrello
Aerospace Systems Directorate
U.S. Air Force Research Laboratory

Dr. Lakshmi Sankar
School of Aerospace Engineering
Georgia Institute of Technology

Date Approved: November 7, 2017

To my wife, my family
and my newborn daughter
– I'm so excited to meet you!

ACKNOWLEDGEMENTS

TABLE OF CONTENTS

LIST OF TABLES

LIST OF FIGURES

LIST OF SYMBOLS AND ABBREVIATIONS

Re	Reynolds number (dimensionless)
S_L	Laminar flame speed (m/s or cm/s)
T_0	initial or inlet temperature (K)
p	pressure (atm or Pa)
t	physical time (s)
U	velocity magnitude (m/s or cm/s)
ϕ	equivalence ratio (dimensionless)
σ_X	uncertainty of the variable X (the same unit as X)

SUMMARY

Combustion plays a vital role in transportation and power generation. However, concerns of efficiency, emission, and operations at extreme conditions highlight the needs to enhance combustion process. If the rate-limiting chemical pathways can be modified, the ignition and combustion process could be dramatically accelerated. Following this idea, addition of ozone (O_3) is proposed as a potential solution. O_3 is one of the strongest oxidizers. It can be efficiently and economically produced *in situ* at high pressures, and transported to the desired region from an injection location to modify fuel oxidization and control the combustion process.

To serve as a basis for future application on practical combustion systems, this dissertation investigates the effects of O_3 addition on two fundamental combustion processes: the propagation of laminar premixed flames and the stabilization of non-premixed jet flames in autoignitive environment. Previous studies have shown that O_3 addition can enhance flame propagation, stability and ignition, but the dependence on pressure and temperature were not clear. Furthermore, few studies have been conducted on the effects of ozonolysis reactions, which are rapid even at room temperature for unsaturated hydrocarbons. The results presented in this dissertation are an attempt to address these questions.

The effects of O_3 addition on the propagation of laminar premixed flames are investigated with respect to pressure, initial temperature, O_3 concentration and fuel kinetics. For alkane/air premixed laminar flames, high-pressure Bunsen flame experiments in the present work show that the enhancement in laminar flame speed (S_L) increases with pressures. This is due to the fact that O_3 decomposition, which releases reactive oxygen

atoms, becomes a more dominant O_3 consumption pathway at higher pressure. Simulations show that adding O_3 at higher initial temperature is not as effective as lower initial temperatures. A nearly linear relation between the enhancement and O_3 concentration is observed at room temperature and atmospheric pressure. If the fuel is changed from alkanes to C_2H_4, an unsaturated hydrocarbon species, ozonolysis reactions take place in the premixing process. When the heat released from ozonolysis reactions is lost, decrease in S_L is observed. In contrast, if ozonolysis reaction are frozen, either by cooling the reactants or decreasing the pressure, enhancement of S_L by O_3 addition is observed.

The study on flame stabilization with O_3 addition is conducted with a non-premixed jet burner in a quartz tube using C_2H_4 as the fuel. At low-dilution conditions, autoignition events are initiated by ozonolysis reactions. The autoignition timescale is further investigated quantitatively. Overall, this timescale decreases as the inlet velocity increases. At such autoignitive conditions created by ozonolysis reactions, the stabilization of a lifted non-premixed flame is fundamentally different from non-autoignitive conditions. Propagation is enhanced due to the "preprocessing" of fuel by ozonolysis reactions, after which the mass burning velocity of the reactants is increased as shown by simulation. This can increase the propagation speed by several times.

In summary, for the premixed laminar flame propagation, the present results explain the pressure, initial temperature, and fuel dependence of enhancement of flame propagation by O_3 addition. A more comprehensive understanding is thus contributed. Furthermore, this dissertation explores ozonolysis reactions as an alternative to create a platform to conduct fundamental research on flame in autoignitive environment.

CHAPTER 1

INTRODUCTION

1.1   Background and Motivation

Combustion plays a vital role in transportation and power generation. However, concerns of efficiency, emission, and operations at extreme conditions highlight the needs to enhance combustion process. One example is high-speed air-breathing propulsion systems, such as supersonic combustion ramjet (scramjet) engines. The short flow residence times in the engine highlights the need to enhance and control ignition and flame stabilization. If the rate-limiting chemical pathways can be modified, the ignition and combustion process could be dramatically accelerated.

Non-equilibrium plasma assisted combustion (PAC) has shown potential for enhancing and controlling combustion processes [1, 2]. Unfortunately, the operating conditions of non-equilibrium plasma and combustion systems are not well aligned. Most combustion systems operate at elevated pressure conditions, while non-equilibrium plasmas favor pressures below 1 atm [3]. High pressure causes plasma thermal instability, non-uniform structure [1], and collisional thermalization of the discharge [3]. At the same time, radicals have a shorter lifetime at higher pressure [4], and thus they are generally quenched before being transported to the reaction zone (if generation is not *in situ*). The difficulty of generating stable, uniform, non-equilibrium plasmas at high pressures can be mitigated by the injection of long-lived, plasma-produced species. One attractive species is ozone (O_3). O_3 is one of the strongest oxidizers. It can be efficiently and economically

produced *in situ* at high pressures, which corresponds to the operating condition of most practical combustion devices. O_3 has a very long lifetime. Compared to the time scales in most combustors, the lifetime of O_3 is long enough to be transported to the desired region from an injection location to modify the fuel oxidization and control the combustion process.

1.2   Literature Review

1.2.1   An introduction to ozone

Ozone (O_3), or trioxygen, is a pale blue gas with distinctively pungent smell at room conditions. It plays an important role in our life in many ways. The O_3 in the stratosphere (O_3 layer) protects us from biologically-damaging ultraviolet radiation. On earth, it is used in industrial processes and as a disinfectant. It can be toxic, and it is involved in the formation of photochemical smog.

The discovery of O_3 was in 19th century, although it was known as an accompaniment to electrical storms during the history of mankind. Only after the invention of static electricity machines were people able to identify such species on the earth. When first detected, O_3 was recorded as the "odor of electricity" [5]. C. F. Schönbein, Figure 1, a German-Swiss chemist, firstly formally proposed O_3 as a distinct chemical substance in the 1840's [6]. He proposed the name "ozone" for this substance, from the Greek word "ozein", meaning "to smell". The molecular formula of O_3 was determined in 1865 by Jacques-Louis Soret [5] and confirmed by Schönbein. A few decades later, a French chemist, M. P. Otto, started a company that was the first one specialized for manufacturing

and installing O_3 generators, and filed a U.S. patent in year 1915 [7] for water treatment and other applications.

Figure 1 C. F. Schönbein, 1799-1868
(from Ref. [5])

1.2.2 Ozone reactions

An enormous number of reactions involving O_3 have been studied. For example, searching O_3 on the National Institute of Standards and Technology (NIST) Kinetic Database[1] returns 1974 records of different reactions. However, O_3 reactions did not draw much attention in the combustion community, as O_3 rarely exists in a conventional combustion system. To the author's knowledge, prior to the study of O_3 assisted combustion, the only topic in the combustion community involving O_3 reactions is the O_3

---

[1] http://kinetics.nist.gov/kinetics/index.jsp, webpage visited on Aug 26, 2017

decomposition flame, such as in Ref. [8-12]. In such flames, O_3 thermally decomposes in the preheat zone.

$$O_3 + M = O_2 + O + M$$
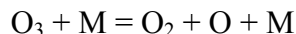
where M stands for a third-body reactant representing the all species. Heat is released from this decomposition reaction and sustains the flames. Such flames were studied primarily for two reasons: the practical safety problems involved in the storage of O_3, and as a platform to study flame structure and dynamics, as only a small number of reactions needed to be considered. The kinetic rates of this reaction have been extensively studied [13]. The dependence on temperature is expressed using an Arrhenius expression with a relatively small uncertainty (approximately 20%).

O_3 reactions are an important topic in atmospheric chemistry because of atmospheric O_3. Interest in atmospheric O_3 dated from the very beginning of Schönbein's discovery of O_3. Schönbein considered the possibility that O_3 was found in the atmosphere [14]. However little direct evidence was obtained until 1885. Schöne measured the spectrum of the atmosphere and found bands characteristic of O_3 [15]. Later, people realize the existence of an O_3 layer in the atmosphere. O_3 absorbs radiation in the ultraviolet. Without an O_3 layer, the organic molecules in living organisms may decompose. Furthermore, the reactions between O_3 and alkenes may form photochemical air pollution [16, 17]. Due to these important issues, the kinetics and mechanisms of the gas-phase reactions of O_3 have been extensively studied. The direct reactions between O_3 and (usually unsaturated) hydrocarbons are generally referred as "ozonolysis reactions". While the rate constants for these reactions are now reliably known [18, 19], significant uncertainties still exist in the

detailed reaction mechanisms and the products formed. Such information could be critical for its application in combustion systems, especially for the ozonolysis reaction with fuel species.

$$O_3 + Fuel = Products + Q$$
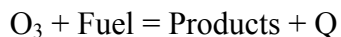
Ozonolysis reactions generally release heat. In the ozonolysis process of hydrocarbons, there could be a dramatic difference in the behavior of alkanes and unsaturated hydrocarbons [20]. The reaction between O_3 and CH_4 is very slow (reaction rate constant at 300 K is 0.99 cm^3/mole-s [21]) at room temperature and atmospheric pressure. However, the reaction between O_3 and ethylene (C_2H_4) is explosive [20, 22] (reaction rate constant at 300 K is 1.12×10^6 cm^3/mole-s [23]) at the same conditions. The rates of ozonolysis reactions have been measured for several species, as listed in Table 1.

Table 1 Ozonolysis reactions rates constants, k, at room temperature and pressure

		k (cm^3/mole-s)	Reference
Alkanes	CH_4	0.99	[21]
	C_2H_6	8.95	[24]
	C_3H_8	4.19	[24]
	C_4H_{10}	6.05	[21]
Unsaturated Hydrocarbons	C_2H_4	1.12×10^6	[23]
	C_3H_6	6.29×10^6	[25]
	iso-C_4H_8	7.13×10^6	[26]
	1-C_4H_8	5.82×10^6	[26]

As the ozonolysis of alkanes are generally very slow at room temperature and can be neglected, the ozonolysis of unsaturated hydrocarbons is the focus in this dissertation. A well-known ozonolysis mechanism was suggested in 1975 by Criegee [27] for alkenes. The first step is a 1,3-dipolar cycloaddition of O_3 to the alkene. In this step, combining with O_3, the double carbon-carbon bond is broken and a 5-member cyclic structure is formed. The

product is called primary ozonide (POZ), which decomposes to give a Criegee intermediate (a carbonyl oxide) and a carbonyl compound. POZ is not collisionally stabilized under atmospheric conditions [28]. In case of C_2H_4, the carbonyl compound is CH_2O, and the carbonyl oxid is H_2COO [29]. Recently, a method has been experimentally demonstrated by Berndt *et al.* [30] to detect Criegee intermediate directly from ozonolysis reactions for close to atmospheric conditions.

The subsequent reactions are not clear and various pathways have been proposed. Criegee suggests that the carbonyl oxide and the carbonyl compound combine and yield a secondary ozonide (SOZ). More recent investigations suggest that the carbon oxide formed in the POZ cleavage may decompose unimolecularly [28, 29, 31]. Several pathways for the unimolecular reaction of the carbonyl oxide have been proposed: 1) the ester channel, which forms dioxirane and subsequently decomposes into simpler species, 2) the formation of an OH radical via H migration, and 3) the split-off of $O(^3P)$ atoms. The relative branching fractions of the reactions of the Criegee intermediate are predicted to be pressure dependent [28]. As the products of these channels are highly reactive, secondary reactions can be initiated and large uncertainties can be introduced, which complicates the investigation of ozonolysis. The mechanism of these reactions is still not fully understood.

Besides the decomposition of O_3 and the ozonolysis reactions with unsaturated hydrocarbons, there are several O_3 reactions that are expected to be important in combustion systems involving O_3. For $O_3 + H = O_2 + OH$, the earliest research may date back to 1962 [32], which only reports a kinetic rate. But more recent works include activation energy, such Ref. [33]. It seems such kinetics measurement have been well accepted, and no further measurements are reported. For $O_3 + H = O + HO_2$, fewer studies

have been conducted. The only measurement reported is in 1980 by Howard and Finlayson-Pitts [34], and the temperature dependence is not investigated. $O_3 + OH = O_2 + HO_2$ and $O_3 + HO_2 = OH + O_2 + O_2$ are relatively well studied, and are reviewed in [35].

1.2.3   Fuel processing using ozone

Due to its unique chemical properties, O_3 is used in fuel processing. It has been attempted in coal desulphurization by Steinberg *et al.* [36]. In this work, enrichment of the sulphur element in the effluent gas was detected after O_3 treatment, indicating the possibility of desulphurization. However, such enrichment could not indicate a practical desulphurization process unless it can be significantly increased. As O_3 can react with almost all functional groups of lignite organic matter, even with polyaromatic fragments at room temperature [37], O_3 has been used as one treatment of lignite. Sharypov *et al.* [38] investigated such treatment on the properties of Kansk-Achinsk lignite. Loosening of the overall molecular structure of lignite was observed to take place during ozonization. Ozonized lignites were reported to have higher reactivity in hydrogenation processes in the presence of hydrogen –donor solvents and pyrite catalyst. Gao *et al.* [39] demonstrated that O_3 is able to reduce the surfactant absorptivity of fly ash carbon. A more recent work by Patrakov [40] studied the treatment of coal organic matter by O_3. Redistribution of O atoms in the functional groups were detected. Ozonoization changes the macromolecular organization. One important kinetic effect is that the effective activation energy of thermal liquefaction decreased by O_3 treatment, as shown in Figure 2. O_3 has also been applied to treat renewable fuels. The crystallization of saturated fatty acid methyl ester (FAME) during cold seasons can cause fuel starvation and operability problems. For this reason, the pour point needs to be depressed for neat biodiesel derived from vegetable oils. O_3 was

investigated as a pour point depressant by Soriano Jr. *et al*. [41]. Microscopic analysis revealed that ozonized vegetable oils prevent the agglomeration of crystals, thus maintaining the fluid flow properties and improving the pour point of biodiesel.
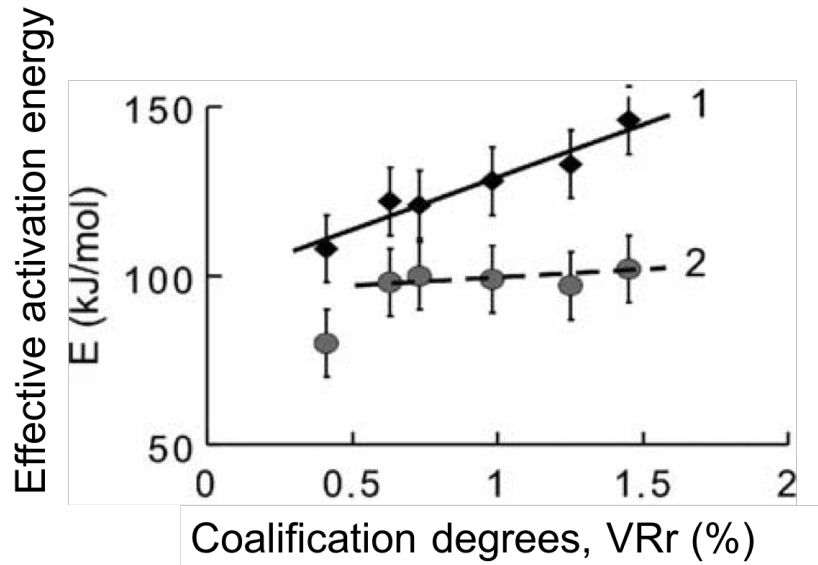
Figure 2 The effective activation energy of thermal liquefaction process of (1) initial and (2) ozonized coal vitrinites

(reproduced from [40])

Ozone treatment has also been investigated as way to modify the fuel reactivity adaptively to control ignition timing. Schönborn *et al.* [42] demonstrated a method to control the point of ignition under HCCI combustion conditions by adapting the molecular structure of the fuel. This was achieved by reacting a variable proportion of the fuel with air that contains O_3 prior to entering the combustion chamber. Such design allows the generation of fuel of a variable ignition quality from a single fuel supply in a practical application. The reactions with O_3-containing air converted a proportion of the acetal fuel

to peroxide, which was suspected to promote the autoignition. It was shown that as the proportion of oxidized fuel increases, the ignition timing is advanced. As a continuation of this work, Schönborn *et al*. [43] investigated the possibility of controlling the ignition timing of another fuel, 1-hexene, by altering its molecular structure using prior reaction with O_3. Correspondingly, an engine system utilizing such "smart fuel" was proposed, as shown in Figure 3. A portion of fuel is oxidized and then mixed with the non-oxidized fuel. The ignition timing is advanced, likely due to the early decomposition of peroxidic structures formed in the case of O_3 utilization. Then the ignition timing is controlled via the fuel mixture composition.
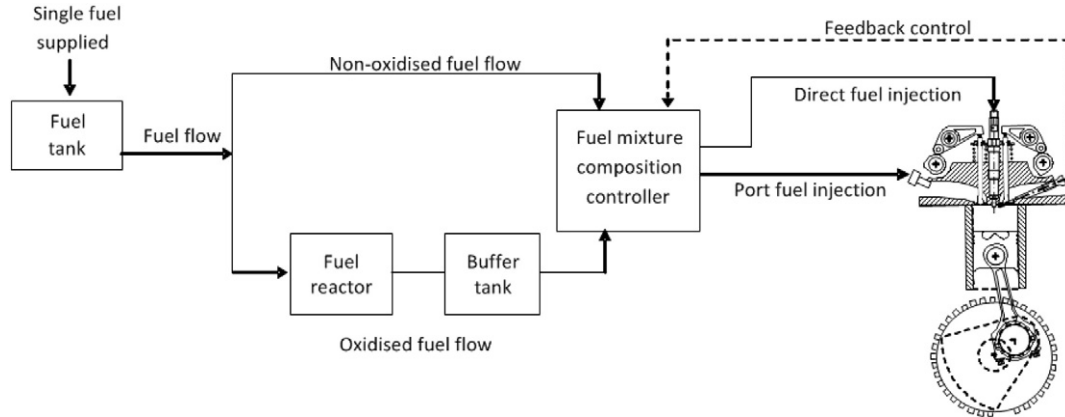
Figure 3 The engine system utilizing the "smart fuel" producing by fuel preprocessing using O_3

(from[43])

1.2.4   Effects of ozone addition on emissions

The effect of O_3 addition on the pollutants from combustion systems have been investigated as well. In 1980, Slater and Rizzone [44] experimentally demonstrated that,

9

by injecting O_3 in a dry, synthetic flue gas., the oxidization of SO_2 is rapid. However the effects were reduced in the presence of NO. Tahibana *et al.* [45] measured the concentration of CO, unburned hydrocarbons, and NOx in the exhaust gas of a diesel CFR (Cooperative Fuel Research) engine with O_3 addition. The composition of NOx was not analyzed. Filter paper was placed in the exhaust to trap particulates, and the contamination level was estimated using the light intensity passing through the filter paper. As more O_3 added, the concentrations of CO and unburned hydrocarbons decreased. The contamination level decreased as well, though not as much as for CO and unburned hydrocarbons. In contrast, the concentration of NO_x increased. The authors suspected that this change was caused by the changes in the combustion temperature. This is a reasonable suggestion as the enthalpy increased by adding O_3. Similar results were observed by Wilk and Magdziarz [46], who supplied natural gas and air mixtures to a modified Mecker burner. The concentration of CO, unburned hydrocarbon, NO and NO_2 were measured for the case with and without O_3. Consistent with Ref. [45], adding O_3 reduced CO and unburned hydrocarbons, and slightly increased NO. No effects on NO_2 were detected. Besides the addition in the oxidizer, O_3 injection has also been used in processing flue gas. Cannon Technology Inc. and BOC Gases developed a low temperature oxidation (LTO) process for removing NOx emissions using O_3 injection in 2003 [47]. O_3 was injected into the cooled exhaust flue gas from the boiler. The NOx was then oxidized in the oxidation chamber to N_2O_5, with part of CO oxidized to CO_2, and SO_2 oxidized to SO_3. Further multi-objective optimization and analysis works [48, 49] have been conducted. Later, a two-step technique was proposed by Mok and Lee [50] to remove NO_x and SO_2 simultaneously using O_3, where NO was oxidized to NO_2 in the ozonizing chamber. Wang *et al.* [51]

investigated the possibility of simultaneously removing NO_x, SO_2, and Hg using O_3. Another process simultaneously removing NO_x and SO_2 by O_3 was investigated by Sun *et al*. [52]. A general observation of these works is that NO in flue gas can be effectively oxidized by O_3. However, as O_3 decomposes at high temperature, the effect of O_3 injection on pollutant oxidization may be reduced. For example, as shown in Figure 4, at 373 K, adding 200 ppm O_3 oxidized more than 80 % of NO, but at 673 K, adding O_3 essentially did not oxidize NO as O_3 decomposed and recombined to O_2 before oxidizing NO.
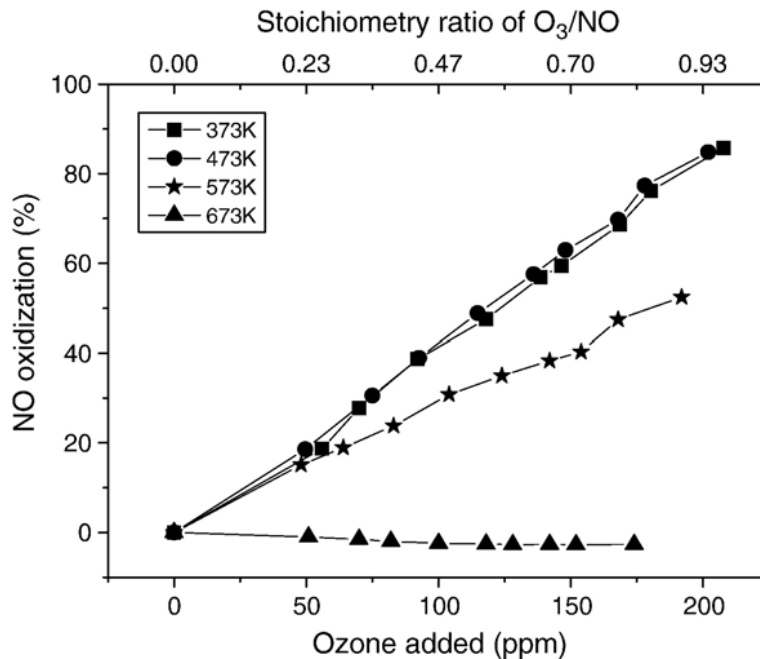
Figure 4 NO conversion property with O_3 added at different temperature
(from Ref. [51])

1.2.5 Ozone assisted combustion via ozone decomposition

Initially, studies of O_3 assisted combustion focus on the effects of O_3 addition on ignition, especially in engines. In 1988, Nomaguchi and Koda [53] investigated spark ignition experiments using electric pulses in a closed vessel at reduced pressure for premixed fuel (CH_4 or CH_3OH) and ozonized air. It was found that the minimum spark pulse duration for successful ignition could be shortened considerably by O_3 addition of 0.2% in O_2. Simulation shows that the acceleration of ignition is due to the O atom attacking fuel molecules. Later, Tahibana *et al.* [54] used a Diesel CFR engine to examine the effect of O_3 addition on compression ignition engines. Adding O_3 accelerated ignition, increased the cetane number and lowered the compression ratio of the ignition limit. These are consistent with the work by Nomaguchi and Koda [53]. These findings on ignition inspired researchers to develop O_3 addition as an ignition control technique. Such an attempt was proposed in a patent [55] filed in 1997. Several ways of using O_3 were proposed in this patent: i) by adjusting the amount added, O_3 can be used to control the start of combustion; ii) O_3 can be used as a cold starting aid; and iii) O_3 can be used to reduce cold start emissions. The first use, ignition controlling, was later investigated by Nishida and Tachibana [56] in 2006 in homogeneous charge compression ignition (HCCI). The ignition timing and combustion duration of HCCI are governed by chemical reactions, not by spark or injection, and thus techniques to control ignition timing are essential. They carried out a numerical analysis, showing the feasibility of controlling ignition timing by varying the amount of O_3 added, as illustrated in Figure 5. They also found that adding O_3 is more effective than addition of OH radicals, and is as effective as injection of O radicals. Further investigations were conducted by Foucher *et al.* [57] and Masurier *et al.* [58-60].
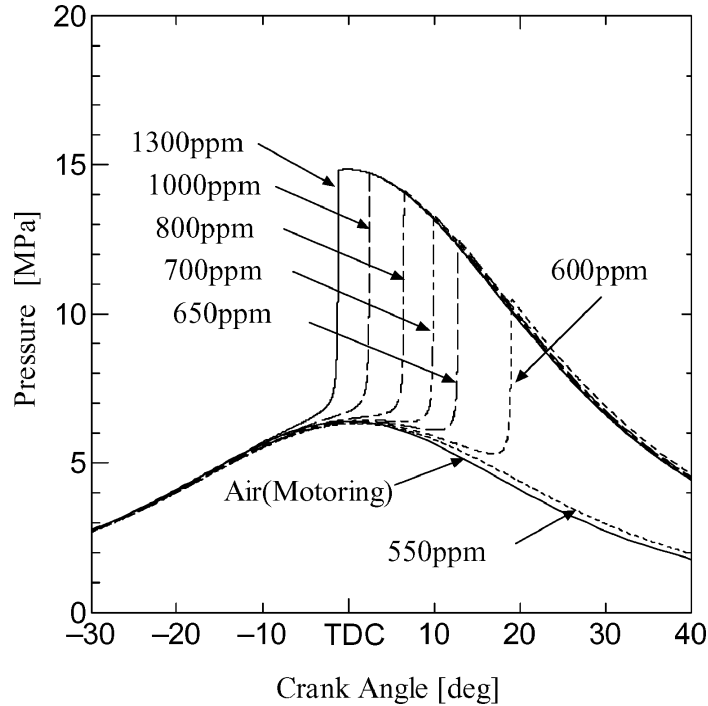
Figure 5 Calculated ignition process in HCCI for different O_3 concentrations
(from Ref. [56])

The effects of O_3 addition on laminar flames has also drawn attention. Besides the work on ignition, Nomaguchi and Koda [53] also measured the burning velocity of CH_4/air at room temperature and atmospheric pressure. Their data showed that adding 5000 ppm O_3 increased the burning velocity by 5% at stoichiometric conditions and that the enhancement was greater for fuel-lean and fuel-rich cases. Another fuel, propane (C_3H_8), was investigated by Ombrello *et al.* [4, 61]. A lifted laminar flame, in which liftoff height is very sensitive to S_L, was employed. O_3 addition was observed to decrease the liftoff height, as shown in Figure 6, indicating an increase in S_L. When accounting for the kinetic and hydrodynamic effects, an approximately 4% enhancement of S_L at a stoichiometric condition was reported with 1260 ppm O_3 addition. These observations were later supported by Halter *et al.* [62] with simulations and a similar experimental approach. A

more recent experiment by Wang *et al*. [63] using the heat-flux burner showed a 3.5%

increase in S_L with 3730 ppm O_3 addition at stoichiometric conditions, and 9% increase for

7000 ppm O_3. Generally, the enhancement increases with O_3 concentration, shown in

Figure 7. Syngas has also attracted much attention. An approximately 9% enhancement to

S_L was reported with 8500 ppm O_3 addition at stoichiometric conditions for a $H_2/CO/N_2/air$

mixture by Liang *et al*. [64].
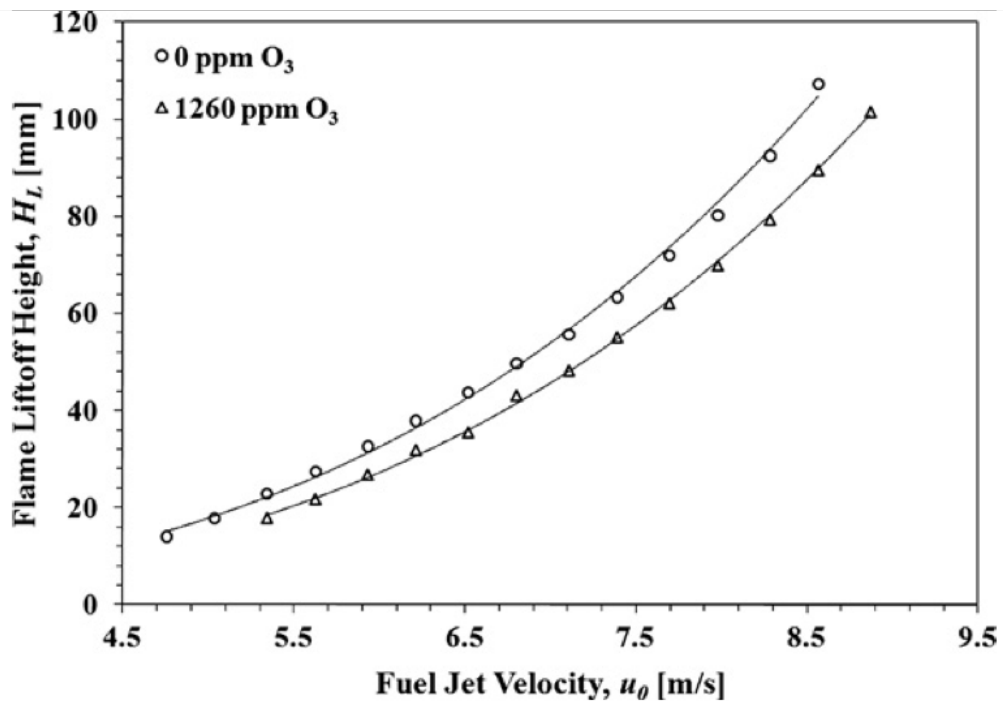
Figure 6 Flame liftoff height as a function of fuel jet velocity with or without O_3
(from Ref. [61])
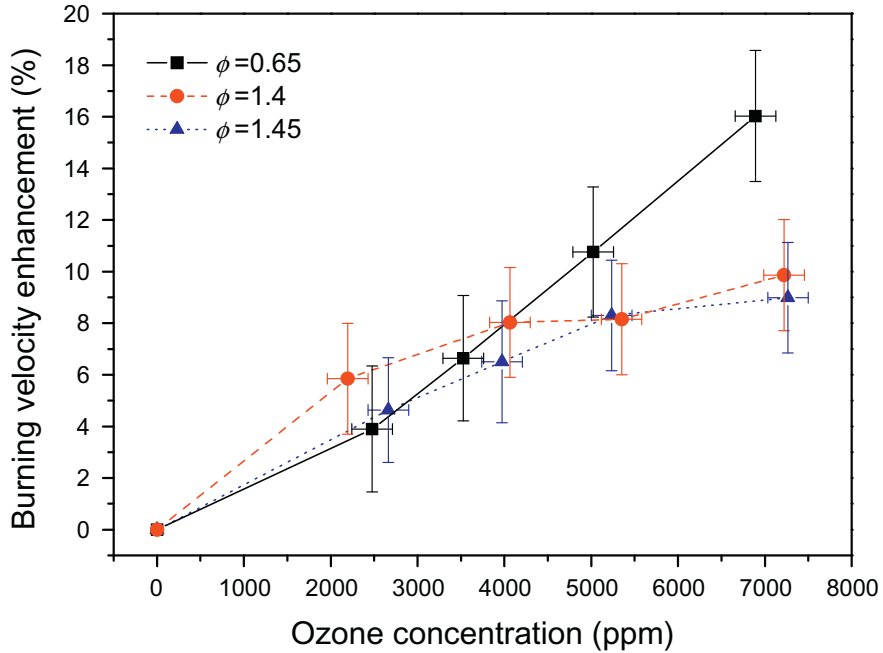
Figure 7 Enhancement of flame speeds as a function of O$_3$ concentration
(from Ref. [63])

O$_3$ addition can also improve flame stability of laminar flames. Recently, Vu *et al*. [65] demonstrated increased blowoff velocity and extended flammability limits in a Bunsen burner at atmospheric pressure using CH$_4$ and C$_3$H$_8$ as the fuels. They observed that an unstable flame can be stabilized by O$_3$ addition, as illustrated in Figure 8. With 3810 ppm O$_3$ addition, the enhancement of blowoff velocity at stoichiometric conditions was approximately 9% for CH$_4$ and 11% for C$_3$H$_8$ [65]. Consistent with their work, Zhang *et al*. [66] found that the flammability limits of syngas were substantially expanded by O$_3$ addition. Furthermore, O$_3$ sustains the syngas flame at higher dilution ratios. The kinetics effect of O$_3$ addition was further investigated by Weng *et al*. [67]. A significant increase of CH$_2$O concentration due to O$_3$ addition was detected in a laminar Bunsen flame using CH$_2$O-PLIF (planar laser-induced fluorescence), with effect greater at rich conditions

15

compared to the stoichiometric case. The experimental measurements agree well with the simulation results. To isolate the effects of the flame, they measured the CH_2O production in heated reactants (no flame), and found that the temperature needed to produce CH_2O was significantly lowered by adding O_3.
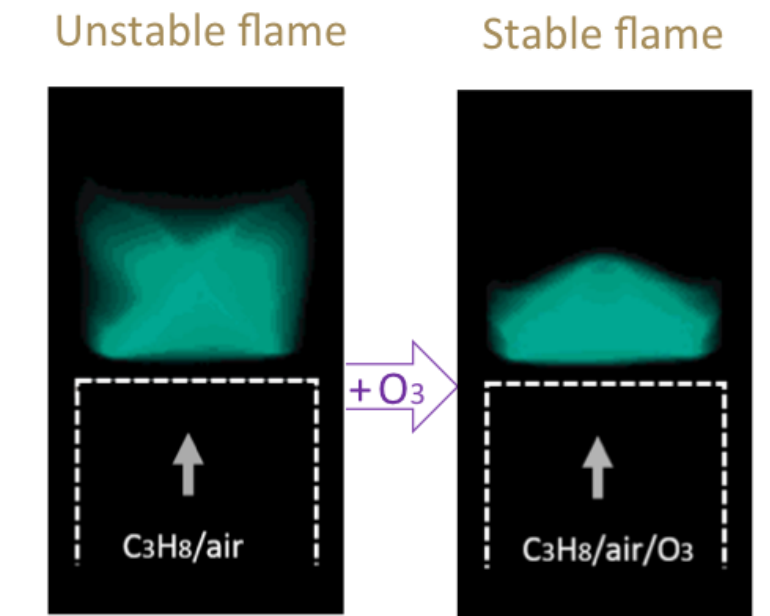
Figure 8 Enhancement of flame stability by O_3 addition
(reproduced from Ref. [65])

Only few works focus on the effect of O_3 addition on turbulent flames. Ehn *et al*. [68] investigated this using laser diagnostics and large eddy simulations. They observed increase in CH_2O as small amounts of O_3 were added, and reported increase in laminar flame speed and extinction strain rate due to O_3, implying that flame can burn under more turbulent conditions that would be possible without O_3 addition. Weng *et al*. [67] also measured the concentration of CH_2O in turbulent flame with or without O_3 addition, using a water-cooled McKenna burner with a centered jet tube. Consistent with Ref. [68] and the

laminar case, they also observed increases in CH_2O concentration in turbulent flames, as shown in Figure 9. Such enhancement effect of O_3 addition on CH_2O production was greater than in laminar cases.
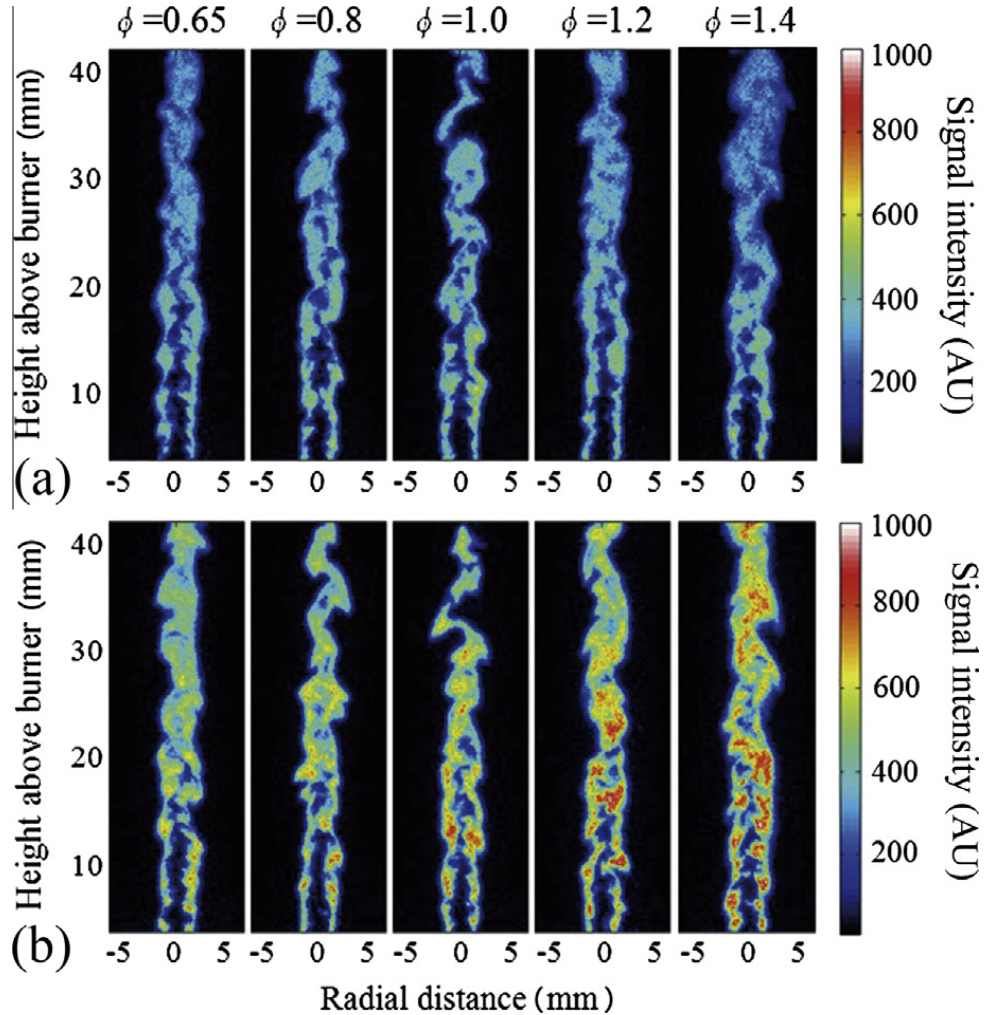
Figure 9 CH₂O-PLIF for the case (a) without O₃ and (b) with 4500 ppm O₃
(from Ref. [67])

The conventional understanding of these enhancements is that, due to its long lifetime, O_3 can be transported to the preheat zone and then decompose to release O atoms, which accelerate reactions by attacking fuel molecules [53, 61]. A general observation

from previous studies is that as one of the strongest oxidizers, O_3 always enhances the combustion process. However, this interpretation is based on the understanding that O atoms are always produced, which may not always be the case. It is possible that O_3 reacts with fuel (ozonolysis) before it decomposes to release O atoms. This process can be either beneficial or detrimental to enhancement. Recent experiments [69] conducted at low pressures shows that S_L with C_2H_4-based flames were enhanced by O_3 addition. However in the 1950s, Gluckstein *et al*. [70] reported that the S_L of C_2H_4 was decreased by O_3 injection at room conditions. The contradictions of previous results raise the following question. Does O_3 always enhance flame propagation, and how does ozonolysis of fuels affect S_L at different pressures and temperatures? Glucksein *et al*. [70] suspected that the detrimental effect of O_3 addition was due to production of formaldehyde (CH_2O) from the reaction between O_3 and C_2H_4. This explanation may not be complete because i) CH_2O has a greater effect on S_L than C_2H_4 and ii) other reactive species such as H_2 could be formed by ozonolysis of C_2H_4 [71, 72]. Replacing a portion of C_2H_4 by H_2 and CH_2O should have a positive effect on S_L. To the authors' knowledge, this is the only reference reporting a detrimental effect of O_3 on flame propagation. However, the uncertainty of the experimental data in this work is large, and the experiments may suffer from uncertain reactant composition. This is because a significant concentration of O_3 may have already been consumed before entering the flame zone due to the fast C_2H_4 ozonolysis reaction. Therefore, experiments with clear boundary conditions are necessary.

1.2.6 Ozone activated cool flames

Ozone also promotes the formation of cool flames [73-77]. Cool flames were observed accidentally more than 100 years ago [78]. Unlike normal high-temperature flames, the temperature of the cool flames is generally around or below 1000 K. It receives attention as low temperature chemistry, which plays a key role in formation of cool flames, is also relevant to practical problems such as engine knock and fire safety. However it is challenging to obtain stable self-sustaining cool flames as the radical chain-branching process is limited at low temperatures. Therefore, addition of O_3, which might assist the initiation and branching of radicals, has been proposed as a solution to stabilize cool flames. Won *et al.* [76] confirmed this possibility experimentally using a counterflow burner with O_3 added to the oxidizer side. The fuel was diluted by N_2 and heated to 550 K. Activated by the addition of O_3, cool flames were observed as illustrated in Figure 10. However, they become unstable at high strain rate or high fuel dilution level. Also low strain rate or low fuel dilution level, normal high-temperature flames were observed instead of cool flames. O_3 plays a key role here in the formation of cool flames [76]. It was suggested that the decomposition of O_3 releases atomic O, which then initiates the low temperature chemistry necessary for cool flames.
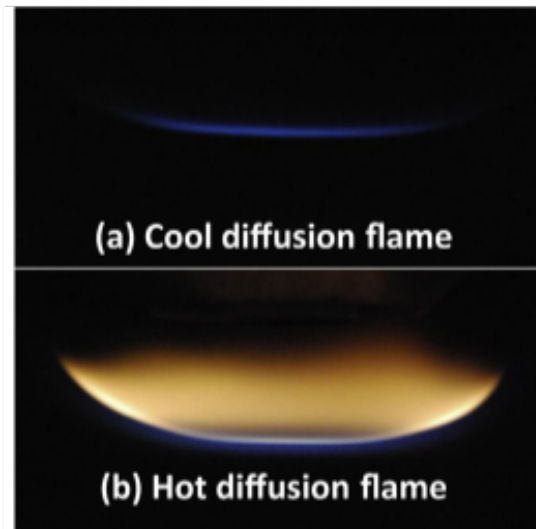
Figure 10 Direct photos of (a) cool and (b) normal high temperature diffusion flames

(from Ref. [76])

Later, Ju and coworkers conducted numerical simulations on premixed dimethyl ether (DME) flames [73]. Three branches were observed: normal high-temperature flames, double flames, and cool flames, as shown in Figure 11. It was observed that the cool flames can exist at the conditions beyond the flammability of conventional high temperature flames, thus significantly extending the flammability of the DME flames. However, at 300 K, for freely propagating flames, only a normal high temperature flame branch is observed. To observe cool flames, the reactants temperature must be raised to 530 K, or O_3 needs to be added in the reactants. It is true that the enthalpy is increased as part of O_2 is replaced by O_3, but the authors [73] argue that the formation of cool flame at 300 K when O_3 is added is not solely a thermal effect. They showed that even at a lower mixture enthalpy, O_3 addition increases the flame reactivity more significantly compared to heating the reactants. Instead, it is believed that O_3 kinetically promotes the formation of cool flames. O_3 decomposition releases O in the preheating zone of the cool flame, thus accelerating the

chain-branching and enabling cool flames at low temperature. Similarly, for stretched counterflow flames, it is reported that O_3 addition extends range of stretch rates for the cool flame formation [73].
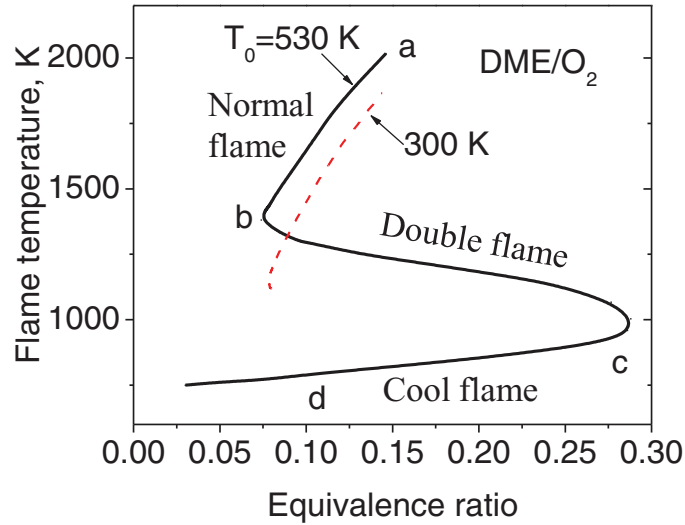
Figure 11 Dependence of flame temperature on equivalence ratio for DME/O$_2$ freely propagating premixed flames

(from Ref. [73])

The numerical prediction of the DME premixed cool flame activated by O_3 addition was later experimentally demonstrated by Reuter *et al*. [74]. The experiment was conducted at atmospheric pressure in a counterflow burner, with premixed reactants at 300 K and very lean conditions, and the counterflow being N_2, which is heated to 600 K. The cool flames were observed when O_3 was added, and exhibited different flame dynamics compared to normal high-temperature flames. For example, the location of the cool flame showed little dependence on equivalence ratio, indicating the weak dependence of its flame speed on equivalence ratio. In contrast, for the normal high-temperature flames, there was a well-known strong correlation between the flame speed and equivalence ratio. A difference in flame structure was also observed. For example, the PLIF measurement

21

showed that CH_2O profile for the cool flame was much thicker than its normal high-temperature flame counterpart, as illustrated in Figure 12. This might be linked with the different flame dynamics mentioned above, but was not discussed in this work.
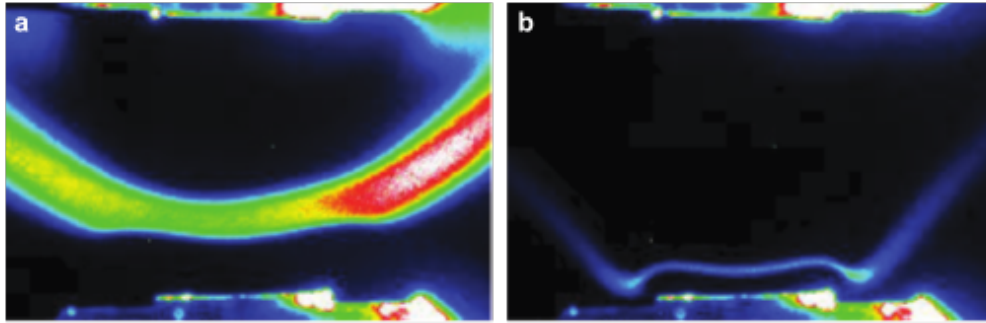
Figure 12 Raw CH$_2$O PLIF images of (a) a cool flame and (b) a normal high-temperature flame at the same flow conditions

(from Ref. [74])

Hajilou *et al*. [75] further investigated the DME premixed cool flames using a Hencken burner at sub-atmospheric pressures. Such a platform has been used to study freely propagating flames [79]. The propagation speeds of the cool flames were measured [75]. Consistent with previous work [74], the flame speed seems to be not sensitive to equivalence ratio at very lean condition. However, it was also reported that the propagation speed decreases as the equivalence ratio increases from 0.6 to 1.4, shown in Figure 13. The peak flame temperatures depressed as equivalence ratio increased in the reported range, which is different with the normal high-temperature flames.
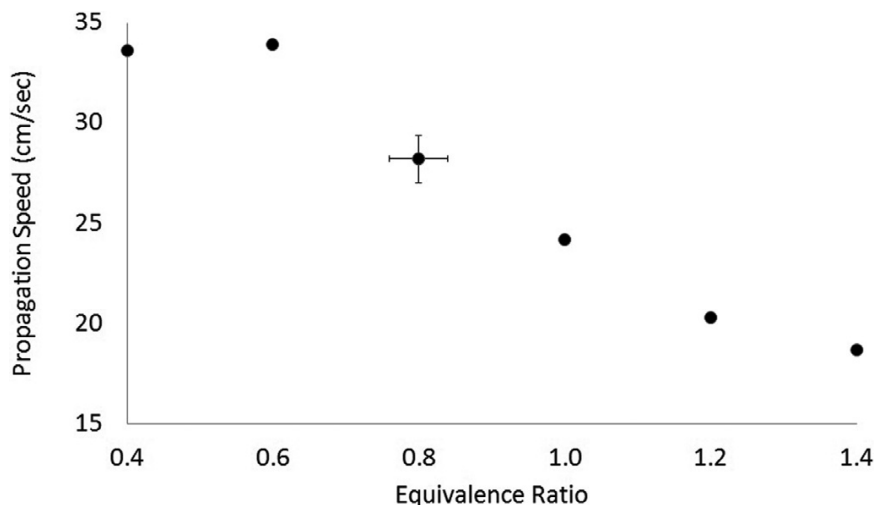
Figure 13 Cool flame propagation speeds derived from lift-off height analyses
(from Ref. [75])

As a continuation of the previous work [74], Reuter *et al.* [77] investigated the cool diffusion flames for large n-alkanes. As the presence of O_3 slightly complicates the chemical kinetics, they generated "ozone-less" cool flames by turning off the O_3 generator after cool flames were established. Without O_3, the cool flames were much weaker in terms of the chemiluminescence intensity, shown in Figure 14. "Ozone-less" cool flames were generated using this method for large n-alkanes ranging from n-heptane to n-tetradecane. Similar to previous works, the cool flames show different behavior compared to normal high-temperature flames. For example, the chain length of the n-alkanes significantly affects the ozone-less cool flame reactivity, and larger n-alkanes produce stronger ozone-less cool flames. In contrast, the normal high-temperature flames were not very sensitive to the chain length, in terms of the extinction limit. However, for the case with O_3, as the low-temperature reactivity is significantly promoted, the reactivity of the cool flames was also essentially independent of the size of the n-alkanes.
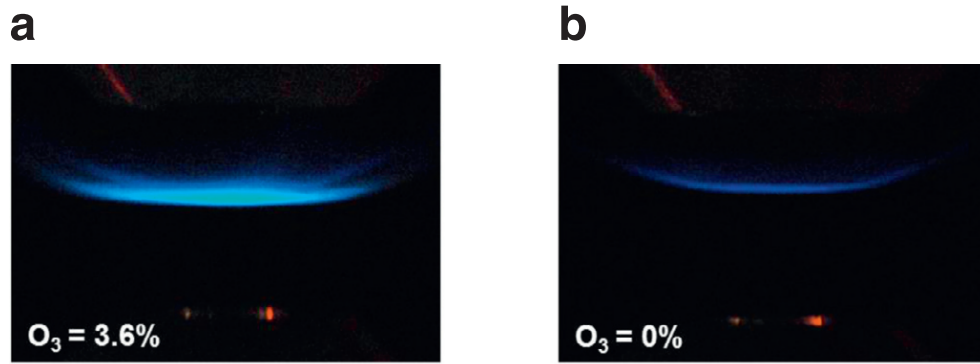
Figure 14 Direct photographs of cool flames with (a) and without (b) ozone addition
(from Ref. [77])

1.3   Research Objectives

The first objective is to investigate the effects of ozone addition on laminar flame propagation. The question attempted to be answered is how does ozone (O_3) addition affect the laminar flame speed S_L for different fuels, and how this effect changes with the operating conditions (temperature and pressure). The present work provides the knowledge to understand the effects of O_3 addition on S_L more comprehensively. This includes the underlying mechanisms of the effects of O_3 addition (e.g. thermal vs. kinetic effects), and the dependence of the effects of O_3 on pressure, temperature and fuel types, which allows a more general conclusion on the effects of O_3 addition on S_L, in contrast to previous studies conducted under limited conditions.

The second objective is to demonstrate the use of ozonolysis reactions as an alternative way to create a platform for the fundamental research on flame in autoignitive environment.   With this platform, several questions are addressed. At low initial

temperature, i) how do ozonolysis reactions affect early fuel oxidation and autoignition, and ii) how do such effects affect flame stabilization. In addition, models are presented to explain the dependence of autoignition events on conditions such as Reynolds number and O_3 concentration. The stabilization mechanism is compared with classical non-premixed jet flames.

1.4 Dissertation Outline

The dissertation is organized into nine chapters. Chapter 2 describes the theoretical framework, which include the theories on the propagation of laminar premixed flames, and the stabilization of non-premixed jet flames. The experimental diagnostics technique and simulation tools employed in this work are introduced in Chapter 3. Then, Chapters 4-7 cover the work on O_3 assisted combustion. This includes two topics. Firstly, the effects of O_3 addition on premixed flame propagation are covered, and this includes the effects on alkanes (Chapter 4) and unsaturated hydrocarbons (Chapter 5). The second topic is the effect on non-premixed jet flame stabilization at the autoignitive conditions created by ozonolysis reactions. This includes a study on ozonolysis activated autoignition (Chapter 6) and the enhancement of flame stabilization due to these autoignition events (Chapter 7). Finally, the contributions and conclusions are summarized in Chapter 8, followed by the recommendations of future research works on O_3 assisted combustion (Chapter 9). The appendix documents a novel chemistry mechanism reduction algorithm, Global Pathway Selection, which generates the reduced mechanism for the 3D simulation in Chapter 6 and 7.

CHAPTER 2

THEORETICAL AND EXPERIMENTAL FRAMEWORK

This chapter firstly covers the theories on the propagation of laminar premixed flames, which serves as the basis for O_3 assisted flame propagation later investigated in Chapters 5 and 6. Then, theories on the stabilization of non-premixed jet flames are covered, for the comparison with flame stabilization under the conditions that ozonolysis reactions are dominant factors, as discussed in Chapter 7 and 8.

2.1 Propagation of laminar premixed flames

2.1.1 Laminar premixed flames

For laminar premixed flames, fuel and oxidizer are premixed at the molecular level and provided in the laminar state. The research on such flames is a fundamental topic in the combustion community. The oldest theory is the thermal model for flame propagation proposed by Mallard and Le Chatelier [80] in 1883. It was assumed that the flame propagation is controlled by heat conduction back to the unburned reactants. In later works, the diffusion of species was considered. A theory was proposed by Zeldovich and Frank-Kamenetskii and presented by Semenov in detail [81]. This theory takes the diffusion of molecules (but not free radicals or atoms) into consideration. Tanford concluded that diffusion plays a more important role than heat transfer [82].

The structure of the laminar flame can be interpreted at several levels of complexity. The simplest interpretation for a laminar premixed flame is a flame sheet. The thickness and internal structure of the flame is neglected. It is seen as an interface that separates the burned and unburned gas. Transport and finite-rate chemistry are not considered. A more

realistic model is a two-zone model [83]. The flame is assumed to consist of a preheat zone and a thin reaction zone. The preheat zone is governed by the diffusion process of heat and mass. Chemistry is assumed to be only dominant at the reaction zone. Due to the development of simulation techniques and programs such as PREMIX [84], a comprehensive model of the premixed flame, considering convection, diffusion and chemistry, can be built and solved without making strong assumptions about the flame structure.

2.1.2 Propagation speed of laminar premixed flames

The laminar flame speed, S_L, is the velocity at which unburned gases move through the flame in the direction normal to the flame surface [85]. Ideally, it is defined for a steady, adiabatic planar flame, which corresponds to an unstretched laminar flame speed, S_L^0. However, such flame is rarely achieved experimentally.

Besides heat loss and the possible stretch introduced by the geometry of the flame sheet and unsteadiness, the propagation speed also depends on pressure, temperature and the composition of the reactants (fuel kinetics, equivalence ratio, dilution species and dilution ratio, etc). For pressure dependence, a general observation is that the flame speed decreases with increasing pressure. Some examples are given in Figure 15. This trend can be explained by the pressure dependence of reaction rate, diffusivity, and density [83, 85]
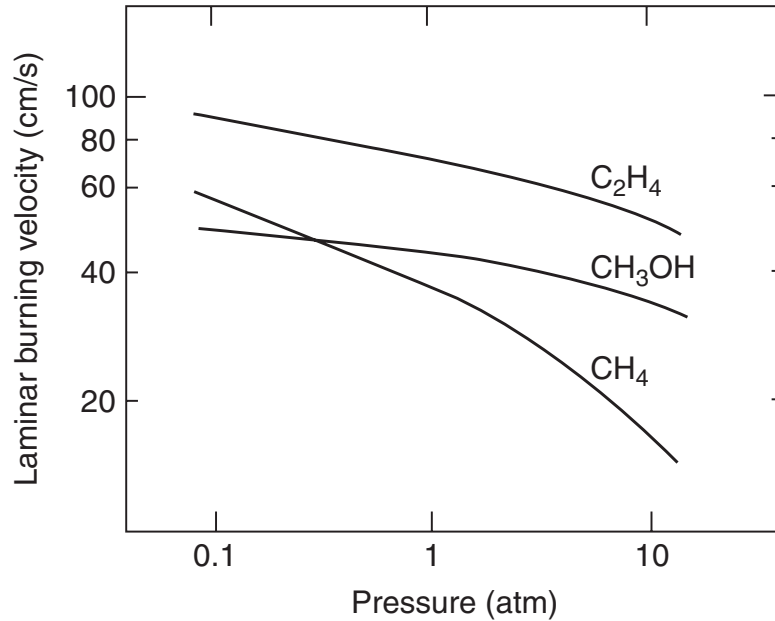
Figure 15 Pressure dependence of the flame speeds for some stoichiometric fuel/air mixtures

(reproduced from [86])

Equivalence ratio generally has a non-monotonic relation with the flame speed. The peak position depends on fuel, as illustrated in Figure 16. For most fuels, it peaks near the stoichiometric condition where the flame temperature also reaches its maxima. However, when diffusivity is strongly dependent on the equivalence ratio, which is the case for H_2, the flame speed may peak at off-stoichiometric conditions. Besides diffusivity, fuel kinetics also affect the results. For example, CO favors fuel-rich conditions because the radical-termination steps at such conditions become slower than that at fuel-lean conditions [85].
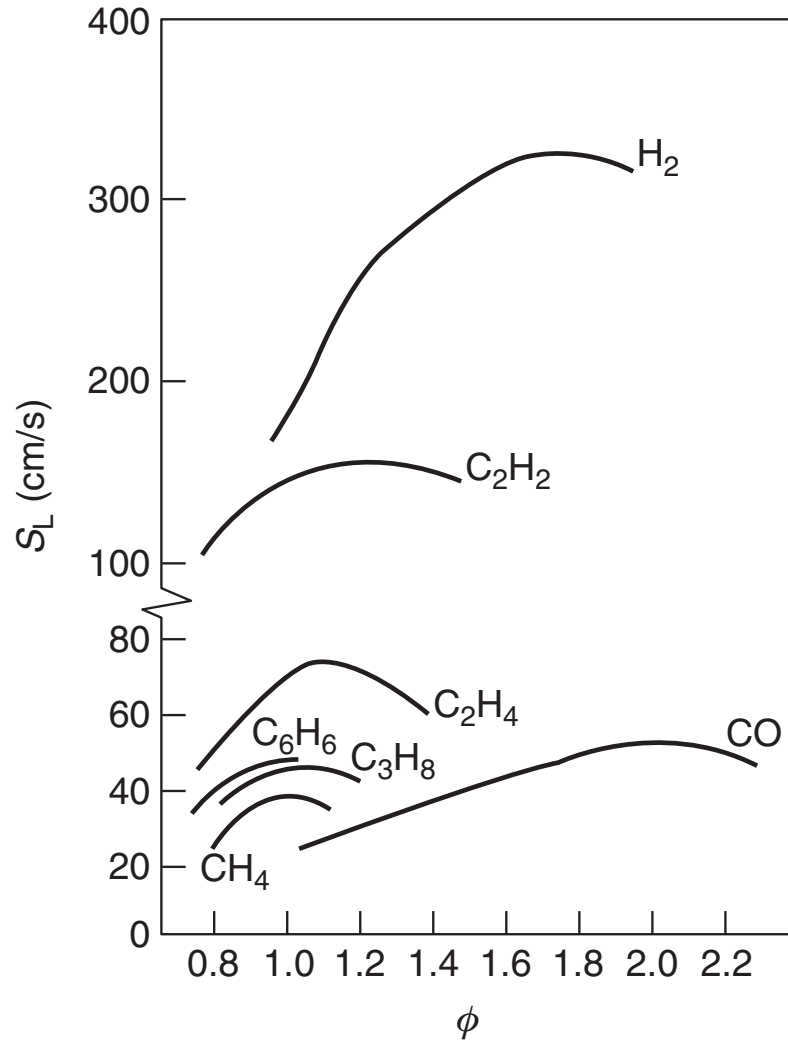
Figure 16 Equivalence ratio dependence of the flame speeds for some fuel/air mixtures

(from [85])

2.1.3 Experimental measurement methods of laminar flame speed

Several experimental methods have been proposed to measure the flame speed, although all methods suffer from uncertainty, as it is not easy to achieve a steady, adiabatic planar flame. Some commonly used methods are introduced in this section.

The spherically expanding flame method was first explored by Lewis and Von Elbe [87] in 1934. The configuration is a spherical bomb filled with fuel/oxidizer mixture. It is ignited at the center of the chamber. Then the propagation speed of the generated spherical expanding flame is measured in the outward direction. The unstretched laminar flame speed is then inferred using linear or non-linear extrapolation [88] to zero stretch rates. The advantage is that this system is nearly adiabatic. The disadvantages come from the uncertainty caused by stretch from unsteadiness and the spherical shape. The possible distortion may arise from the influence of the ignition process, the flame instabilities at elevated pressures, or the auto-oxidization of reactants at high preheating temperatures.
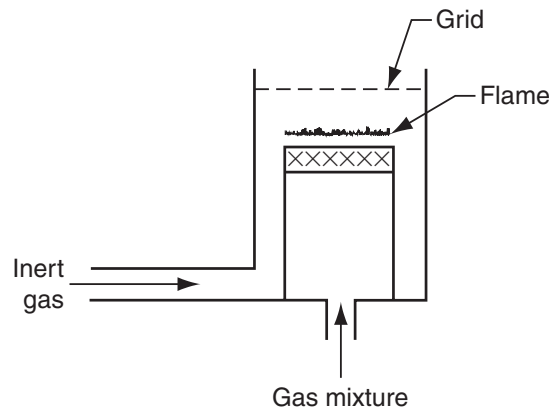
Figure 17 A flat flame burner
(from [85])

The flat flame method is usually attributed to Powling [89] in 1949. Later Botha and Spalding [90] extended it to higher flame speeds by cooling the plug. A premixed planar flame is stabilized through heat loss to the surface of the burner, as illustrated in Figure 17. Then heat loss is varied to determine the flame speed without heat losses by extrapolating

the heat loss rate to zero. The advantage is the nearly zero stretch of the flames. One uncertainty source is the possible depletion of radicals when the flame is too close to the burner surface at higher pressure. Another limitation is that, if the flow rate is high (corresponding to high burning speed), it becomes difficult for the flame to remain flat.
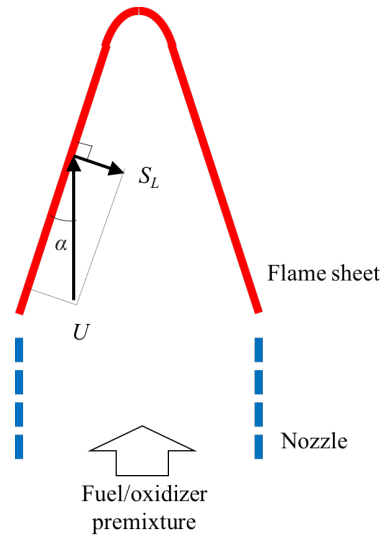
Figure 18 A sketch for a Bunsen flame

The Bunsen flame approach provides one of the simplest examples of a stabilized premixed combustion system. It is employed in this study. The premixed flame is stabilized on the lip of a Bunsen burner or a slot burner. The flame speed can be determined either using a flame angle approach, or deduced from the total flow rate and the flame area. For the flame angle approach, the flame speed is determined from

$$S_L = U \sin \alpha$$

where U is the local flow velocity , and α is the half cone angle of the flame, as illustrated in Figure 18. This result may depend on the point where α is measured, as α is not a

constant value along the flame surface. In contrast, the flame area method defines an average flame speed over the whole flame surface

$$S_L = \dot{Q}/A$$

where $\dot{Q}$ is the total volumetric flowrate at the nozzle exit, and A is the area of the flame surface. To create a conical flame, usually the nozzle of the burner is contoured to create a nearly uniform velocity profile at the nozzle exit. Bunsen flames can stabilize themselves by adjusting the shape (e.g. cone angle) of the flame sheet within the proper range of flowrate, therefore, this method is more robust regarding the range of burning velocity being measured, compared to the flat flame method. The disadvantages, however, are the stretch effects due to the non-flat flame shape. Such effects are especially significant near the flame tip, though they generally exist due to azimuthal curvature. The heat loss to the burner lip also contributes to uncertainty. Another source of uncertainty is the discrepancies of the boundaries detected by different imaging techniques, such as schlieren, PLIF, chemiluminescence and shadowgraph.

2.2. Stabilization of non-premixed jet flames

2.2.1 Classical non-premixed jet flames

Traditionally, the study of non-premixed jet flames, either lifted or burner stabilized, is a central topic in combustion research. The following review focusses on the lifted flames for future comparison with the dynamics at autoignitive conditions, which is relevant when explosive ozonolysis reactions play dominant roles. The utilization of a lifted jet flame reduces the damage to nozzle material by minimizing contact between the flame and nozzle, which leads to practical applications, like burners in commercial boilers. The mechanisms that control the liftoff, stabilization and blowout have been investigated extensively.

For the laminar case, the triple flame (also known as tribrachial flame) has been generally accepted as the stabilization structure of the lifted jet flame. It is a composite flame of a rich premixed flame, a lean premixed flame and a diffusion flame, all trailing from the tribrachial point. Such a flame structure was initially observed in layered CH_4/air systems by Phillips [91] in 1965, as illustrated in Figure 19. Decades later, Chung and Lee [92] noticed its relation with the lifted non-premixed flame, and confirmed the existence of triple flames in laminar lifted flames, as illustrated in Figure 20. The stabilization has been explained based on the balance between the propagation speed of the tribrachial flame edge and local flow velocity [92, 93]. Chung and his colleagues [92, 93] also theoretically showed that for fuels with Schmidt number, Sc, smaller than 1, the lifted flame is not physically realistic (not stable). This is consistent with the experimental observation that for CH_4 (Sc = 0.7), the flame blowout directly without a lifted flame was observed [92].

33
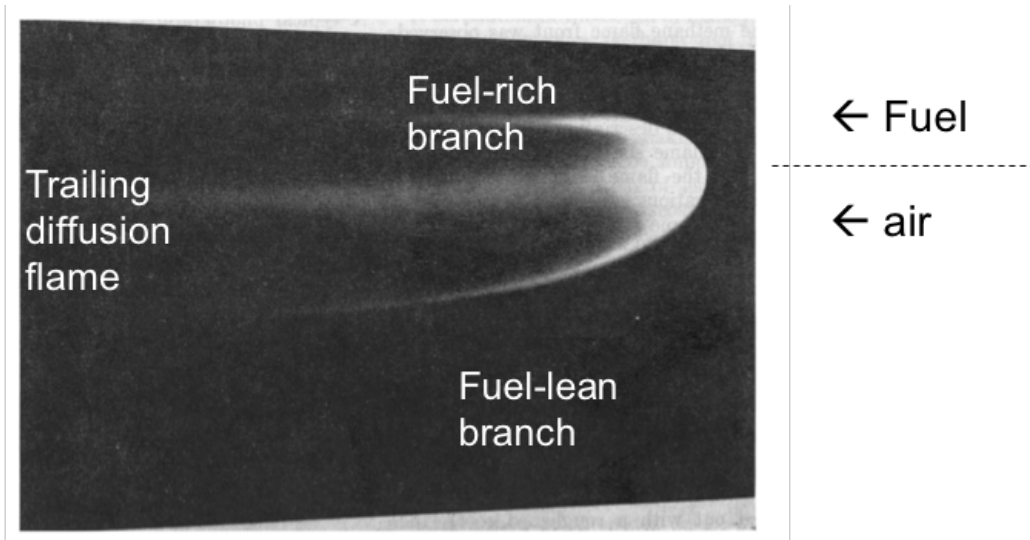
Figure 19 Stabilized triple layer flame

(reproduced from Ref. [91])
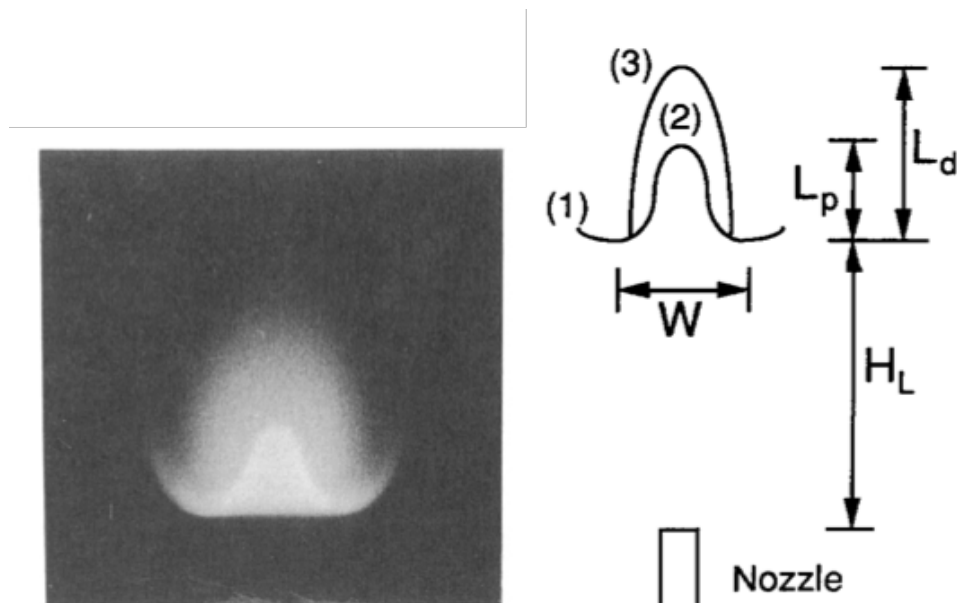
Figure 20 Triple flame structure of a lifted laminar non-premixed flame

(reproduced from Ref. [92])

The effects of heat release were investigated by Ruetsh [94]. They emphasized that

the streamline in front of the flame front is redirected and consequently the effective flow

34

velocities are decreased. This mechanism further stabilizes the flame, which is absent in planar flames. Boulanger *et al*. [95] further studied this issue using Direct Numerical Simulation (DNS) for a round lifted jet diffusion flame, and concluded that the as flow deflection is induced by heat release, the flame is stabilized much closer to the burner than expected. The effects of dilution and exit velocities are studied as well [96]. For the transition region from the laminar to the turbulent case, the liftoff height increased with the exit velocity, while for laminar and well-developed turbulent cases, a inverse relation was reported. More recently, the effects of coflow on flame liftoff height, reattachment and blowout have been predicted using an approximation solution [97].

While the laminar non-premixed jet flames are successfully analyzed using the triple flame concept, many theories are proposed for the turbulent case, and it seems a definitive one is still not in hand. Primarily there are three categories of theories, as reviewed by Pitts [98], Lyons [99] and Lawn [100]:

1. The partially premixed model. This stabilization mechanism was proposed by Vanquickenborne and van Tiggelen [101] in 1966. The fluid at the flame base is assumed to be premixed, then the flame is stabilized as a result of the balance between the local turbulent burning velocity and the local jet velocity. The lack of the consideration of the large eddy structures in the jet and the intermittency of the turbulence limit the validity of this model [98], but it seems to be adequate when the jet velocity is high enough to lift the flame to a height greater than about 40 jet radii [102]. Attempts have been made to model the burning velocity using turbulence intensity [103], where a positive relation between burning velocity and turbulence intensity is assumed. The concept of edge flames is also applied to determine the flame propagation speed at the liftoff flame base [104]. Edge

flames stabilize themselves by decelerating the oncoming flow due to the divergence of streamlines, as reviewed by Buckmaster [105]. Upatnieks *et al.* [106] have reported PIV measurement results supporting the edge flames approach. They found little correlation of the turbulent burning velocity with turbulence intensity or the passage of eddies.

2. The extinction model. Peters and Williams [107] developed the idea that the extinction of laminar diffusion flamelets by flame stretching determines the flame front. However, later Bray and Peters [108] found that the scalar dissipation rate at the liftoff heights is much smaller than the critical value for quenching. Schefer *et al.* also concluded that the primary factor controlling flame stability is not the scalar dissipation based on their imaging measurement [109]. However, even if the stretch effects are not sufficient for quenching, they still may affect the rate of combustion. Local extinction or stretching may decrease the overall rate of propagation [100].

3. The large eddy model. Broadwell *et al.* [110] emphasized the importance of large eddies. They predicted blowoff velocity using the ratio of timescale of the mixing of re-entrained hot products into fresh reactants and timescale of chemical reaction. Miake-Lye and Hammer [111] assumed that at the lifted flame height, the large-scale strain rate must be below its critical value thus determining the stability. Based on this, they proposed a linear relation between the liftoff height and the jet exit velocity.

These theories are not necessarily exclusive. For example, Kelman *et al.* [112] proposed that the stabilization mechanism is a combination of premixed propagation and extinction due to the interaction of large scale turbulent structures. The large scale structures are assumed to cause extinction by drawing ambient air in and convecting the

reaction zone downstream. More recently, Su *et al.* [113] conducted simultaneous planar laser induced fluorescence (PLIF) and particle image velocimetry (PIV). The results are more consistent with the partial premixing than the quenching model. But the large-scale structures seem to be important, and a stabilization mechanism is proposed, as shown in Figure 21 and Figure 22.
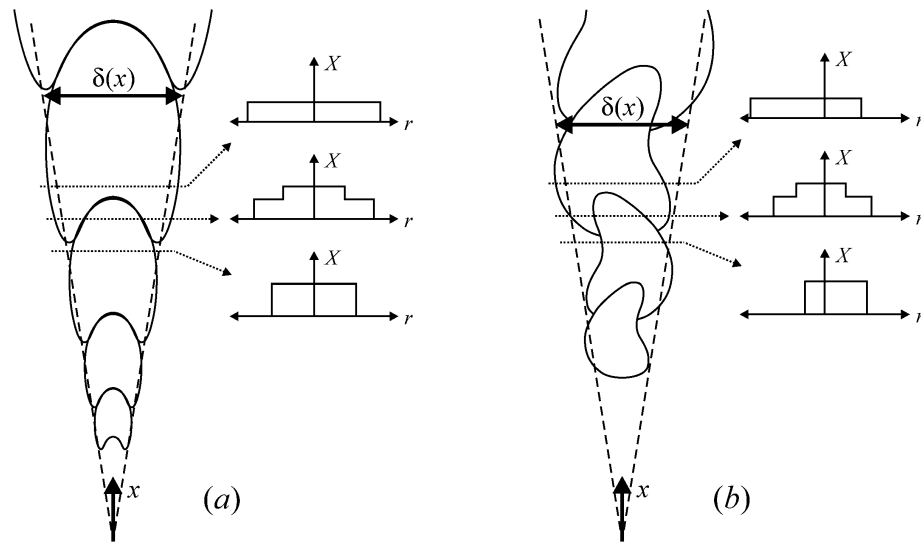
Figure 21 The (a) axisymmetric and (b) helical mode of jet large scale structure.
(from [113])
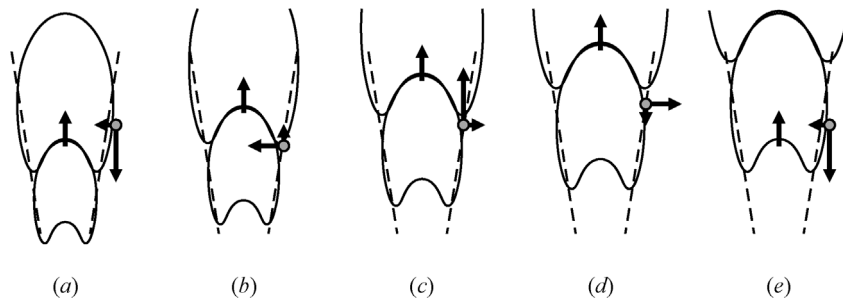
Figure 22 Lifted flame stabilized in large scale structures
(from [113]. Time advances from left to right. The instantaneous stabilization point is represented by a gray circle)

2.2.2 Non-premixed jet flames at autoignitive condition

Autoignition plays an important role when the jet is heated to sufficiently high temperature. However, investigations with autoignition have mostly concentrated on uniform mixtures. For autoignition in non-uniform mixtures, the counterflow configuration is dominant in the early years. Then, the study of jet-in-hot-coflow flames attracted attention, motivated by clean combustion techniques such as MILD (moderate and intense low-oxygen dilution) combustion. In addition, these conditions are related to the recirculation zones in practical engines. For such flames, the autoignitive conditions are created by the high temperature of the coflow. The studies at autoignitive conditions are reviewed as they are related to the autoignitive conditions induced by ozonolysis reactions, which is one of the topics of this dissertation.

For turbulent jet-in-hot-coflow flames , Dally *et al*. [114] used a Jet in Hot Coflow (JHC) burner, where the hot coflow (oxidizer) was produced by a secondary burner and the center jet (fuel) is a mixture of H_2 and CH_4. Although the coflow temperature is 1300 K, no autoignition events are observed. They observed that the flame temperature and the levels of CO, NO and OH are substantially lowered when the coflow is further diluted. In the same year, Cabra *et al*. [115] reported their results from a vitiated coflow burner. The diluted H_2 jet was surrounded by the coflow of hot combustion products from a lean premixed flame (vitiated coflow, temperature above 1000 K). Their instantaneous scalar measurements suggested that a thickened turbulent partially premixed flame exists at the flame base. Though autoignition events were not observed below the liftoff height, they suggested that autoignition or the ignition introduced by turbulent mixing of products and reactants may contribute to the stabilization of the flame. Later, Markides and Mastorakos

[116] experimentally investigated the autoignition behavior of a hydrogen jet in coflow of heated air (up to 1015 K) at atmospheric pressures. Random occurrence of autoignition kernels was observed and the probability density function was measured for the axial location. Large uncertainty existed, as illustrated in Figure 23. Gordon applied the vitiated burner previously used by Cabra *et al*. [115], and simultaneously measured temperature via Rayleigh scattering, OH and CH_2O LIF. The images are classified in three categories: i) CH_2O only, ii) ignition kernels, and iii) liftoff flames. Type i) and ii) dominate the upstream of the jet, while type iii) dominates the downstream part after the stabilization height. CH_2O peaks prior to the autoignition and then decays after ignition, and OH is found to peak at ignition. This sequence is analogous to the evolution of autoignition. Oldenhof *et al*. [117] used the Delft JHC burner, where the center jet is natural gas, and the hot coflow is 1460~1540 K. In contrast to the conventional one in cold coflow, which produces a sharp interface, ignition kernels are continuously being formed near the flame base of the jet flames in hot coflow, as illustrated in Figure 24. This ignition frequency increases with the coflow temperature. Furthermore, a non-monotonic relation between the Reynolds number and the location where ignition first occurs is reported. These observations indicate the flame base in hot coflow behaves fundamentally different with the lifted jet flame in a cold coflow. Later Oldenhof *et al*. [118] further investigated the role of entrainment of the hot coflow in the stabilization of such flames, and emphasized the dominant role of autoignition as the stabilization mechanism. With the development of computational diagnostic techniques [119-124], more feasible tools have become available to analyze the flame dynamics. For example, chemical explosive mode analysis (CEMA)

[119] has identified autoignition as the dominant stabilization mechanism for jet flames in hot co-flow.
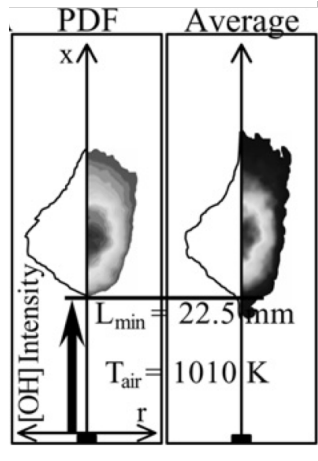
Figure 23 PDFs of autoignition location and average OH chemiluminescence.

(from [116])
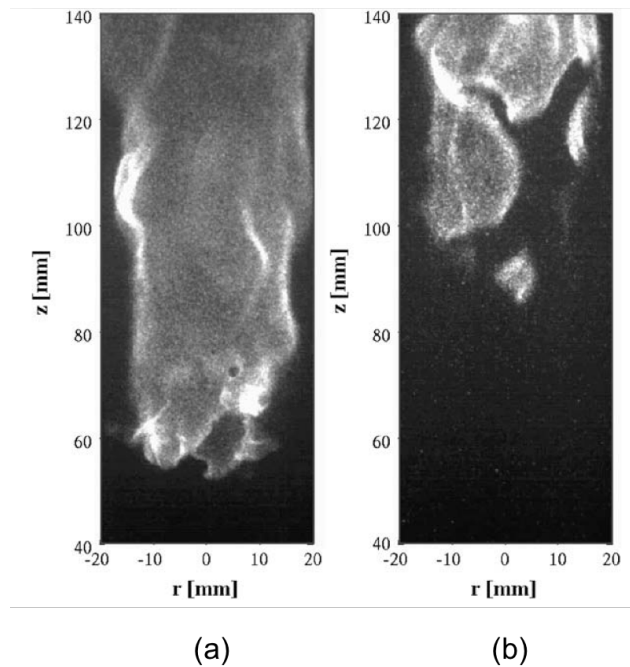
Figure 24 Non-premixed jet flame in (a) cold coflow and (b) hot coflow.

(from [117])

To focus on the autoignition events shortly after the injection of fuel, rather than the burning flames, pulsed fuel injection is applied. Due to the discontinuous supply of fuel, autoignition events are easily to be observed. Meier *et al*. [125] designed a new vitiated coflow burner, but the fuel jet is pulsed and the injection frequency is on the order of 1 Hz. Autoignition was observed to occur at the periphery of the CH_4 jet, and multiple autoignition kernels ("islands") can appear nearly simultaneously. As a continuation of this work, Arndt *et al*. [126] conducted more detailed measurements. The histogram of the detected autoignition heights are presented and the variance is on the same scale as the mean value, similar to [116], indicating large uncertainty. Simultaneously formed autoignition kernels are observed merging rapidly to a connected flame sheet. Furthermore, the autoignition kernels were observed frequently below the flame base, as illustrated in Figure 25, indicating that the lifted jet flame is stabilized by autoignition. Later Arndt *et al*. [127] further investigated the influence of temperature, by varying the coflow temperature between 1566 and 1810 K. They showed that the autoignition delay decreases as temperature increases, as expected.
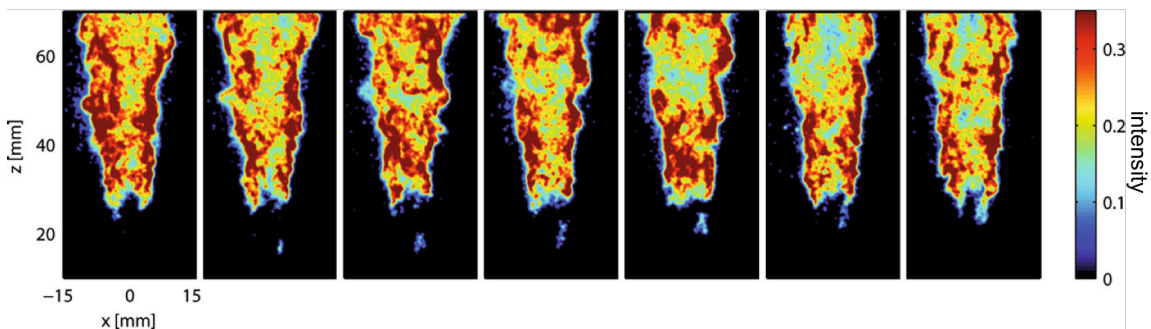
Figure 25 OH* chemiluminescence image of the formation of autoignition kernels below the flame base

(from [126])

41

For laminar cases, the studies of the lifted non-premixed jets in hot coflow have emerged in recent years. Choi *et al*. [128] experimentally studied such flames using diluted propane (Sc > 1) as the fuel jet in 2009. They found that when the initial temperature is below 860 K, typical tribrachial structures are observed. For the temperature above 860 K, the jet was autoignited. For this case, tribrachial edge structure is not observed if the fuel is excessively diluted, and instead, a mild combustion zone is observed. For the autoignited flame with tribrachial edge, autoignition and extinction are repetitively observed at critical conditions. For all cases, the liftoff height has a positive relation with exit velocity, though the nonlinearity depends on the specific conditions. Later, Choi and Chung [129] repeated the experiment for different fuels with Sc smaller than 1 (CH_4, C_2H_4 and C_2H_6) and one greater than 1 (n-C_4H_{10}). Similar to previous work [128], they observed autoignited lifted flames with tribrachial edge or mild combustion at high initial temperatures. The important observation is that such lifted non-premixed jet flames exist regardless of the Sc of fuel, as shown in Figure 26. In contrast, for cold coflow, lifted non-premixed jet flames can only stabilize for the fuel with Sc>1. This implies a fundamentally different stabilization mechanism. They concluded that the adiabatic ignition delay time plays a crucial role in stabilization. They further investigated such flames using a mixture of CH_4 and H_2 as the fuel. The addition of H_2 allows the lifted CH_4 flame to be stabilized at lower coflow temperature. An interesting observation is that the liftoff height increases with jet velocity for higher initial temperature, but decreases as the jet velocity increases. Further investigations are necessary to explain this. More recently, Deng *et al*. [130, 131] studied the case for Dimethyl ether (DME), which features NTC (negative temperature coefficient) chemistry. They concluded that at 700-900 K, autoignition was the dominant stabilization

mechanism, while at 1100 K the kinematic balance between the flame propagation and flow velocity stabilize the flame.
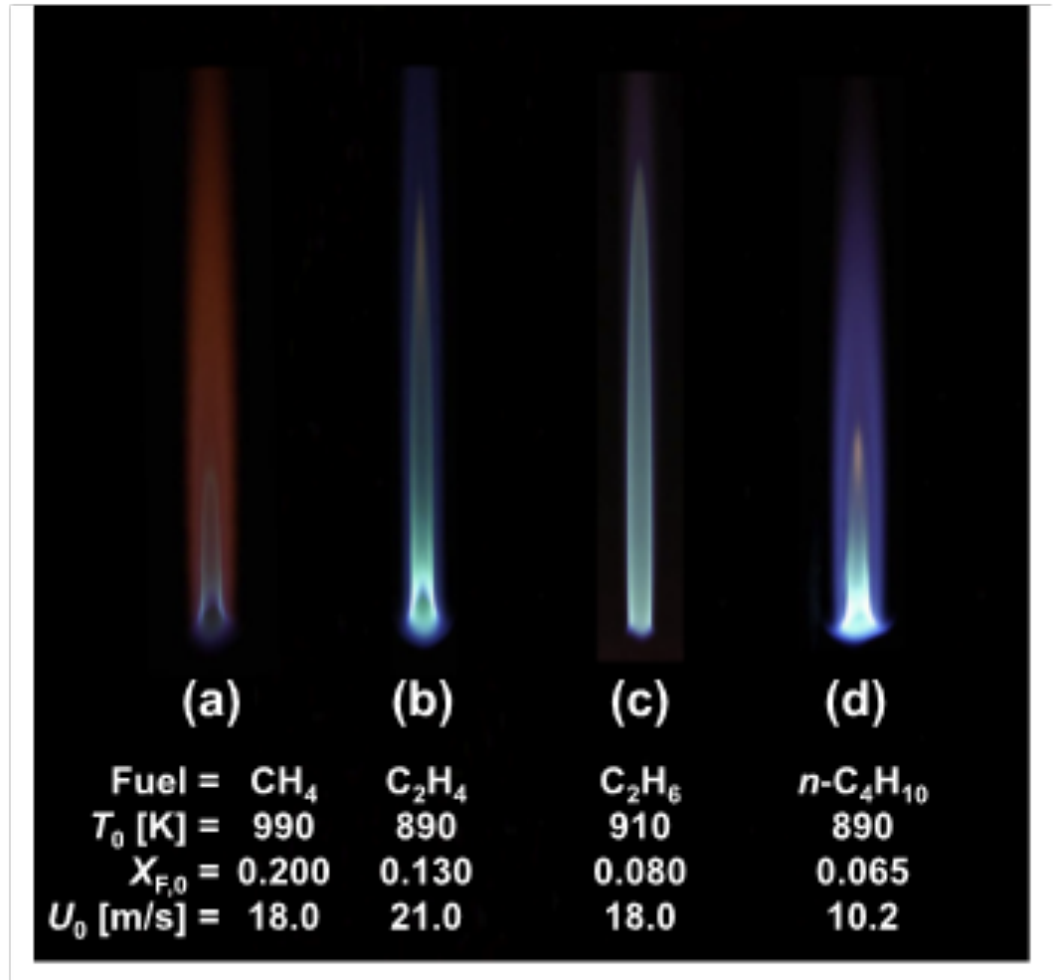
Figure 26 Lifted non-premixed flames at autoignitive conditions.

(from [129])

The transient process from ignition kernel to the fully burning state was also investigated. Ko and Chung [132] ignited free jets of CH_4 with a Nd:YAG laser and measured the propagation speed of the laminar tribrachial flame. This value is found to be correlated with flame curvature and mixture fraction gradient, and estimated to be 1.5-2

times the corresponding stoichiometric laminar flame speed ($S_{\mathrm{L,st}}$). For the turbulent case, Ahmed and Mastorakos [133] estimated the average propagation speed of the edge flame after spark ignition and found that the speeds are 3 to 6 times $S_{\mathrm{L,st}}$. In the case of turbulent flame initiation due to autoignition in high temperature air co-flow, as in reference [134], the averaged flame propagation velocities during the transient process are reported to be 0.5 to 1.2 times $S_{L,st}$. Concerning the ignition of non-premixed turbulent flames, a comprehensive review can be found in [135].

CHAPTER 3

METHODOLOGY

3.1. Chemiluminescence

Optical diagnostics techniques are one desired technique in analyzing of combustion system. Generally, the sensors do not need to experience the harsh environment inside the combustor. Furthermore, such methods are non-intrusive and usually the sensors can respond quickly. These features are important for the collection of high resolution and reliable data in combustion systems.

Chemiluminescence measurement is one popular optical diagnostics technique, and is employed in this study. It collects the light emitted from electronically excited species, which are produced by chemical reactions. There is no need for external illumination. As species differ in their emission spectra, filters can be applied to control which species, or emission sources, are investigated.

3.1.1   OH* and CH* chemiluminescence

OH* and CH* are common species whose chemiluminescence is measured in hydrocarbon combustion. They are narrow band emitters, as illustrated in Figure 27 for a typical CH_4/air flame [136]. One can observe that the emission from OH* is centered near 308 nm, and for CH* it is centered near 431 nm. Their emission intensity in hydrocarbon flames can be used to observe the location of the primary combustion region. They have been used for identification of the reaction zone [136], as a marker of heat release rate [137], and to measure flame equivalence ratios [138]. A more recent work is done by

Guiberti et al. [139]. Chemiluminescence signals from OH*, CH* and CO_2* are measured experimentally from a conical CH_4/air flame diluted with CO_2 or N_2. Measured intensities agree reasonably with the results from a 1D premixed flame simulation using the Lindstedt detailed chemistry mechanism [140] extended with sub-mechanisms for the chemistry of OH∗ and CH∗ [141].
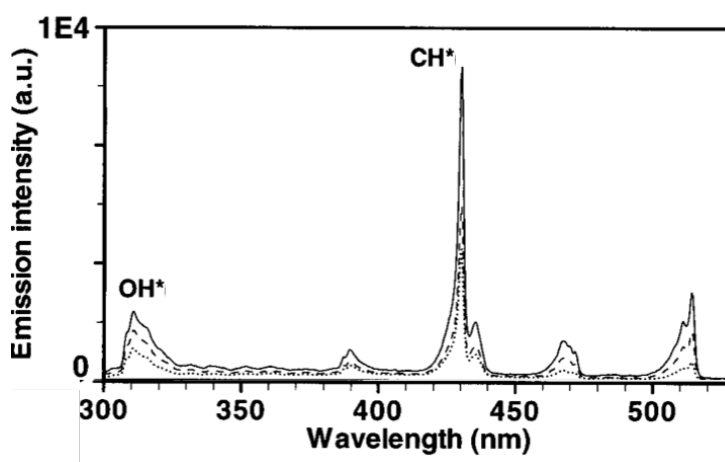
Figure 27 Chemiluminescence spetrum of a CH_4/air flame
(reproduced from [136])

3.1.2 CH_2O* chemiluminescence

In the present work, CH_2O (formaldehyde) is expected to be produced by the ozonolysis reactions of C_2H_4 and exist primarily at low temperature (<1000 K). Therefore, the detection of this species using chemiluminescence can provide a tool to visualize the region where ozonolysis reactions are significant. The spectra of CH_2O* have been measured in previous works [142-144]. Generally, its signal covers a wide range of wavelengths, significant in range from 400 to 450 nm and centering near 430 nm.
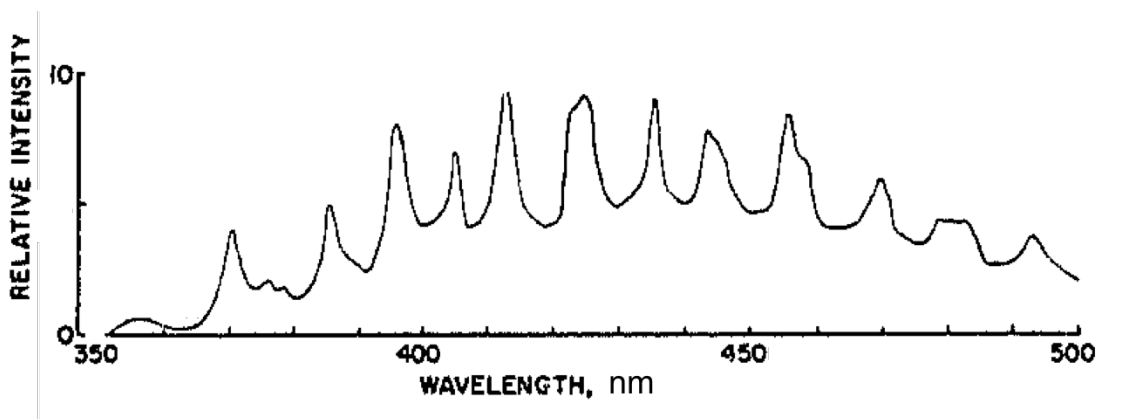
Figure 28 Chemiluminescence emisson from acetaldehyde cool flame
(reproduced from [142]. the primary emission source is CH_2O^*)

Sheinson and Williams [142] obtained a resolved chemiluminescence spectra from cool flames using acetaldehyde and n-butane as fuels. The temperature of the cool flame reaction zone is very low (200-400 °C). The spectra for acetaldehyde cool flame is shown in Figure 28, where the primary emission source is CH_2O^*. It is observed that the emissions of CH_2O^* are centered near 430 nm. They considered other possible emission sources such as CO^* and radicals (CH^*, C_2^*, OH^*, and HCO^*), and concluded that, at such conditions, none of them is significant. Particularly, CH emissions, which also centers near 430 nm, only become comparable with CH_2O^* signal at higher temperature (400-800 °C). In the same year, Toby [143] investigated the chemiluminescence from the reaction between O_3 and allene. They concluded that the obtained spectra is from the produced CH_2O^*. It is qualitatively similar to the one shown in Figure 28, and also shows high intensity near 430 nm. Later Bogan *et al*. [144] observed a similar chemiluminescence spectra from the reaction of ethyl vinyl ether and $O_2(a^1\Delta g)$, which produces CH_2O^*. This spectrum also features high intensity near 430 nm. CH_2O chemiluminescence intensity was measured by Deng *et al* [145] in a DME diffusion flame in a counter-flow burner. A filter centered at

400 nm is used to capture the corresponding chemiluminescence. CH_2O^* is expected to be observed at low-temperature flame. Due to the weak intensity at such condition, a photomultiplier tube is used. The trends of the measured CH_2O^* chemiluminescence intensity is consistent with the calculated maximum CH_2O^* mole fraction. This signal is used to indicate the production of CH_2O^* and as an indicator of the low-temperature chemistry.

Although both CH_2O^* and CH^* chemiluminescence spectrum are centered near 430 nm, it is still possible to distinguish them. CH_2O^* is a low-temperature species while CH^* is a high-temperature species. For example, Sheinson and Williams [142] concluded that in their chemiluminescence measurement of cool flames, CH_2O^* is the primary emission source and CH^* is negligible.

3.2. Experimental setup and procedure

In this study, two premixed burners are employed to measure S_L: a high-pressure Bunsen flame facility [146-148] and a low-temperature system [148]. In addition, a non-premixed coflow burner [149] is employed.

3.2.1 High-pressure Bunsen burner

The high-pressure facility was built in the Ben T. Zinn Combustion Laboratory at Georgia Institute of Technology. It has been validated and documented in previous studies [146, 147]. In this study, this facility is coupled with equipment to generate and monitor O_3, as illustrated in Figure 29. Oxygen (O_2 99.994% purity from Airgas) flowed through an O_3 generator (Ozone Solutions, TG-40) and was partially converted to O_3. It was confirmed by thermocouple measurement that this ozonization process did not change the

temperature of the flow. An O_3 monitor (Teledyne Instruments, Model 454) was connected downstream of the O_3 generator to measure O_3 concentration. The fuel, O_2, and N_2 streams were mixed before entering the burner. The source of the uncertainties in the S_L measurement include uncertainties in flow rate measurements of the reactants, the reaction zone area [146] and O_3 concentration (±130 ppm).
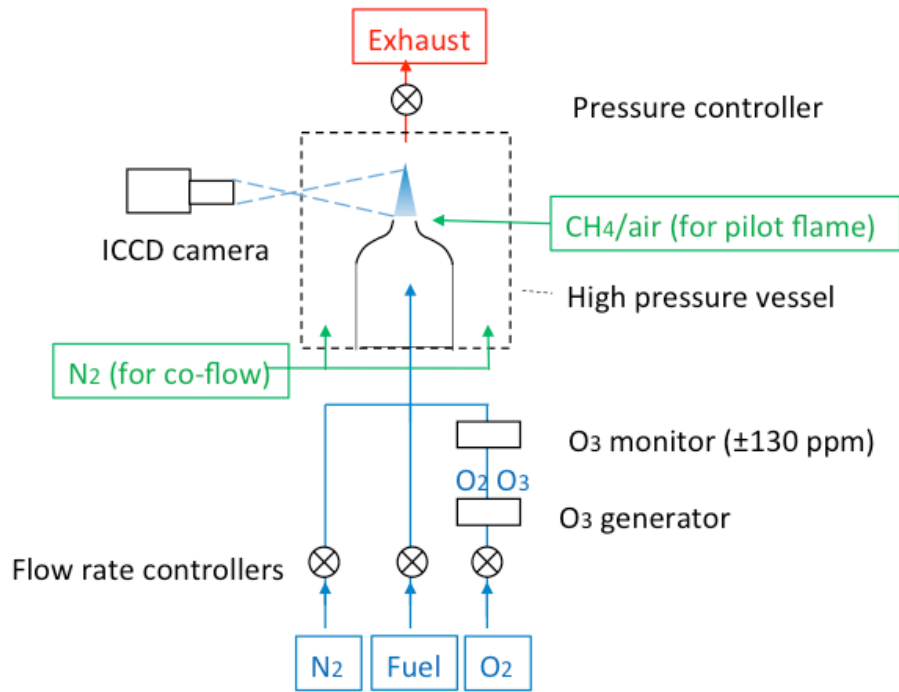
Figure 29 Experimental setup for flame speed measurement at elevated pressures

S_L is calculated using the flame area method discussed in Section 2.1.3. The flame area is estimated from the flame chemiluminescence image, using a gradient-based algorithm to detect the flame edge [146-148].

As the measured inlet temperature T_{expt} may differ from the desired value T_0 (difference $<$ 15K), the total volumetric reactants flow rate $\dot{Q}$ is converted from the measured total volumetric flow rate $\dot{Q}_{expt}$

$$\dot{Q} = \frac{T_0}{T_{expt}}\dot{Q}_{expt}$$

The reported value is the average of values measured in such way from 50 frames taken at the same condition, and the standard error is reported using the error bar.

3.2.2 Low-temperature Bunsen burner

The low-temperature system is employed to freeze the ozonolysis of C_2H_4 to provide experimental results with clear boundary conditions. Axisymmetric Bunsen flames are produced with a contoured laminar nozzle at atmospheric pressure, as shown in Figure 30. The burner and the reactants are cooled by liquid N_2, and the temperature is monitored by a Fluke 52 II thermometer and an E-type thermocouple. In the present work, the temperature was maintained at 200±10 K. The reactant streams of C_2H_4/N_2 and $O_2/O_3/N_2$ are separately provided from two inlets to ensure that the mixing process and potential ozonolysis reaction are restricted within the burner. The flow rate for each species is controlled using a combination of a sonic nozzle (O'Keefe Controls Co.) and a pressure regulator. The sonic nozzle creates choked flow given sufficiently high pressure upstream. Then the mass flow rate is controlled by adjusting the upstream pressure using a pressure regulator. The uncertainty in flow rate is estimated to be 1%. The internal volume of burner is minimized to decrease the residence time. Simulations were conducted using the CHEMKIN [150] plug-flow reactor model with USC Mech II [151] combining a C_2H_4

ozonolysis mechanism [22] to estimate the O_3 loss due to ozonolysis. According to the simulation results, less than 10% of O_3 would be consumed in the mixing process at the experimental conditions. As with the high-pressure experiments, pure O_2 was partially ozonized by the O_3 generator, combined with N_2, and then flowed through the O_3 monitor before entering the burner.
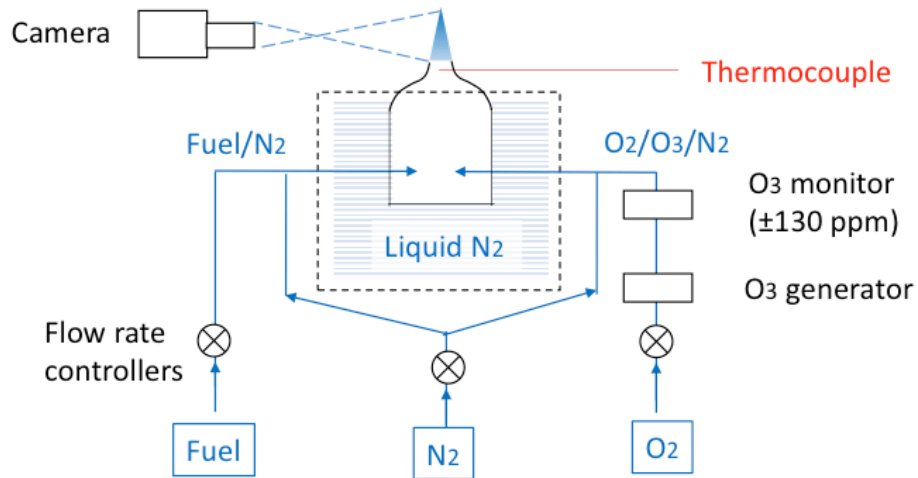
Figure 30 Experimental setup for flame speed measurement at low temperatures

During the experiment, the reactants are flowing through the burner, which is immersed in the liquid N_2. The temperature is measured at the exit of the nozzle by a Fluke 52 II thermometer and an E-type thermocouple. When the temperature at the nozzle exit reaches the desired temperature at steady state, the flame is initiated using a lighter. Then S_L is measured using flame area method.

3.2.3   Non-premixed burners

The non-premixed co-flow burner is illustrated in Figure 31. The fuel (C_2H_4) is the center jet and the oxidizer ($O_2/O_3/N_2$) is the coflow jet. The exit of the nozzle tube

supplying the fuel has an outer diameter (OD) of 0.317 cm, and inner diameter (ID) of 0.178 cm. To block the dilution effects of the ambient air, the reactants jets are surrounded by a quartz tube, which has a length of 30 cm, ID of 0.787 cm and OD of 1.27 cm. N_2, O_2 (99.994% purity), and C_2H_4 are sent through a bank of calibrated flow controllers. Same as the previous section, such flow controller is a combination of sonic nozzle and a pressure valve. O_2 is sent through an O_3 generator (Ozone Solutions, TG-40, during data acquisition the fluctuation of O_3 concentration is within 2.5%) to be partially ozonized. An O_3 monitor (Teledyne Instruments, Model 454, accuracy ±130 ppm) is connected downstream of the O_3 generator to measure O_3 concentration. N_2, O_2, and O_3 are mixed (as the oxidizer stream) and sent to the burner. A high-frame-rate camera (NAC, Memrecam GX-3) is used to record the intensity of the chemiluminescence from the flames. The chemiluminescence at a specific range of wavelength is also recorded with an intensifier (Lambert Instruments, HiCATT) and an optical bandpass filter centered at 430 nm to capture the chemiluminescence from CH* and CH_2O^*.
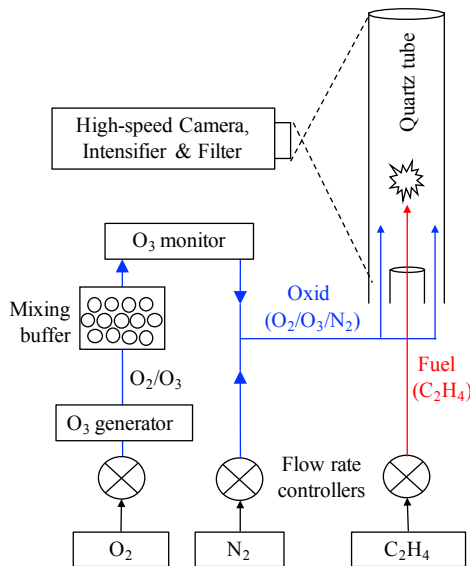
Figure 31. Schematic of the experimental setup.

52

The experiments are conducted at room temperature (~300 K) and pressure (~1 atm) conditions. The O_3 generator applies a high-voltage pulse (5k-30k Hz) to convert O_2 to O_3. To minimize this unsteadiness effect, a mixing buffer is added between the O_3 generator and the O_3 monitor. This stainless-steel buffer has a volume of approximately 0.3 liter and is full of glass beads (diameter of 6.35 mm) to let O_2/O_3 be well mixed before reaching the burner. During the experiment, initially the oxidizer and O_3 generator are turned on but the fuel stream turned off. At least 30 seconds are given to let the generation of O_3 reach steady state. Then, fuel is turned on, and autoignition may occur, which is recorded using the camera. It is observed that certain products from ozonolysis reactions (and its subsequent reactions) are liquid at room temperature and stayed on the wall of the quartz tube. Therefore, after each experiment, the quartz tube was replaced and cleaned. Please note the products from ozonolysis are not clear and still under further investigation.

3.3. CHEMKIN simulation

CHEMKIN [150] provides a package of several programs to perform simulation for the chemistry process in zero- and one-dimensional reactors. As the problems have been simplified, these models and their results are often easier to be interpreted and analyzed. In addition, the simulation cost is much less than running a three-dimensional simulation. Three models: SENKIN, PLUG, and PREMIX are used in the present study and their assumptions are briefly introduced.

3.3.1 SENKIN: Closed homogeneous reactor

SENKIN is a program developed by Lutz *et al* in 1988 [152]. It is designed to predict the time-dependent behavior of chemically reacting gas in a closed homogeneous reactor. It can model the following systems: an adiabatic isobaric system (constant pressure), an

adiabatic isochoric system (constant volume), an adiabatic system with specified volume history, a system of constant pressure and temperature, a system of constant volume and temperature, and a system with specified histories of pressure and temperature. The governing equations include the conservation equations for mass and energy. Initial reactants, temperature and pressure need to be provided as initial conditions.

3.3.2 PLUG: Steady, laminar, 1D Plug-flow reactors

This model was developed by Larson and coworkers in 1996 [153]. It is designed to model steady, laminar plug-flow reactors. The governing equations are the equations of continuity, species, energy, and momentum. It is assumed that there are no variations in the transverse direction, and the axial diffusion is negligible comparing to the convective term. Therefore, the model is 1D and diffusion terms are not considered. The inlet composition, flow rate, and temperature are given as the boundary conditions. By default, the pressure is assumed to be constant along the reactor, but a user-specified pressure profile is also available.

3.3.3 PREMIX: Steady, laminar, 1D premixed flames

This model was developed by Kee and coworkers in 1985 [84]. It is designed to model steady, isobaric, quasi-one-dimensional flame propagation. It can model two types of flames: burner-stabilized and adiabatic freely propagating premixed laminar flames. The governing equations are the equations of continuity, energy, species and state. Unlike the PLUG flow reactor, the diffusion terms are considered.

The boundary conditions are different for the burner-stabilized flames and freely propagating flames. For burner-stabilized flames, the mass flow rate, inlet temperature and

inlet mass flux fractions are known. Gradients are assumed to vanish at the outlet (the hot boundary). For freely propagating flames, the mass flow rate is not known. It is an eigenvalue and needs to be solved. For this purpose, an additional condition is added by fixing the location of the flame by specifying the temperature at one point. By definition, for freely propagating premixed laminar flames, there are no heat losses. Therefore, this point, where the temperature is fixed, should be chosen such that the temperature and species gradients should "nearly" vanish at the cold boundary (inlet) [84]. These assumptions and requirements imply PREMIX should not be applied in cases where the inlet is autoignitive, as it is not steady, and for these cases the zero gradients at the incoming flow boundary is a bad assumption.

3.3.4 Kinetic mechanism

USC Mech II mechanism [151], combined with an O_3 sub-mechanism summarized by Wang *et al.* [63], is used as the kinetic mechanism for the CHEMKIN simulations. Furthermore, several ozonolysis reactions are proposed and added in the kinetic mechanism, adapted from the literature [71, 72].

$$C_2H_4 + O_3 = CH_2O + OH + HCO$$

$$C_2H_4 + O_3 = CH_2O + 2H + CO_2$$

$$C_2H_4 + O_3 = CH_2O + H_2 + CO_2$$

$$C_2H_4 + O_3 = CH_2O + H_2O + CO$$
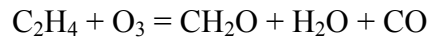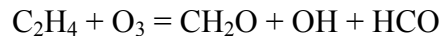
Due to the lack of detailed kinetic information, the branching ratio is assumed to be ¼ for each of these pathways. That is, they are assumed to have the same Arrhenius rates

$$k = Ae^{-E/(RT)}$$

where R is the universal gas constant, T is the temperature, $A = 1.81 \times 10^9$ mole/cm-sec-K is the pre-exponential factor, and $E = 5227$ cal/mole is the activation energy, based on reference [23].

Guiberti. [139] summarized the sub-mechanisms for OH*, CH* and CO_2* [141]. These sub-mechanisms are added to USC Mech II for the discussion of chemiluminescence emitters in Section 6.2.1.

3.4. FLUENT simulation

Comparing to CHEMKIN, FLUENT [154] provides more comprehensive and flexible modeling capacities at the cost of more complexity and higher computational cost. It can model a wide range of incompressible and compressible, laminar and turbulent, steady-state or transient, reacting or non-reacting problems. Therefore, for the simulation corresponding to the non-premixed burner discussed in Chapter 6 and 7, a FLUENT model is used.

3.4.1 Model geometry

The simulation model is corresponding to the non-premixed coflow burner documented in Section 3.2.3. Consistent with this experimental setup, the geometry dimensions and the unstructured grid for the simulation model are illustrated in Figure 32. The number of grid nodes in this model is 35,891. To ensure reasonable accuracy and the maximum node size is less than 1 mm. The model is axisymmetric.
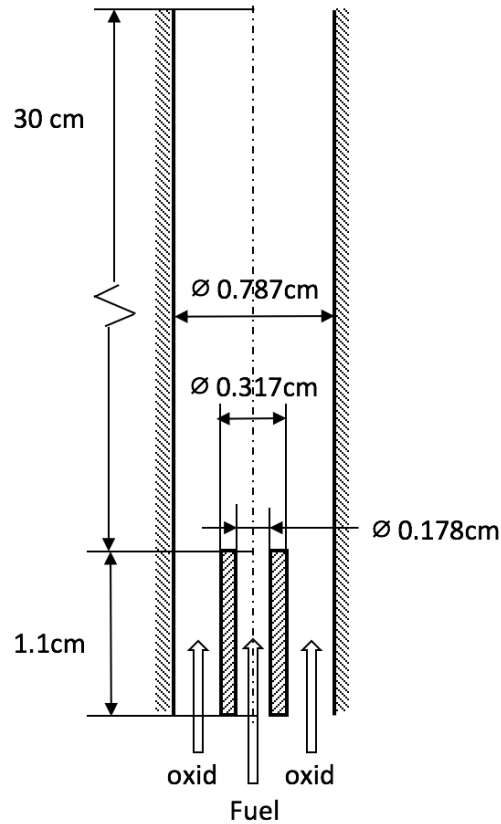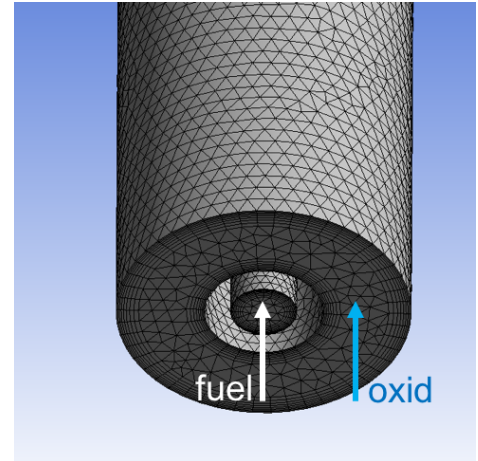
<div align="center">(a) Dimensions   (b) Grid</div>

Figure 32. The gemotry of the 3D FLUENT model for the non-premixed experiment

As for the boundary conditions, the velocity and species at the fuel and oxidizer inlet are fixed. Temperature is fixed at 300 K. For the outlet, a pressure-outlet boundary condition is set. The walls are set to be adiabatic and no-slip.

3.4.1 Chemical model and kinetic mechanism

Chemical process can be modelled using several approaches in FLUENT. For non-premixed combustion, the mixture fraction approach is available. Equations for individual species are not solved but derived from mixture fraction, with help of a look-up table. For

premixed systems, the reaction progress variable is available. However, for the present work, a general finite-rate chemistry approach is used for volumetric reactions. Other reactions such as wall surface reactions, particle surface reactions, and electrochemical reactions are also available but are not be considered in the present work.

Several solvers are available to solve the chemistry process. The one applied in this study is the Stiff Chemistry Solver, which applies a two-step approach. Firstly, the chemistry in each cell is reacted at constant pressure for the given flow time step. Then, the convection and diffusion terms are treated as in a non-reacting flow. This solver enables efficient integration of stiff chemical kinetics. It works with the finite-rate assumption.

Due to the expensive CPU time to run a 3D simulation using a detailed mechanism, a 28-species mechanism, GPS28, is generated using the Global Pathway Selection algorithm (see Appendix) for the fuel and oxidizer mentioned above. This mechanism is reduced from the detailed mechanism introduced in Section 3.3.4. This skeletal mechanism is validated using a homogenous reactor (SENKIN [152]) for the fuel and oxidizer used in the experiment. The fuel is C_2H_4, and the oxidizer is $O_2/O_3/N_2$ mixture. The ratio of nitrogen and oxygen atoms in oxidizer is 0.28, and the mole fraction of O_3 in the oxidizer is 4.1%. Comparison with the detailed mechanism is illustrated for a wide range of ϕ, which corresponds to different mixture fraction (Z) in the non-premixed system. The results are illustrated in Figure 33. The results found using GPS28 agree very well with the detailed mechanism, with its maximum discrepancies at the fuel-rich side. But the error is still within 15%.
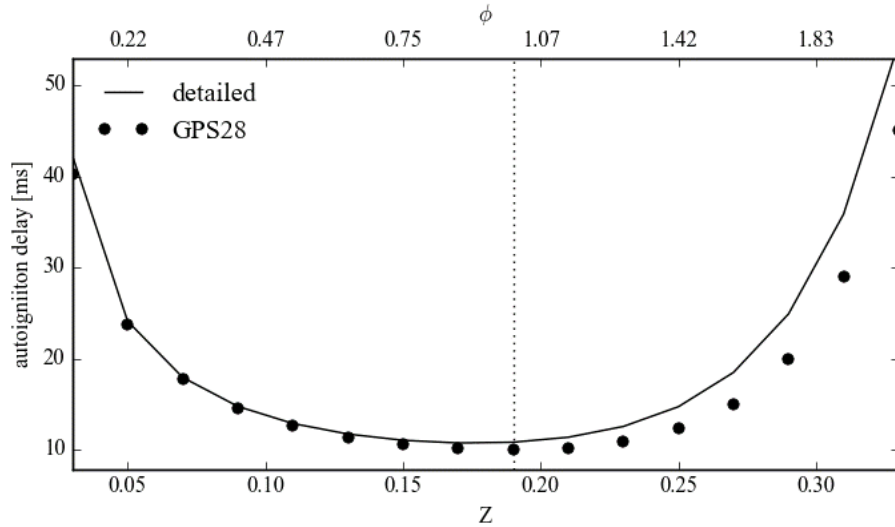
Figure 33. Autoignition delay at different ϕ and Z calculated using the detailed and skeletal mechanism (GPS28)

(Dotted line is $Z = Z_{st}$)

3.4.2   Turbulence models

Turbulent flows are characterized by fluctuating velocity at a wide range of scales in space and time. It is too computationally expensive to simulate directly all of them. To remove such small scales, the instantaneous governing equations can be manipulated (e.g., time-averaged). However, this results in additional unknown variables, and turbulence models are needed to determine these variables. Several models are available in FLUENT, including Reynolds-averaged approaches (e.g., k-ε models and k-ω models) and large eddy simulation (LES).

The simplest model may be a two-equation model: the standard k-ε model, proposed by Launder and Spalding [155]. It is a semi-empirical model based on model transport equations for two important parameters: the turbulent kinetic energy (k) and its dissipation

59

rate (ε). It assumes that the flow is fully turbulent and molecular viscosity is negligible. This model is used in the present work due to its simplicity.

CHAPTER 4 THE EFFECTS OF OZONE ADDITION ON ALKANE FLAME PROPAGATION

4.1   Introduction

The effects of O_3 addition on some small-molecule alkanes fuels, CH_4 and C_3H_8, are investigated using the Bunsen burner described in Section 3.2.1. The ozonolysis reaction of alkanes at room temperature and pressure conditions is typically very slow. Previous kinetic studies indicate that at such conditions the reaction rate constant of the ozonolysis reaction of CH_4 is 0.994 cm^3/mole-s [21] and that for C_3H_8 is 4.93 cm^3/mole-s [156]. So, the ozonolysis of alkanes is generally ignored [63, 157]. It is also confirmed that the O_3 concentration is the same between the O_3 monitor location and burner exit, measured at 300 K using CH_4 and C_3H_8 as the fuel.

4.2   Uncertainty quantification

The uncertainty of flow rate is estimated as $\frac{\sigma_{Q_{fuel}}}{Q_{fuel}} \approx \frac{\sigma_{Q_{oxid}}}{Q_{oxid}} \approx 1\%$. As the equivalence ratio can be written as $\phi = C \frac{Q_{fuel}}{Q_{oxid}}$, where C is a constant depending on the fuel and oxidizer composition. Then, based on propagation of uncertainty, we have

$$\frac{\sigma_\phi}{\phi} = \sqrt{\left(\frac{\sigma_{Q_{fuel}}}{Q_{fuel}}\right)^2 + \left(\frac{\sigma_{Q_{oxid}}}{Q_{oxid}}\right)^2} \approx 1.4\%$$

The uncertainty in measured S_L, $\sigma_{S_{L,\text{with } O_3}}$, is defined as the standard error of 50 samples. The enhancement of S_L is defined as

$$E_{S_L} = \frac{S_{L,\text{with } O_3}}{S_{L,\text{no } O_3}} - 1$$

Therefore, the uncertainty of enhancement can be related to the uncertainty of S_L

$$\frac{\sigma_{E_{S_L}}}{E_{S_L}} = \sqrt{\left(\frac{\sigma_{S_{L,\text{with } O_3}}}{S_{L,\text{with } O_3}}\right)^2 + \left(\frac{\sigma_{S_{L,\text{no } O_3}}}{S_{L,\text{no } O_3}}\right)^2}$$

The uncertainty of the variables mentioned above is presented using error in the following sections.

4.3   The effect at room temperature and atmospheric pressure

The S_L of CH_4/air mixtures was initially measured at atmospheric pressure to validate the experimental setup. As illustrated in Figure 34, the present CH_4 S_L data agree well with archival experimental results [63, 158-160], as well as the computed results. The effect of O_3 addition on S_L of CH_4 and C_3H_8 were then investigated at the same conditions. As shown in Figure 35 and Figure 36, with O_3 addition of 6334 ppm at 1 atm and an initial reactant temperature (T_0) of 300 K, both the CH_4/air and C_3H_8/air S_L increased. This observation is consistent with previous work [53, 61-63, 65]. As illustrated in Figure 35, for the stoichiometric case the simulation predicts the enhancement of CH_4 S_L very well. The experimental result of fractional S_L enhancement is 8.3%, which is very close to the modeling result of 8.7%. However, for off-stoichiometric cases, the simulations overestimate the effect of O_3 addition, especially for fuel-rich cases. For instance, the simulations predict CH_4/air S_L at $\phi = 1.4$ increasing by 16.3% with O_3 addition, while the measured values only show an 8.7% enhancement. When C_3H_8 was used as the fuel, the simulations better match the experiments at all ϕ, but with a tendency to overestimate the effect of O_3 addition. For example, O_3 addition of 6334 ppm (± 160 ppm) increases S_L at ϕ

= 1 by 7.6% in the experiments, which is slightly lower than the prediction of 9.4%. As with CH$_4$, the discrepancy is larger at fuel-rich conditions. The simulation gives an enhancement at ϕ = 1.3 of 10.8%, while experimental results only show an increase of 5.7%. The modest effect of O$_3$ addition on C$_3$H$_8$ S_L at fuel-rich cases is consistent with the work on flame stability by Vu et al. [65], which showed that O$_3$ addition increased C$_3$H$_8$ blowoff velocities (which is strongly tied to flame speed) significantly at stoichiometric and fuel-lean cases but only modestly at fuel-rich conditions.
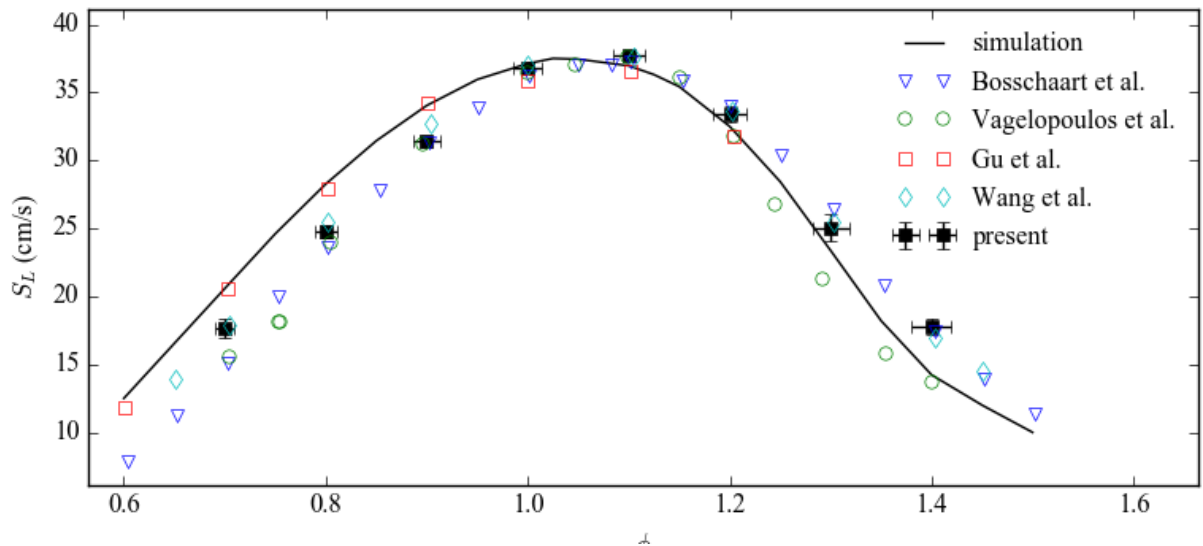
Figure 34 Validation results for the experimental setup using CH$_4$/air at 300 K and 1 atm
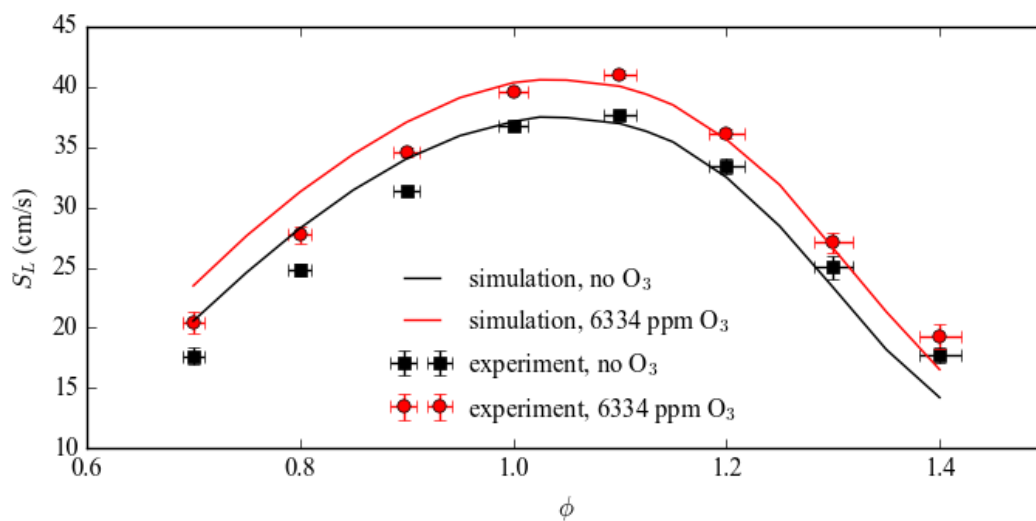
Figure 35 CH$_4$ flame speed with and without O$_3$ addition
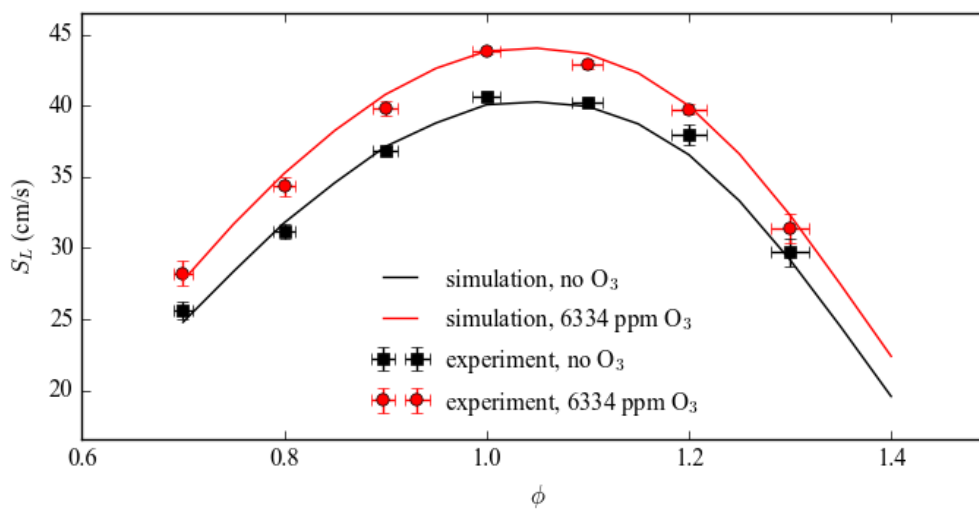
Figure 36 C$_3$H$_8$ flame speed with and without O$_3$ addition
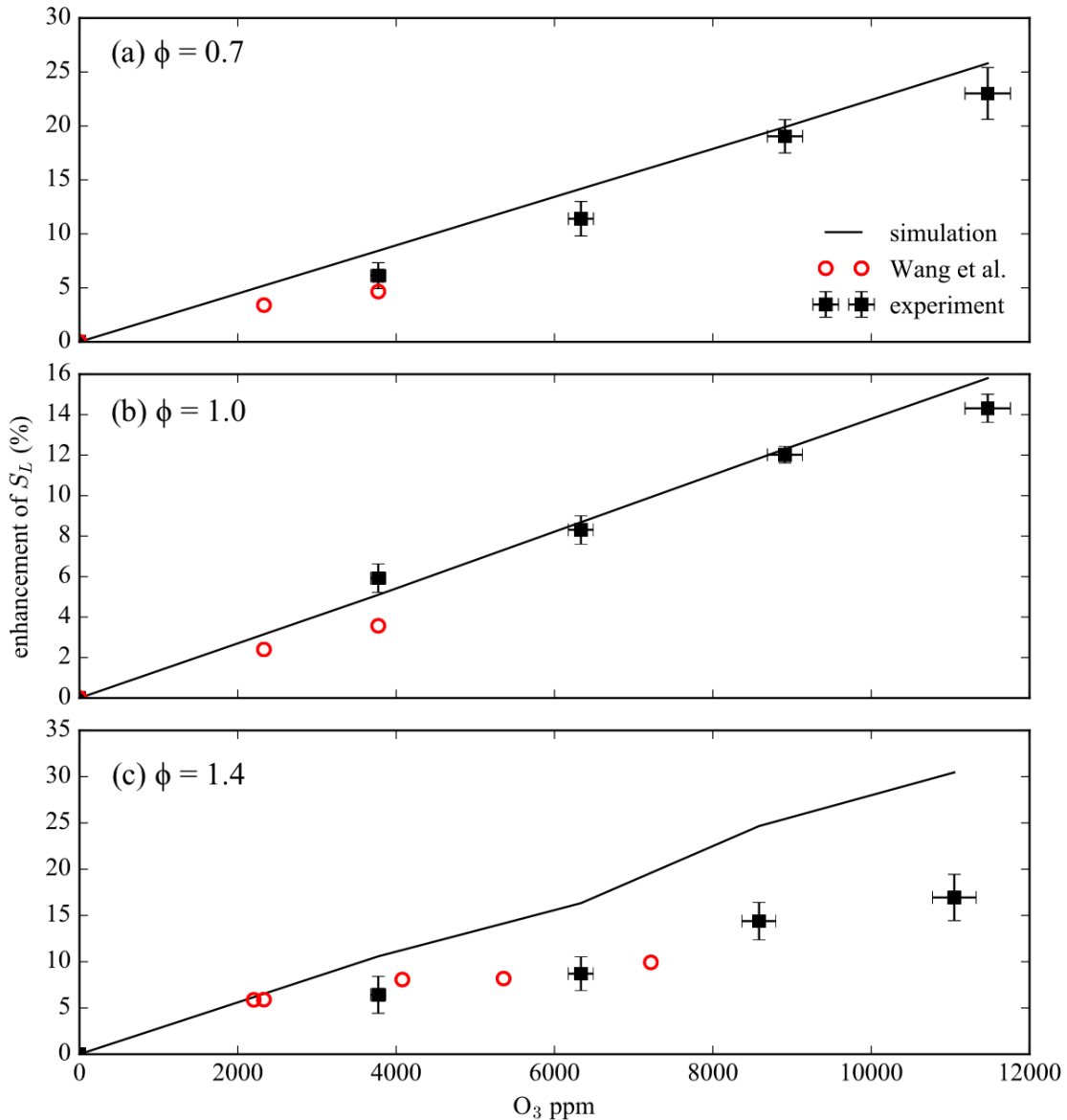
Figure 37 Enhancement of CH$_4$/air flame speed as a function of O$_3$ concentration

The effect of O$_3$ concentration on S_L can be demonstrated by Figure 37. The measured CH$_4$ S_L fractional enhancement has a near-linear relationship with O$_3$ concentration for fuel-lean and stoichiometric cases that is well predicted by the simulations. On average, CH$_4$ S_L increases by 2% per 1000 ppm O$_3$ addition at $\phi = 0.7$ and 1.37% per 1000 ppm O$_3$ addition for $\phi = 1.0$. For fuel-rich cases, however, the measured

enhancement does not increase as fast as the simulation predicts. The higher uncertainties for the non-stoichiometric cases in this figure result from decreased flame stability at these extreme equivalence ratios, and because the absolute S_L is smaller, the fractional uncertainties become larger. Still, the discrepancies between the experiments and simulations suggest a need to improve the kinetic mechanism.
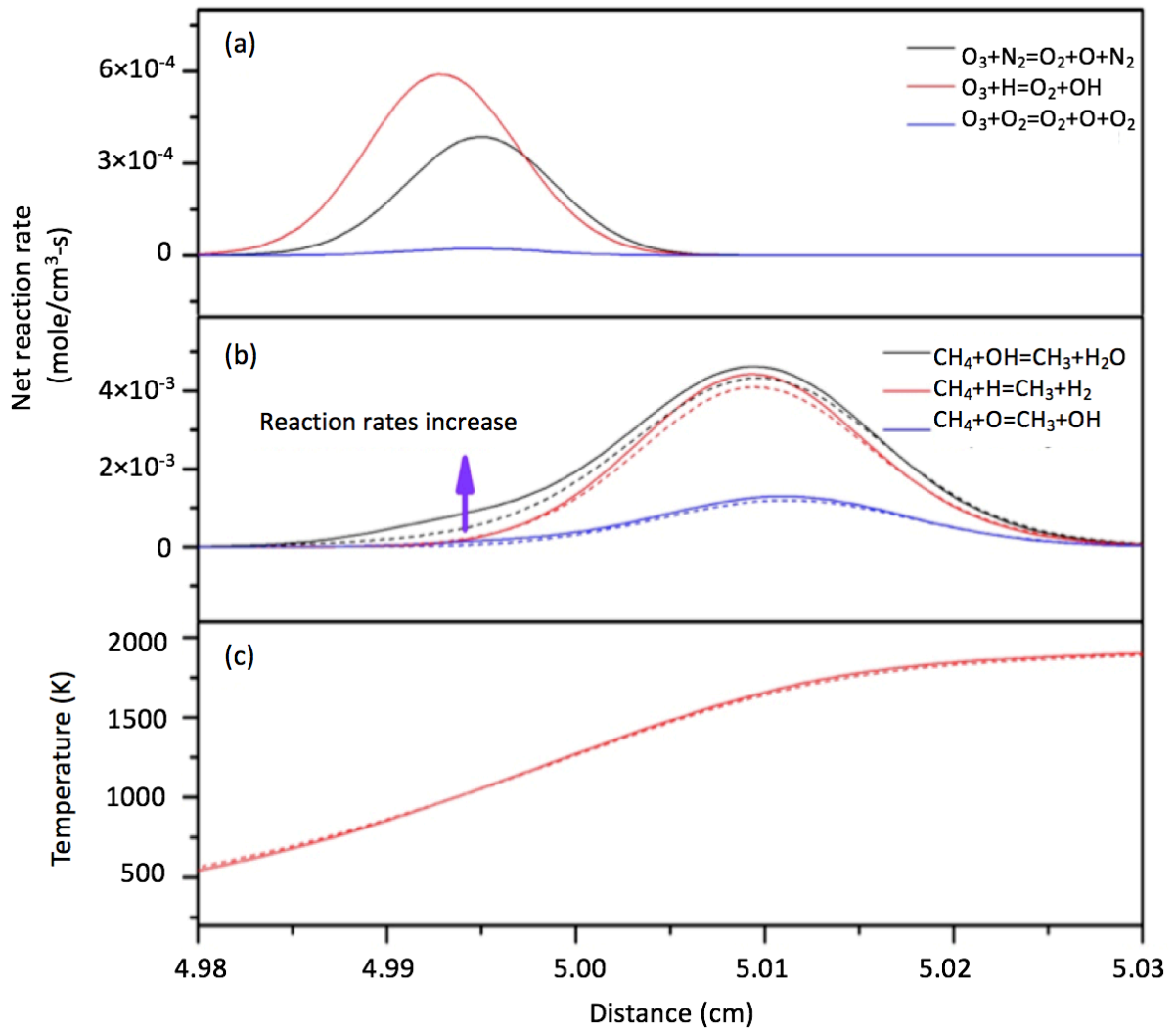
Figure 38 Simulation results for the CH$_4$/air flame with (solid lines) and without (dashed lines) O$_3$ addition. (a) Major O3 consumption pathways. (b) major CH4 consumption pathways. (c) Temperature

For CH$_4$ at 1 atm and 300 K, the enhancement effect of O$_3$ starts with the release of O atoms from O$_3$ decomposition in the preheat zone. Sequentially, O atoms attack fuel molecules [61, 63]. As illustrated in Figure 38(a), the major pathway of O$_3$ decomposition in this study is through the reaction between O$_3$ and N$_2$ in the preheat zone.

$$O_3+N_2=O_2+O+N_2 \qquad\qquad\qquad (R1)$$

The O atoms then react with fuel and produce other radicals such as OH. Consequently, the conversion of CH$_4$ to CH$_3$ is accelerated. For example, as illustrated in Figure 38(b), the net reaction rate of CH$_4$+O=CH$_3$+OH was increased by 10.2% after O$_3$ addition. This accelerated OH production benefits another major CH$_4$ consumption pathway, CH$_4$+OH=CH$_3$+H$_2$O, and increases its net reaction rate by 9.9%. These reactions promote production of CH$_3$ and, consequently, increase its oxidized product, CH$_2$O. The increased concentration of CH$_2$O after O$_3$ addition has been experimentally shown in a recent work [67]. This kinetic effect makes the enhancement higher than the pure thermal effect could achieve. For example, if the energy used to convert O$_2$ to generate 6334 ppm O$_3$ (in this study defined as the enthalpy difference between O$_3$ and converted O$_2$ at T$_0$) was used to heat the stoichiometric CH$_4$/air mixture, the initial temperature of reactants would increase by approximately 30 K. This would result in an increase of 5.4% in modeled mass burning rate (g/s), which is lower than the enhancement (8.3%) achieved by O$_3$ addition. (Here the mass burning rate, rather than S_L, is used because increase in initial temperature would increase flow rate and S_L even without any chemical effect.) The release of O atoms and the subsequent increase in fuel oxidization provides one reaction pathway for enhanced flame propagation. This explanation can be extended to other alkanes such as C$_3$H$_8$.

However, there is another O_3 consumption reaction pathway competing with the O_3 decomposition reaction (R1) in the preheat zone, as indicated in Figure 38(a):

$$O_3+H=O_2+OH \qquad\qquad (R2)$$

Unlike the decomposition reaction R1, which is a chain initiation reaction, R2 is a chain-propagation reaction, or a chain-termination reaction if O_3 is counted as a semi-radical. This chain-termination reaction is detrimental to S_L. For example if this reaction is removed from the kinetic mechanism, the simulated stoichiometric S_L enhancement for CH_4 with O_3 addition of 6330 ppm increases from 8.7% to 11.3%. This negative effect on S_L is consistent with previous work [65], where a negative dependence of S_L on this reaction in sensitivity analysis was reported. In addition, R2 can heavily depend on the diffusion process, which is pressure dependent. This is because H atoms produced in the flame rapidly diffuse to the preheat zone. Though the quantity of H atoms is small at the preheat zone (approximately 100 ppm), the reaction rate constant of R2 is approximately 10^4 times that of R1, and therefore, the net rates of R1 and R2 are comparable. In fact, at the conditions shown in Figure 38, R2 is the dominant consumption pathway for O_3.

Though the reaction R2 had a higher reaction rate compared to the reaction R1, as shown in Figure 38(a), the simulations show that heat absorbed by the endothermic reaction R1 is approximately 200 times that released by the exothermic reaction R2. This heat consumption by the O_3 decomposition is responsible for the decreased temperature in the preheat zone after O_3 addition, shown in Figure 38(c). As O_3 addition increases the total enthalpy of the system, the equilibrium temperature increases after O_3 addition, as indicated in Figure 38 (c).

Besides the reactions R1 and R2, others involved include $O_3+O_2=O_2+O+O_2$ and $O_3+CH_3=CH_3O+O_2$. These reactions account for less than 5% of total O_3 consumption, and their removal of them only affects flame speeds by less than 0.3%. Previous sensitivity analysis has confirmed the negligible effects of the reaction between O_3 and CH_3 and other hydrocarbons in this case [65]. Therefore, reactions R1 and R2 are the focus of the present work.

4.4   The effect at room temperature and elevated pressure

In order to study the pressure dependence of S_L on O_3 concentration, experiments were conducted at elevated pressures. However the question that needs to be addressed is whether it is reasonable to ignore ozonolysis of CH_4 at high pressures. There is inconsistency among the existing kinetic data describing the ozonolysis of CH_4. Based on early work of Schubert et al. [21], the reaction rate constant of CH_4 ozonolysis at 300 K is $k = 0.994$ cm^3/mole-s, while a more recent result [157] is 722 cm^3/mole-s. To resolve this discrepancy, the residence time of the mixing process was increased from 20 to 80 s. This would result in approximately 80% of the O_3 being consumed before exiting the burner with $k = 722$ cm^3/mole-s, while this consumption is only 8% with $k = 0.994$ cm^3/mole-s. The measured S_L for the different residence times were identical, confirming that ozonolysis of CH_4 can be ignored in the following high-pressure experiments. Measurements at high pressure were firstly validated using pure CH_4/air. As shown in Figure 39, our measurements and simulations agree well with published values [161]. Then 6334 ppm O_3 was added to evaluate the pressure effect on S_L. As illustrated in Figure 40, the fractional enhancement of S_L increases with pressure, as predicted by the simulation. The stoichiometric CH_4/air S_L for 6334 ppm O_3 addition increased from 7.7% at room

pressure to 11% at 2.5 atm, and the enhancement of S_L at $\phi = 0.7$ increased from 11.3% at atmospheric pressure to 14.4% at 2.5 atm. Although the simulation properly predicts this trend, the enhancement at the off-stoichiometric case is somewhat high. For example, Figure 40 shows the measured S_L at $\phi = 0.7$ and 2.5 atm increased by 14.4% with O_3 addition, but the corresponding simulation result is 16.3%. This is consistent with results at atmospheric pressure, as discussed previously.
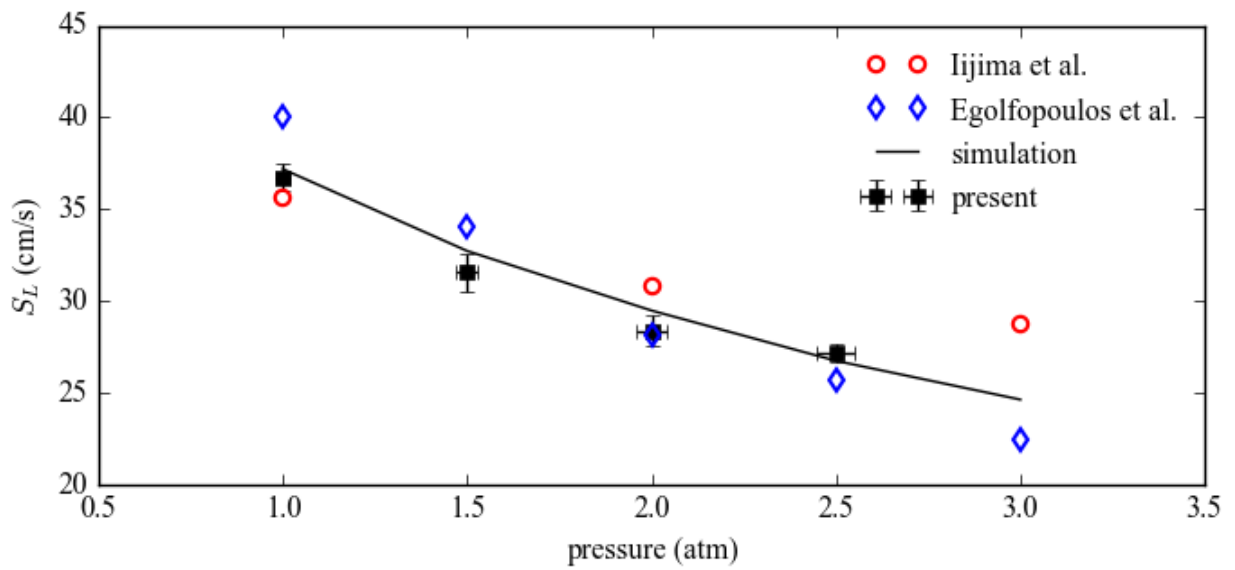
Figure 39 The pressure dependence of CH$_4$/air flame speeds
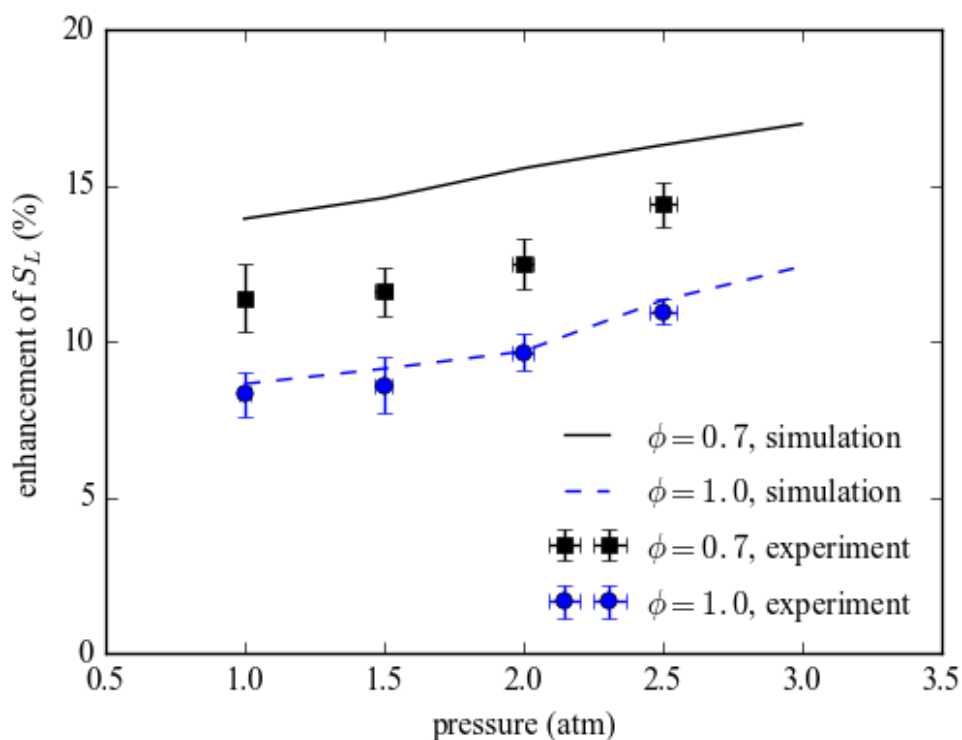
Figure 40 The pressure dependence of the enhancement of CH₄/air flame speeds

Agreement between simulated and measured enhancement of S_L at elevated pressure is good; the implication is that the kinetic mechanism is very similar. As seen in Figure 41(a), O_3 decomposes in the preheat zone through the reaction with N_2, and releases O atoms, which attack fuel molecules and accelerate subsequent reactions. For example, the peak net reaction rate of $CH_4+O=CH_3+OH$ in Figure 41(b) increased by 9.3% after O_3 addition, while for $CH_4+OH=CH_3+H_2O$, the peak net reaction rate increased by 7.2%. In fact, for all major CH_4 consumption reactions, the increase in reaction rates at 2 atm is higher than at 1 atm, which is consistent with the observed results. As at atmospheric pressure, the thermal effects only account for part of the enhancement. For example, if the energy used to convert O_3 to O_2 was used to heat the reactants, the increase in mass burning

rate would be only 5.7% (versus the 9.7% enhancement achieved by O_3 addition with the same energy).
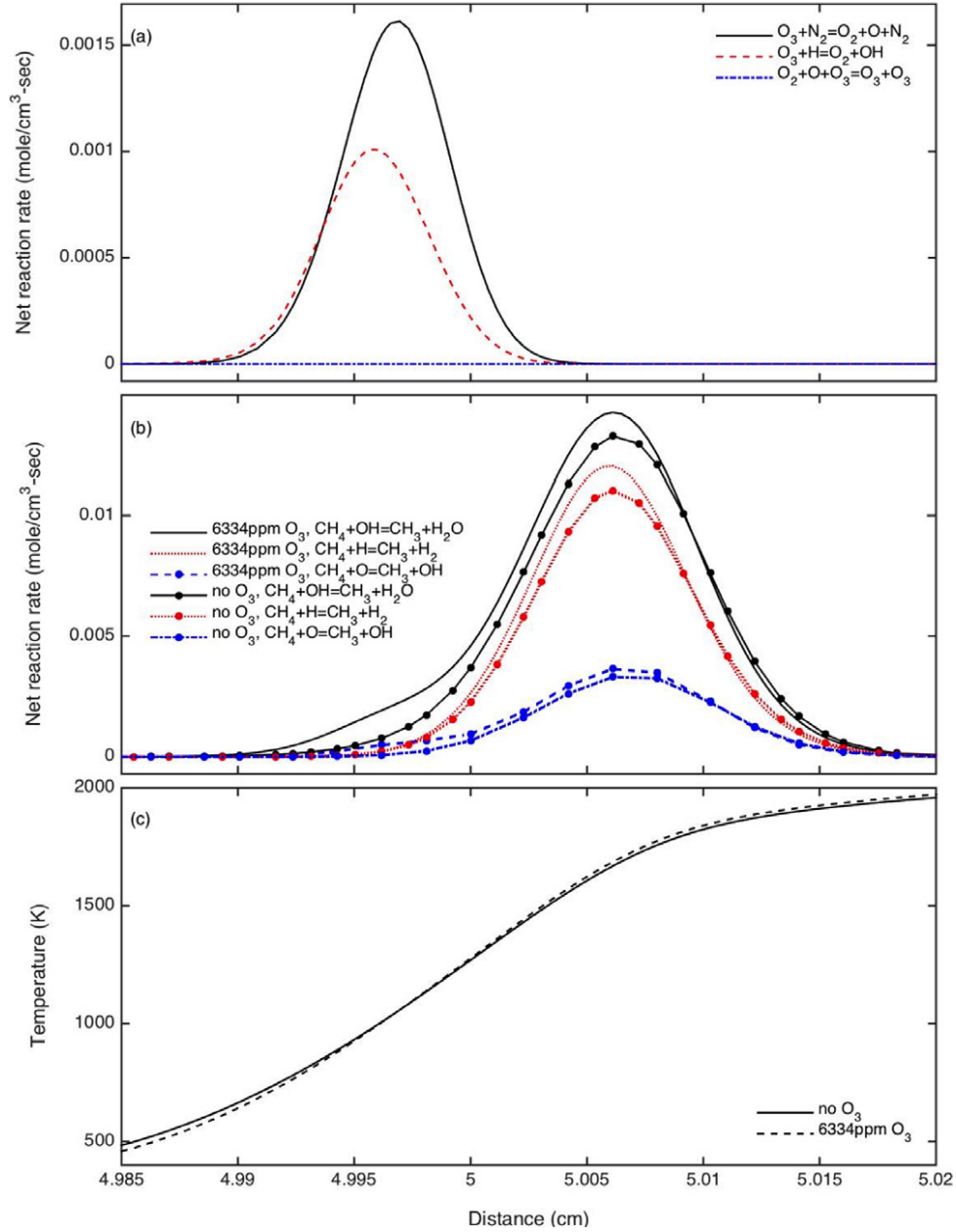
Figure 41 CH_4/air/O_3 flame simulation at P = 2 atm, T_0 = 300 K, and φ = 1 (a) major reactions of O_3 ; (b) major reactions of CH_4 and (c) temperature profile.

An important difference at elevated pressure is that the main O_3 consumption pathway is changed. At atmospheric pressure, the most significant channel is R2, as shown in Figure 38(a), while at elevated pressure, reaction R1 is favored, as indicated in Figure 41(a). This is consistent with observation of higher enhancement at elevated pressure, since R1 produces O, while R2 has a negative effect on S_L. There are two pressure effects that account for this change of O_3 consumption pathway. First, in the presence of CH_4 and other hydrocarbons, O is consumed immediately after being released from O_3. Therefore, the recombination rate (reverse reaction of R1) is nearly zero, and the increase in pressure would only benefit the decomposition reaction (forward reaction of R1). Thus, increased pressure accelerates O_3 decomposition in the preheat zone. This positive pressure dependence can be illustrated by the increase in the reaction rate of R1 at high pressure. For example, compared with atmospheric conditions, the peak net reaction rate of this reaction is increased by 317% at 2 atm.
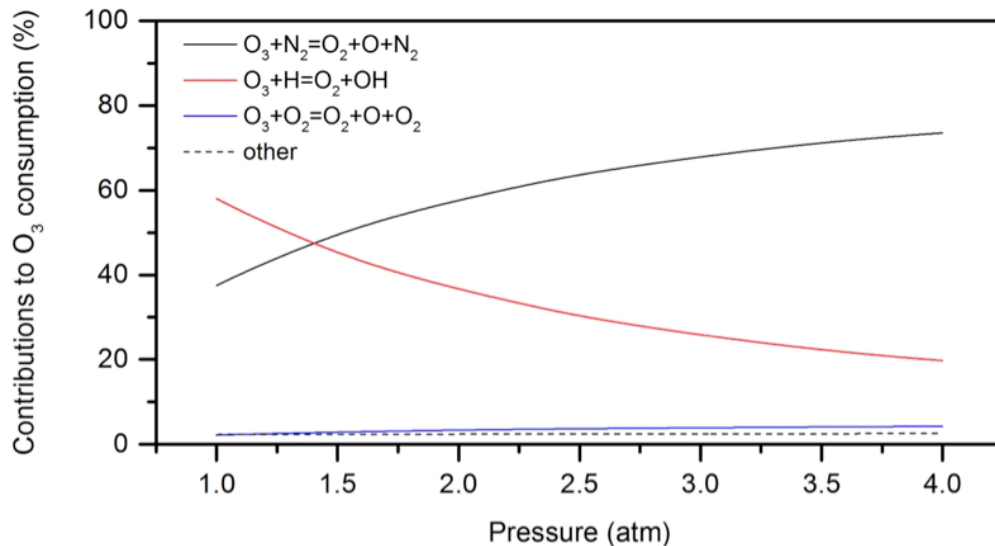
Figure 42 Contribution to the consumption of O_3 by reactions as a function of pressure in simulated laminar CH_4/air flames

Second, the reaction R2 heavily depends on the diffusion of H atoms from the reaction zone of the flame to the preheat zone, but diffusivity is lower at higher pressure. In addition, the dissociation of H-containing species is suppressed. Consequently, although the flame becomes thinner at high pressure, fewer H atoms diffuse to the preheat zone. For example, at the point in the preheat zone where the temperature is 1000 K, the H mole fraction at 1 atm is 110 ppm, while it is 35 ppm at 2 atm. Coupled with the positive pressure dependence of O_3 decomposition, lower diffusivity weakens the reaction R2 and makes the dominance of the reaction R1 greater as pressure increases. For example, at 1 atm the decomposition only accounts for 37.5% of total O_3 consumption; while at 2 atm, 57.6% of O_3 is consumed by the decomposition reaction. This trend of increasing contribution of this pathway continues if the pressure is increased further (see Figure 42). In addition, the peak O production rate within the preheat zone after O_3 addition of 6334 ppm at 2 atm is increased by 664% compared to the value at 1 atm. This is much greater than the effect of pressure on pure CH_4/air flames. For example, the peak CH_4 consumption rate is only increased by 187% when pressure is increased to 2 atm. Consequently, elevated pressure results in greater enhancement of O_3 on flame propagation, as indicated in the experimental results (Figure 40).

4.5   The dependence on initial temperature

Simulation is conducted to investigate the initial temperature dependence of the enhancement of flame speed due to O_3 addition. The results are presented in Figure 43. It shows that the enhancement decreases with increasing T_0.
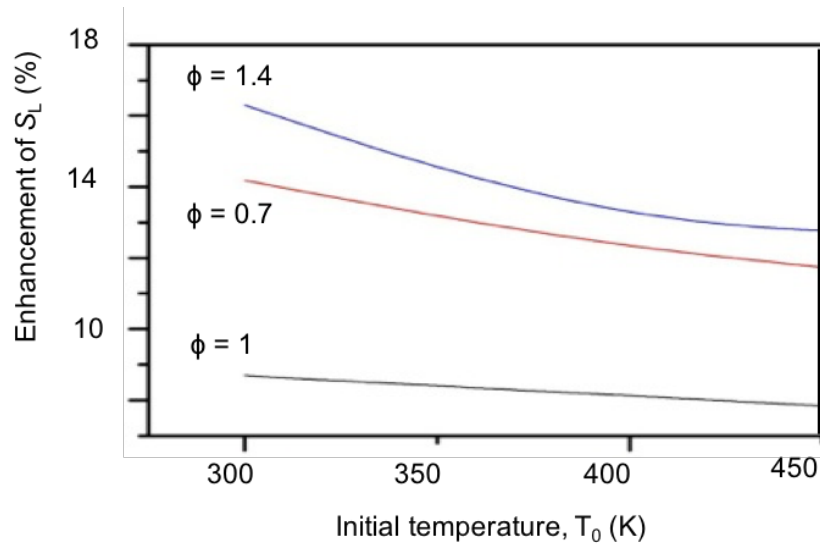
Figure 43 Enhancement of CH$_4$/air S_L as a function of T_0 at 1 atm with O$_3$ addition of 6334 ppm

This trend can be explained by considering the effects of higher T_0 on the reaction O$_3$ + H = O$_2$ + OH. As illustrated in Figure 44, increasing T_0 from 300 to 450 K results in a significant increase of H concentration. This is particularly true in the preheat zone. This is due to 1) higher temperature favors more H due to dissociation of H-containing species, and 2) higher diffusivity at higher temperature transport more H into the preheat zone. Consequently, for the positions of the same O$_3$ concentration, H concentration at T_0 = 450 K is always much higher than that at T_0 = 300 K. Together with higher temperature, this promotes O$_3$ + H = O$_2$ + OH, which is found to negatively affect the flame speed based sensitivity analysis. As a result, the enhancement is reduced at higher T_0.

It is worthy to mention that, O$_3$ decomposes rapidly before entering the preheat zone of the flame at high temperature (>450 K). At such conditions, the conventional flame model, such as PREMIX [84], does not work. Such a model assumes nearly-zero gradient

75

at the inlet, and this assumption is violated when O_3 starts decomposition at the inlet. In such case, residence time matters. The longer residence time between the inlet and the flame, the more O_3 is consumed. An extreme case is that the residence time is sufficiently long that all O_3 is consumed before entering the flame. Such case is modelled using a "PLUG+PREMIX" network. An adiabatic PLUG flow reactor [153] is used to model the reactions before the reactants enter the flame at high T_0, where all of O_3 is consumed. The simulation results are illustrated in Figure 44. With O_3 addition of 6334 ppm at $T_0 = 500$ K, 1 atm, it takes about 0.5 s for all O_3 to be consumed, and then the composition remains constant in the PLUG flow reactor. The composition at the end of the PLUG flow reactor is listed in Table 2. Although some relatively less stable species, H_2O_2 and CH_2O, are produced, no radicals remain.
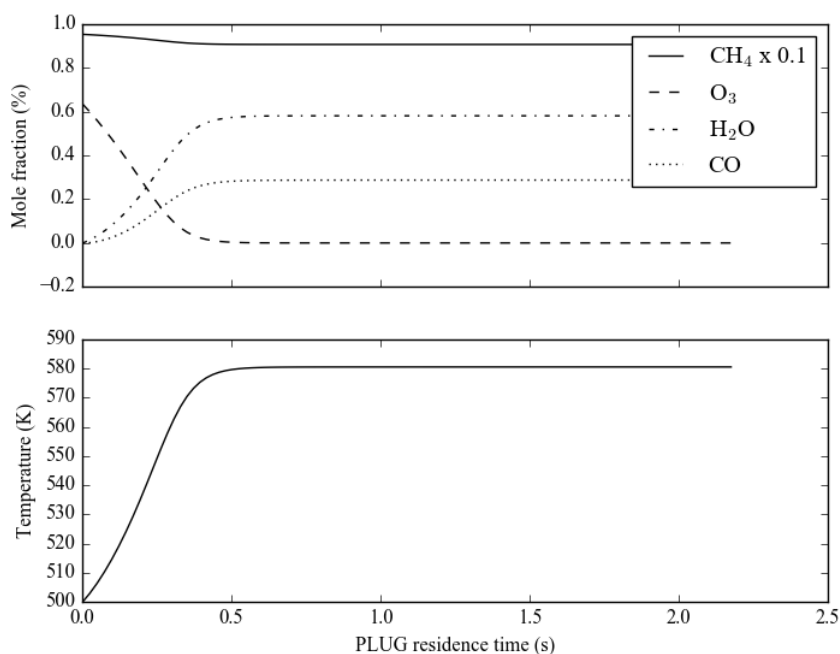
Figure 44 Simulation using an adiabatic PLUG flow reactor with O_3 addition of 6334 ppm at $T_0 = 500$ K, 1 atm

If the composition and temperature of the outflow of the PLUG flow reactor are used as values for the inlet of the PREMIX reactor, one may find the corresponding mass burning rate is 0.065 g/cm^2-s. If no O_3 is added, the mass burning rate is 0.064 g/cm^2-s. This implies that, even if all of O_3 is consumed before entering the flame due to high T_0, the mass burning rate is still only enhanced slightly. However this enhancement is almost negligible compared to the case when O_3 can survive and be transported to the preheat zone. For example, at 300 K, the enhancement is more than 8%. This is because by transporting O_3 into the preheat zone, the released O atoms can attack the fuel more efficiently, and induce the subsequent chain propagating and branching reactions. If O_3 is decomposed too early, the produced O is consumed without affecting the flame significantly.

This suggests that, to enhance flame propagation with O_3 addition, one should either apply it with a low initial temperature, or restrict the residence time to minimize the decomposition of O_3 before it is transported to the flame.

Table 2 Mole fractions at the end of PLUG flow reactor with O_3 addition of 6334 ppm at $T_0 = 500$ K, 1 atm.

N_2	71.4%	CO	0.287%
O_2	18.4%	H_2O_2	0.108%
CH_4	9.07%	CH_2O	0.076%
H_2O	0.58%	C_2H_6	0.025%

(note: the species whose mole fraction are smaller than 0.01% are not listed)

CHAPTER 5 THE EFFECTS OF OZONE ADDITION ON ALKENE FLAME PROPAGATION

5.1 Introduction

As mentioned previously, there is a dramatic difference between the ozonolysis reaction rate of alkanes and unsaturated hydrocarbons. The ozonolysis of unsaturated hydrocarbons is usually rapid and cannot be ignored at room temperature. For example, the reaction rate constant of the ozonolysis reaction for CH_4 is $k = 0.994$ cm^3/mole-s [21], but for C_2H_4, $k = 1.12 \times 10^6$ cm^3/mole-s [23]. The rapid ozonolysis reaction makes the effect of O_3 addition much more complicated than with alkane fuels. Thus, experiments were conducted at various temperatures and pressures to control the ozonolysis reaction and investigate the effect of O_3 addition on flame propagation.

5.2 The effect at room temperature and atmospheric pressure

Experiments are conducted at room temperature and atmospheric pressure using the Bunsen burner documented in Section 3.2.1. In contrast to the results with CH_4 and C_3H_8, reduced S_L was observed with the addition of O_3 at room temperature and pressure with C_2H_4. This observation is consistent with the findings of Gluckstein $et\ al$. [70]. As illustrated in Figure 45, S_L at $\phi = 0.7$ is lowered by more than 50% with O_3 addition of 6410 ppm. Although the changes in S_L became smaller when ϕ is higher, there is still a decrease of 10% in S_L at $\phi = 1.8$. However, for all ϕ, simulations (PREMIX with the USC Mech II mechanism [151] and a O_3 sub-mechanism [63] but ozonolysis reactions are not inclued)

predict an increased S_L (see "simulation (S_L)" in Figure 45). Thus, numerical modeling correctly predicts the change of S_L for CH_4 and C_3H_8 but fails for C_2H_4. The discrepancy results from the missing ozonolysis reaction for C_2H_4.
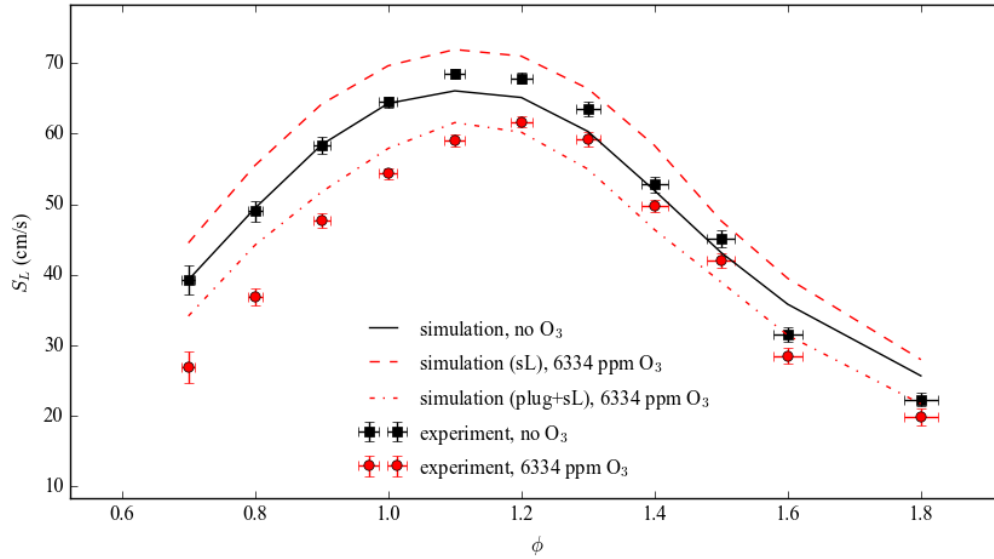
Figure 45 C_2H_4 flame speeds with and without O_3 addition
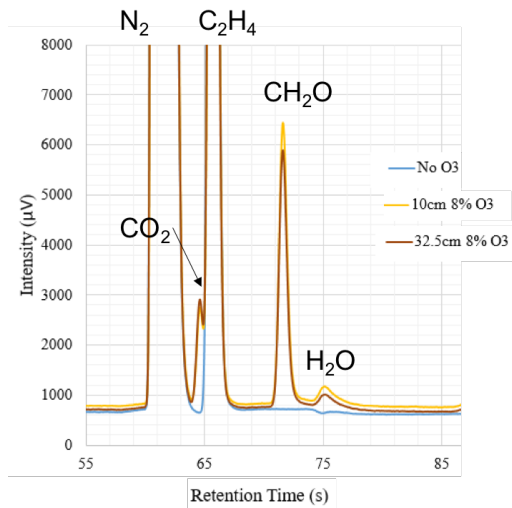
Figure 46 Gas chromatography results of C_2H_4/air without and with O_3 measured at different locations of a plug flow reactor at room temperature

Additional evidence of O_3 consumption is provided by Gas Chromatography (INFICON Micro GC Fusion® Gas Analyzer) at atmospheric pressure and room temperature. Samples were collected at different locations (10cm and 32.5cm) along the mixing tube (before entering the burner). The tube in the mixing section was replaced for each experiment to remove any possible residue liquid/solid substance in the tube. As illustrated in Figure 46, the results shows that significant amounts of H_2O, CO_2, and CH_2O are formed when O_3 is added. The comparison confirmed significant ozonolysis reaction of C_2H_4 at room temperature and pressure. We can expect that heat generated would be transferred into the flow apparatus, and this energy loss could explain the decreased S_L.

A CHEMKIN reactor network model was developed to simulate S_L in the case of the presence of ozonolysis and heat loss using the ozonolysis reaction proposed above. The kinetic mechanism including the ozonolysis reactions (Section 3.3.4) is employed. An isothermal plug-flow reactor model was used to simulate the mixing section. The outlet of this reactor is connected to a 1-D, adiabatic planar flame model (PREMIX). Therefore, the products of the plug flow reactor are also the reactants of PREMIX. The temperature of this reactor was maintained at 300 K, based on the measured wall temperature of the mixing section in experimental setup. It was expected that O_3 would be completely consumed, and the flow would reach steady state within 1 s based on the proposed ozonolysis mechanism. As a result, plug-flow reactor residence times greater than 1 s were found to not affect the simulated S_L. The mixing time in the experimental setup was generally longer than 20 s; therefore, fixing the plug-flow reactor residence time at 20 s, as was done in this study, should ensure reasonable simulation. Furthermore, the plug flow reactor is assumed to be isothermal to account for the heat loss to the burner and the initial temperature of the

incoming flow. The PREMIX module was therefore fixed at 300 K, same as the isothermal plug reactor. Results from this model, labeled as "simulation (plug+sL)" in Figure 45, successfully predict the decrease of S_L. For example, at $\phi = 1.2$, this model predicted a decrease in S_L of 7.8% with O_3 addition of 6334 ppm, which is close to the corresponding experimental result 8.7%. However, this model shows large discrepancies with experimental results at leaner and richer conditions.
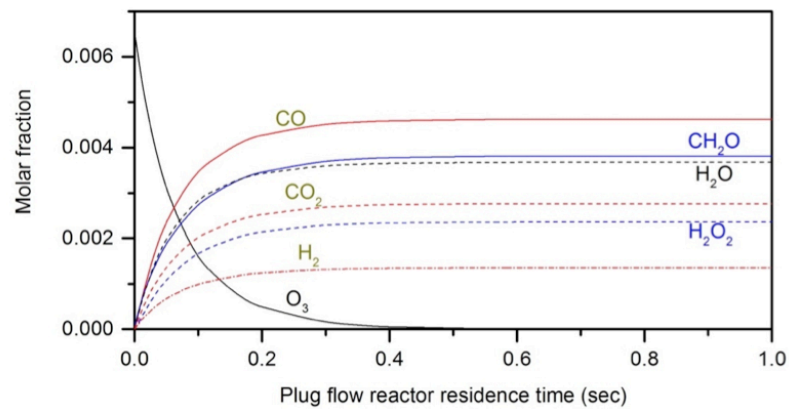
Figure 47 Species profiles in an isothermal PLUG flow reactor with $C_2H_4/air/O_3$ as the inlet species
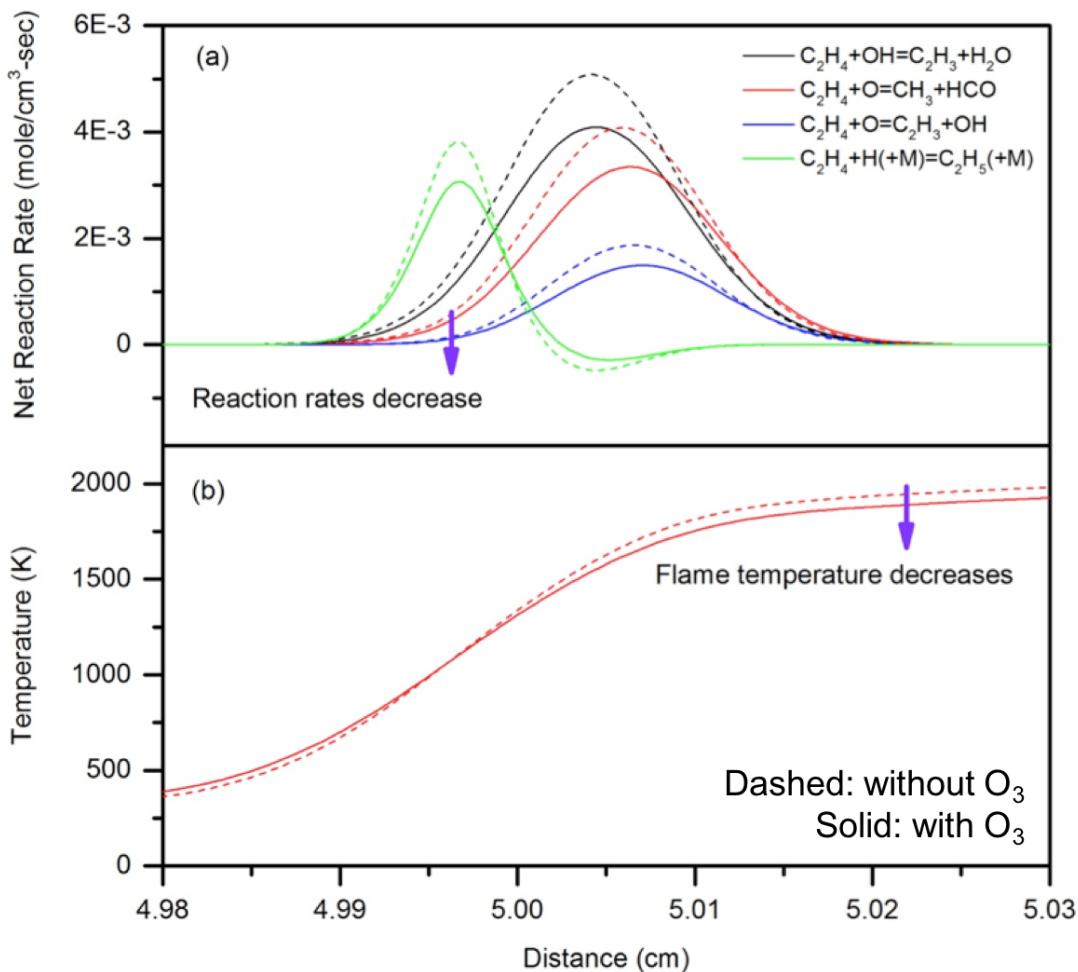
Figure 48 Simulation of C_2H_4 flame with (solid lines) and without (dashed lines) O_3 addition. Inlet species preprocessed in PLUG flow reactor.

Simulations show that this mixing process involves both the change of chemical composition and loss of energy. Radicals such as H and OH are produced by ozonolysis of C_2H_4, and then consumed immediately and generate species such as H_2O, CO, and CO_2, as shown in Figure 47. In contrast, reactive species H_2 and CH_2O could survive and be transported to the flame. If the mixing process is adiabatic, these changes in chemical composition could lead a 3% increase in mass burning rate. This indicates that the pure chemical kinetic effect of ozonolysis of C_2H_4 enhances the flame propagation speed.

However, significant heat loss exists upstream of the burner exit in the present experimental setup and this process is nearly isothermal based on temperature measurements. For example, the simulations show that the enthalpy of the reactants at the burner exit decreases by almost 296 kJ/kg after 6334ppm O_3 addition if the temperature of plug flow reactor is maintained at 300K. Consequently, although the change in chemical composition enhances S_L the heat loss decelerates the reaction rates of fuel oxidization, as seen in Figure 48(a). The overall consumption rate of C_2H_4 was decreased by 16% after 6334ppm O_3 addition. In contrast to alkane fuels, whose flame temperatures generally increase slightly with O_3 addition (see Figure 38(c) and Figure 41(c)), the flame temperature with C_2H_4 was decreased by 3% after O_3 addition, as shown in Figure 48(b), which again indicates the loss of energy.

5.3   The effect at low temperature and atmospheric pressure

Since the detrimental effect of O_3 addition on flame propagation results from the energy loss induced by the exothermic ozonolysis reaction in the mixing process, we should expect increased S_L with O_3 addition if the ozonolysis reactions were minimized. One possible way is to slow the reaction by cooling the reactants. The reaction rate constant of the ozonolysis reaction of C_2H_4 can be modeled as $k = 7.23 \times 10^9 e^{-5226/(RT)}$ [23], which shows that the reaction is slower at lower temperature. As shown in Figure 49, the O_3 lifetime in the reactants is significantly increased as the temperature decreases, as ozonolysis reactions are frozen. These results suggest that O_3 consumption can be ignored in the mixing process if reactants are cooled to 200 K and burner volume is minimized (i.e., the residence time is short).
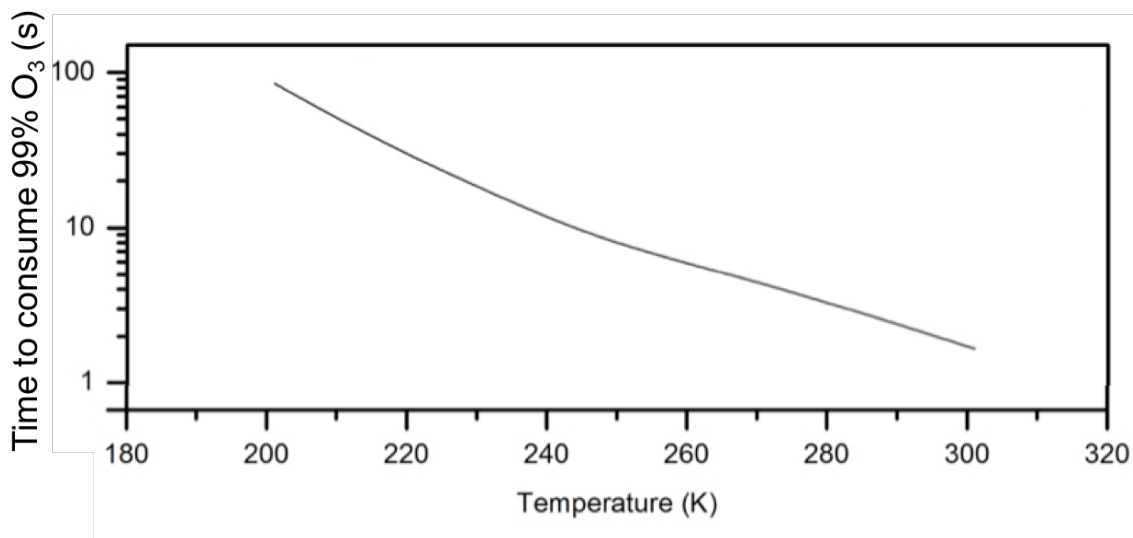
Figure 49 Computed O$_3$ lifetime in C$_2$H$_4$/O$_2$/O$_3$/N$_2$ mixture as a function of temperature at atmospheric pressure

Experiments are conducted at 200 K and atmospheric pressure using the low-temperature Bunsen burner documented in Section 3.2.2. In this experimental setup, the mixing of reactants was limited to 0.4 s at 200 K, so that approximately only 10% of the O$_3$ was estimated to be consumed by the time the reactants exit the burner. This technique provides a clear boundary condition and avoids the difficulty at room temperature of specifying initial conditions and heat loss. As shown in Figure 50, the present results are in good agreement with the experimental data of [162] by Dugger for S_L of a C$_2$H$_4$/air mixture at 200 K. In contrast to the detrimental effect of O$_3$ addition at room temperature, significant enhancements of S_L are observed. At stoichiometric condition, the S_L was increased by 5.7% with O$_3$ addition of 3910 ppm. The enhancement is greater at off-stoichiometric conditions: 13.6% at $\phi = 0.8$ and 10.9% at $\phi = 1.4$. Large discrepancies between the experimental and simulation data are observed. However, USC Mech II has not been validated at such low initial temperature conditions.

84

Based on the analysis of simulations, C_2H_4 shares a similar enhancement mechanism with the alkane fuels. As illustrated in Figure 51(a), O_3 first decomposes in the preheat zone through its collision with N_2 (R1); the released O atoms then accelerate the H abstraction reaction of C_2H_4 as shown in Figure 51 (b). The peak net reaction rate of $C_2H_4+O=CH_3+HCO$ increases by 27.7% with O_3 addition of 13,175 ppm. As with alkanes, the increased reaction rate is not solely a thermal effect. For instance, if the energy used to convert O_2 to form 3910 ppm O_3 at 200 K (defined as the change of enthalpy at this temperature), was used to heat the reactants, T_0 would increase by 19 K, but this only results in an increase of 2.9% in the mass burning rate (versus 5.4% with O_3 addition).
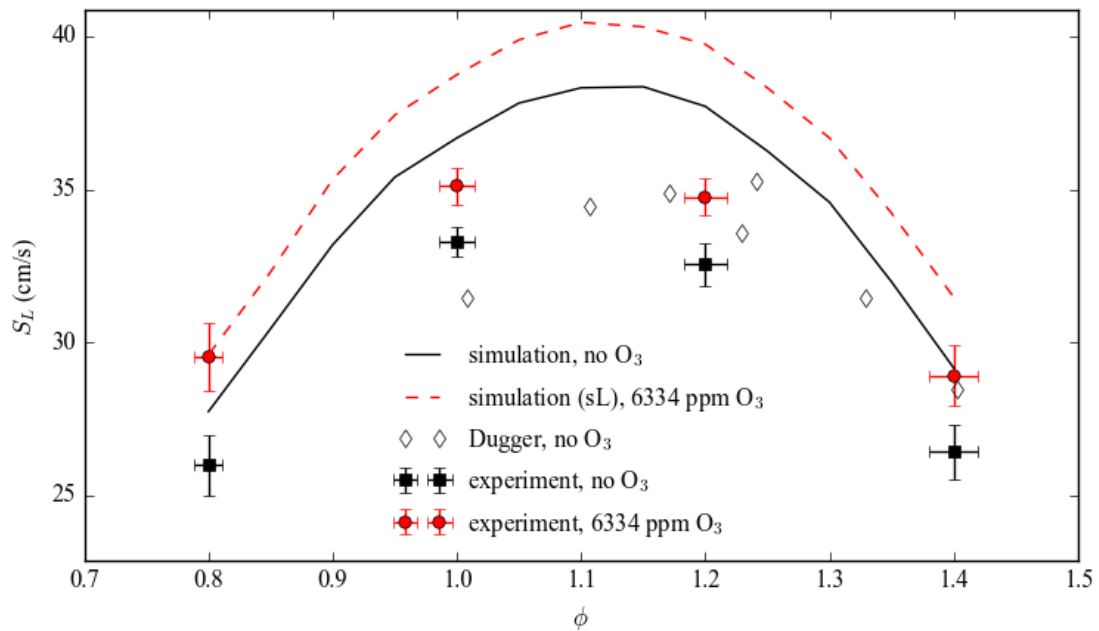
Figure 50 C_2H_4 flame speeds with and without O_3 addition at 200 K.
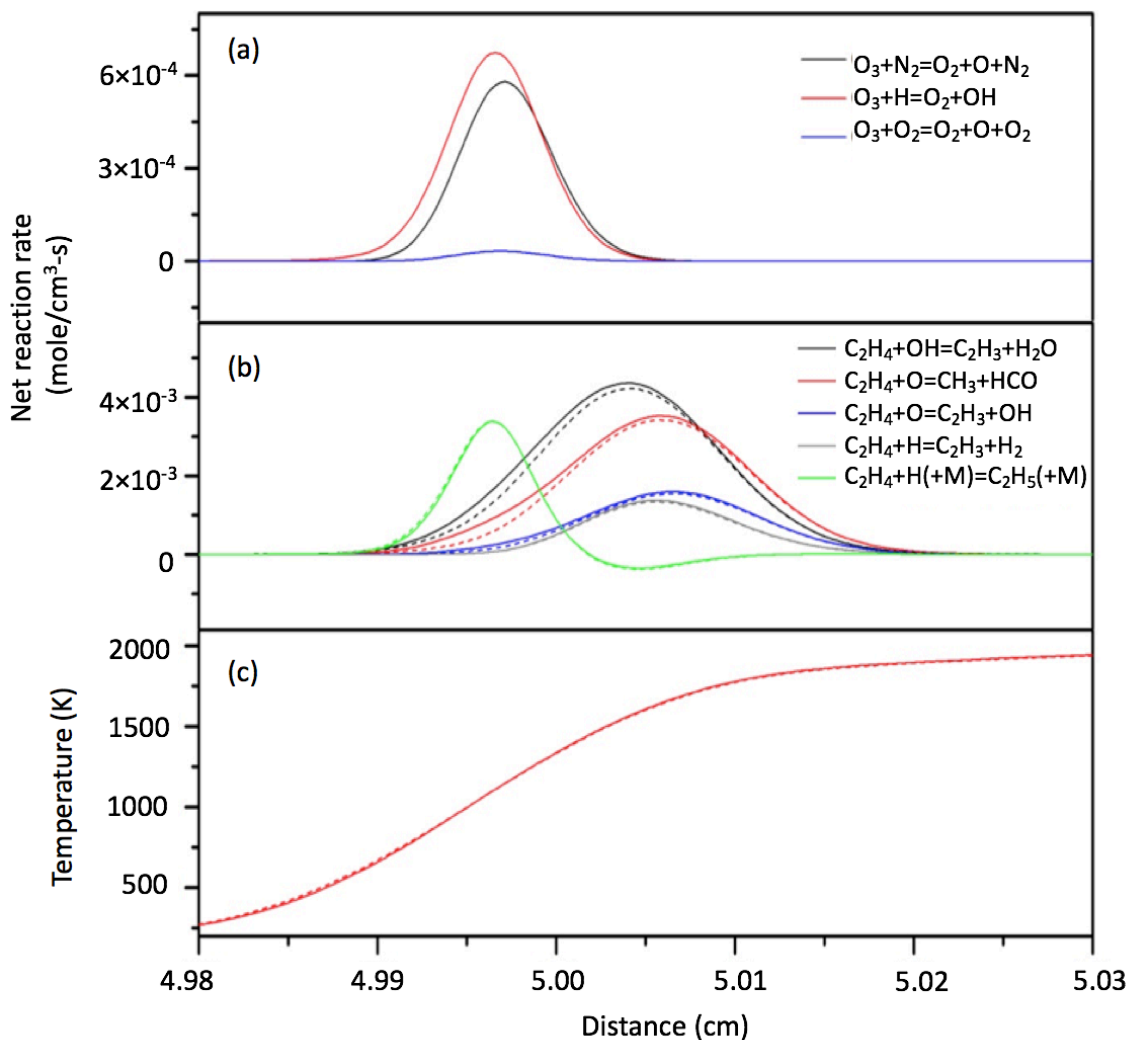
Figure 51 Simulation of C_2H_4 flame with (solid lines) and without (dashed lines) O_3 addition at 200 K.

However, an important difference between C_2H_4 and alkanes is that there are two possible pathways to form the important species CH_3. One is through the reaction $C_2H_4+O=CH_3+HCO$ in the reaction zone. As shown in Figure 51 (b), this "one-step process" would benefit from O_3 addition, due to the released O atoms. Another is a "two-step process". Firstly, a portion of C_2H_4 is consumed in the preheat zone by the reaction $C_2H_4+H(+M) = C_2H_5(+M)$, as shown in Figure 51(b); then, the formed C_2H_5 is converted

to CH_3 through the reaction $C_2H_5+H=2CH_3$. Both the above-mentioned formation and consumption pathways of C_2H_5 happen in the preheat zone, and both consume H atoms. Thus, this "two-step process" would be suppressed by O_3 due to the reaction R2. For example, in the case without O_3 addition, $C_2H_4+H(+M)=C_2H_5(+M)$ consumes 11.3% of C_2H_4, but with 13175 ppm O_3 addition, only 8.7% of the C_2H_4 is consumed. The "two-step process" is less efficient compared to the "one-step process;" therefore, compared to alkanes, reduced C_2H_5 production in the preheat zone by O_3 addition provides more efficient conversion from fuel to CH_3. This provides another mechanism of the enhancement of flame propagation.

5.4   The effect at room temperature and sub-atmospheric pressure

The effect of O_3 addition on flame propagation was also investigated at sub-atmospheric pressures. The experiment was conducted by Dr. Ombrello at U.S. Air Force Research Laboratory [148] and the analysis is presented here as a part of this dissertation. The fuel is C_2H_4 and the pressures is varied from 0.40 atm to 0.92 atm at $\phi = 1$ with and without O_3 addition of 14,400±100 ppm. The residence time for the mixing process was maintained between 0.42 and 0.66 sec. As illustrated in Figure 52, O_3 increased the S_L (decreased its flame height) of the C_2H_4/air mixture at 0.40 atm, which is consistent with the previous work [69]. There is no observable change in S_L was seen at 0.66 atm. At 0.79 atm, S_L decreased with O_3 addition. These results indicate that the effect of O_3 addition on S_L enhancement is pressure dependent. Actually, as shown in Figure 53, the ozonolysis is faster at higher pressure, and therefore more C_2H_4 is consumed and more heat was transferred to the ambient during the mixing process. This results in greater heat loss at

higher pressure and explains the different observations at different pressures. At low pressure, no much heat is lost thus adding O_3 enhance flame propagation. However, the heat loss is significant at higher pressure, ozonolysis reactions become faster and the increased heat loss lead to a decrease in S_L.
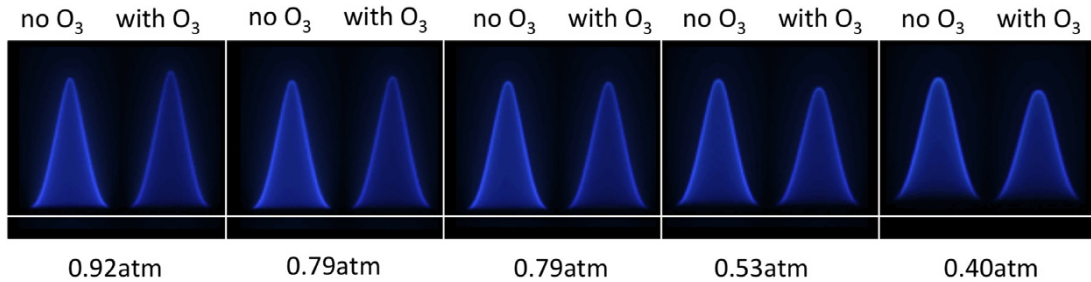
Figure 52 Direct photo of C$_2$H$_4$/air flame with or without O$_3$ addition (14,400 ± 100 ppm), at sub atmospheric pressure. T_0 = 300 K and φ = 1.

(Experiments conducted by Ombrello at U.S. Air Force Research Laboratory [148])
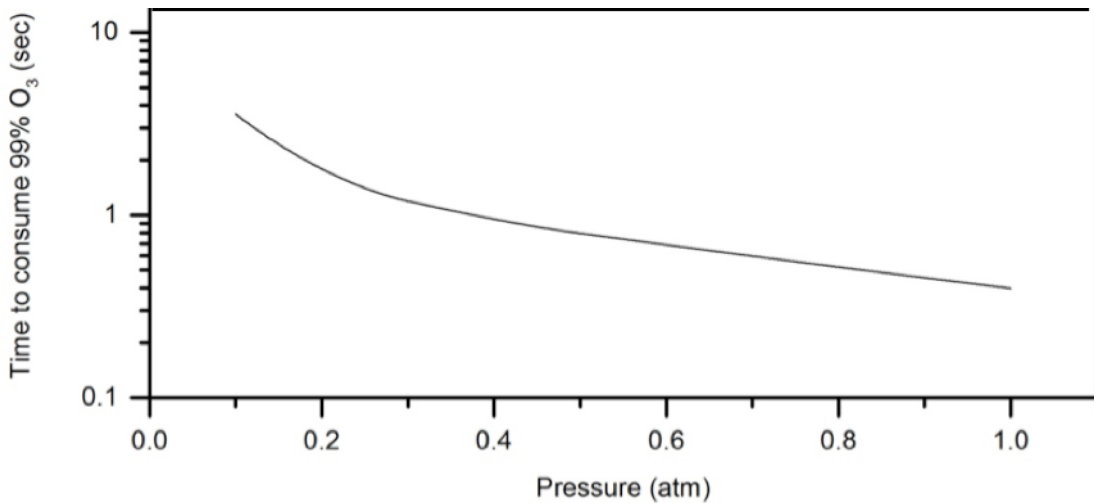
Figure 53 lifetime of 6334 ppm O$_3$ in stoichiometric C$_2$H$_4$/air as a function of pressure at room temperature at constant temperature of 300 K

CHAPTER 6 OZONOLYSIS ACTIVATED AUTOIGNITION

6.1 Introduction

As discussed in Chapter 5, when unsaturated hydrocarbons, such as C_2H_4, and O_3 are premixed, ozonolysis reaction occurs rapidly. But the heat released may be lost if not in an adiabatic environment and resulting in a decrease in reactivity. A natural follow-up question is that, if the heat loss is avoided or minimized, could the heat released from ozonolysis reactions be utilized to initiate autoignition, and affect the flame dynamics?

To investigate such a possibility, a non-premixed burner, documented in Section 3.2.2, is employed. A premixing burner is not used due to safety reasons. As previously discussed, the ozonolysis starts in the premixing section in the reactant feeding lines. The temperature rise may finally induce flashback and is not safe. If a non-premixed burner is used, heat is only released when the oxidizer and fuel are mixed in the desired region in a controlled way. Though cooling the reactants or decreasing the pressure can also minimize ozonolysis reactions, such conditions are not consistent with the practical application to many combustion systems. Additional cost for such efforts may not be worthwhile. However, non-premixed combustion, or more specifically, non-premixed jet flames, is a very common configuration in practical application. Given these concerns on safety and application, a non-premixed burner is preferred as a research platform for this study.

Previously, autoignitive conditions were primarily created using a jet in hot coflow (e.g., turbulent [114-119] and laminar [128-131]). The temperature of the coflow is raised above the flash point to initiate autoignition. Ozonolysis reactions of unsaturated hydrocarbons are proposed as an alternative to create such autoignitive environment. Such

89

reactions release significant heat rapidly even at room temperature, therefore avoiding the difficulties associated with heating flow rate to high temperature. Furthermore, the O_3 concentration can be easily and rapidly controlled.

When autoignition becomes the dominant mechanism, the flame stabilization may be significantly enhanced, as the spread of flame is no longer limited by diffusion. The reactive species can be produced and the heat can be released before the arrive of flame front. This chapter focuses on the ozonolysis-activated autoignition itself. It serves as a basis for the next chapter, where the flame stabilization in such autoignitive environment is discussed.

The non-premixed coflow burner used in this chapter is documented in Section 3.2.3. The dilution level of the oxidizer is low to allow autoignition. The ratio of N atoms and O atoms (including these in O_2 and O_3) in the current experiment is N/O=0.28. The overall equivalence ratio is ϕ=0.4. A nominal flow velocity, U_0, is defined as the total flow rate (fuel and oxidizer) divided by the cross-section area of the quartz tube. U_0 is an overall characteristic flow velocity, not a local velocity or a velocity scale based on a specific velocity profile. A wide range of O_3 concentrations and U_0 is tested in the following sections.

6.2   The role of ozonolysis reactions

6.2.1   Experimental observations

The experimental conditions are set in such way that autoignition can occur at room temperature. 7.7% of O_2 is converted to O_3, which corresponds to 3.7% of O_3 in total

reactants. For this section, U_0 is set to 2.37 m/s. This corresponds to U_{jet} = 13.6 m/s and U_{coflow} = 2.0 m/s. The observed autoignition at such condition is illustrated in Figure 54.
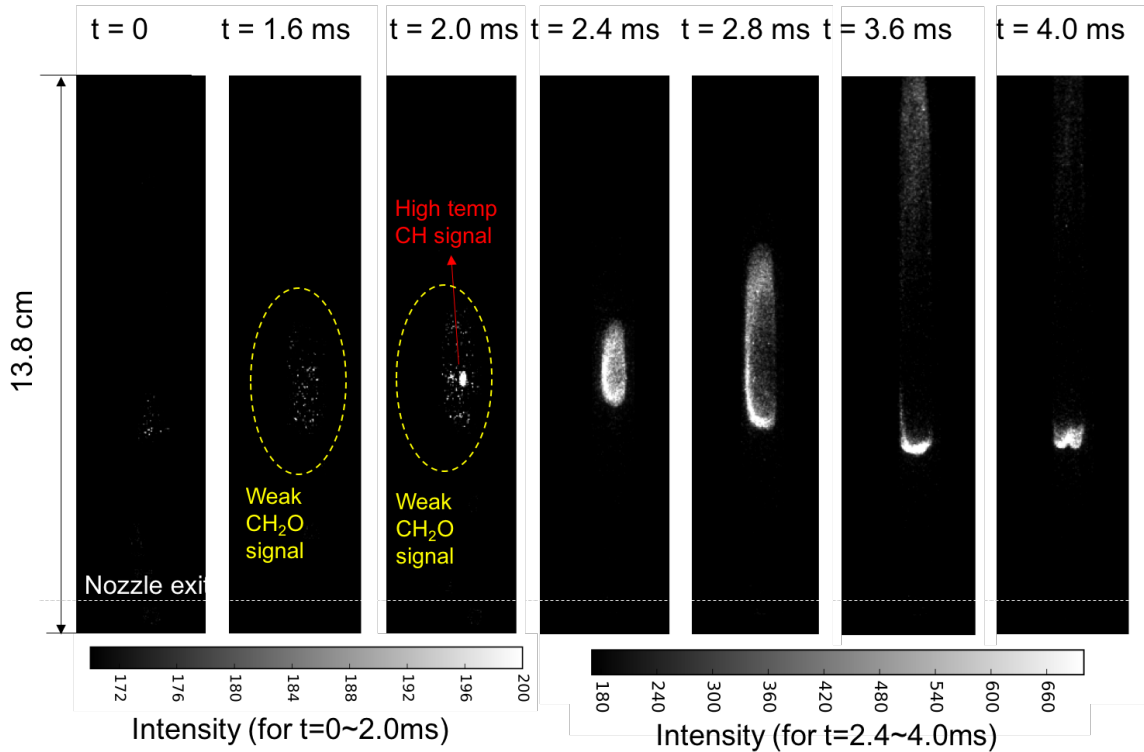
Figure 54. Ozonolysis activated autoignition

Autoignition is initiated by ozonolysis reaction between C_2H_4 and O_3. A simple demonstration is that, if the fuel is CH_4, whose ozonolysis reactions are negligible at room temperature, no autoignition at such condition is observed. This is true even at more favorable conditions, e.g., when more O_2 is converted to O_3.
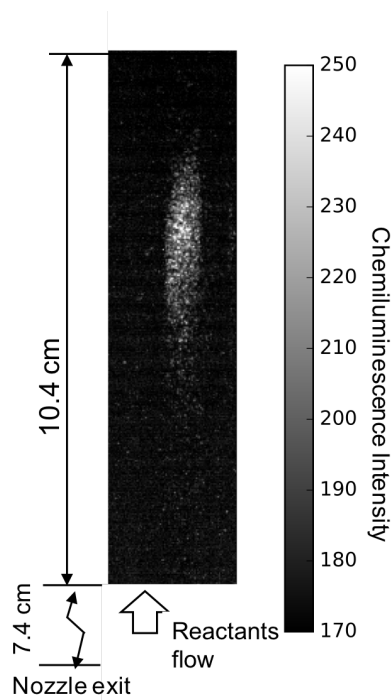
Figure 55. Chemiluminescence passed through a 430 nm bandpass filter at no-flame condition

To confirm that the chemiluminescence from CH_2O^* can be observed in the experiment setup, the reactants are diluted using N_2 so that no autoignition occurs and no flame exists. A temperature rise of approximately 100 K is measured at the exit of the quartz tube. Passed through an optical filter centered at 430 nm, chemiluminescence signal is observable at such condition using a long exposure time (2 ms), as shown in Figure 55. This chemiluminescence is likely to be emitted from CH_2O^*, considering that at this condition the only dominant reaction is ozonolysis and CH_2O is one of its known products. Although CH^* also centers near 430 nm, it is not likely to appear at this low temperature. Simulation conducted using a PLUG flow reactor and USC II mechanism extended with the sub-mechanisms for O_3, OH^*, CH^*, and CO_2^* (Section 3.3.4) shows that at such

condition the mole fraction of CH* is less than 10^{-18} and is not likely to be the major emitter. Similar approaches have been used previously to obtain CH_2O chemiluminescence from the low-temperature flames [142] [145] and the ozonolysis reactions of alkene [143], as discussed in Section 3.1.2

As shown in Figure 54, before the autoignition kernel is formed, a region of weak signals is already formed. Given the above analysis, this chemiluminescence signal is assumed to be emitted from CH_2O^*. This implies that autoignition occurs in such sequence: firstly, oxidizer and fuel are mixed; then ozonolysis starts and releases heat and produces species such as CH_2O; and finally autoignition is initiated by the produced reactive species and released heat from ozonolysis. Furthermore, the location where autoignition kernel is observed is always downstream the location where CH_2O starts to accumulate. These observations also show that autoignition is activated by ozonolysis reactions.
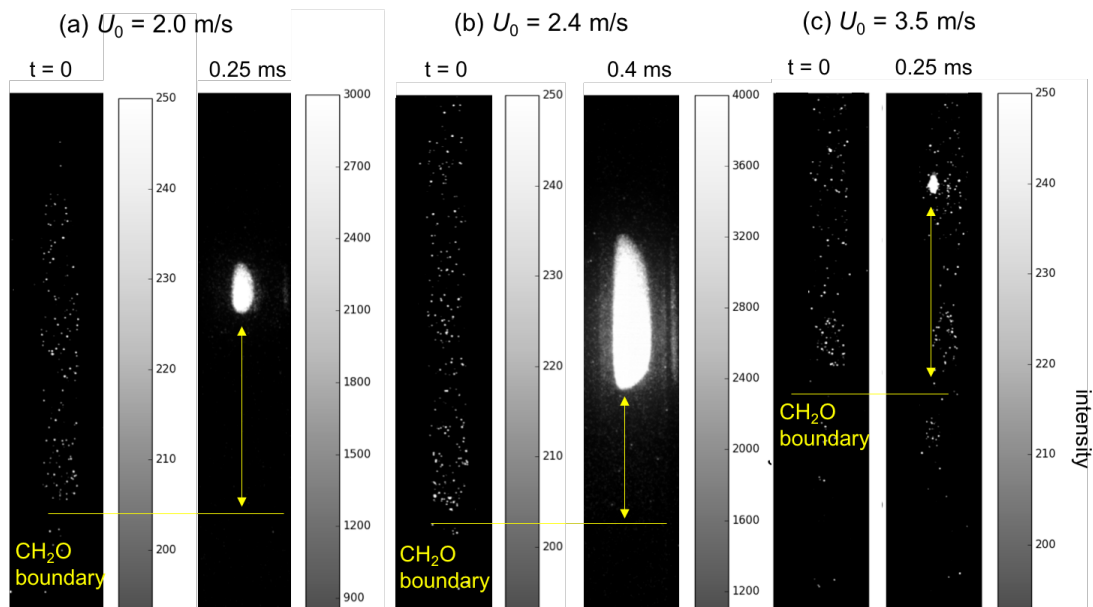
Figure 56. Chemiluminescence passed through a 430 nm bandpass filter before and after autoignition

6.2.3 One-dimensional model

To further investigate the role of ozonolysis reactions, simulation is conducted using the adiabatic steady laminar plug flow reactor model (PLUG) [153]. It is predicted that autoignition occurs at 5.8 cm downstream, as shown in Figure 57. This autoignition is a two-stage process. First stage ignition is activated by the ozonolysis reactions. Only when the temperature becomes sufficiently high (>800 K), the decomposition of O_3 ($O_3+M=O_2+O+M$) and other O_3 reactions become important. This again confirmed that the autoignition is activated by ozonolysis reactions. In fact, if ozonolysis reactions are removed from the chemistry mechanisms, none of these reactions is initiated. As a product of the ozonolysis reactions, CH_2O is produced prior to the significant temperature rise. The peak mole fraction is approximately 1%. This implies it is possible to detect CH_2O chemiluminescence prior to the formation of the autoignition kernel, or even at a no-flame condition (e.g., when the reactants are diluted).
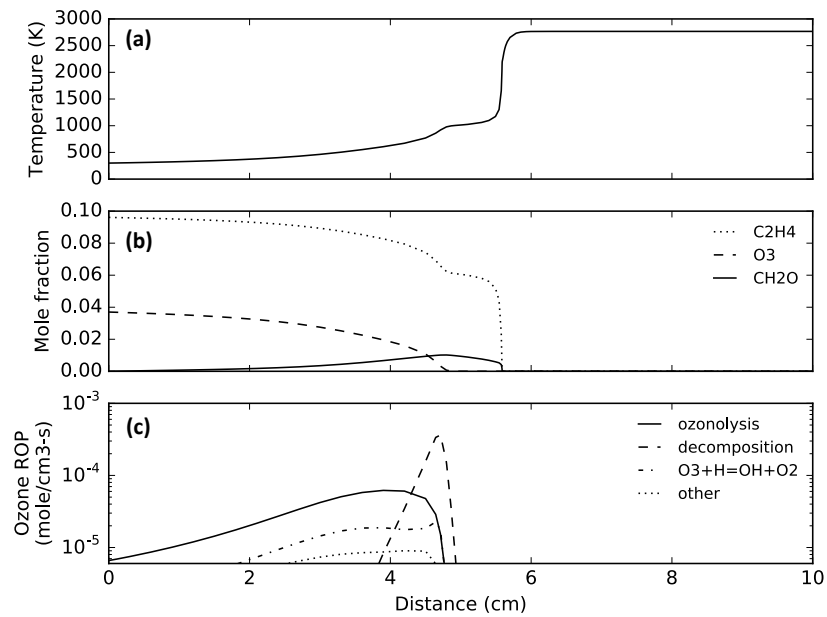
Figure 57. Simulation results of PLUG model

6.2.3 Three-dimensional model

With the skeletal mechanism GPS28, transient simulation is conducted with a 3D model. Similar to the experimental procedure, initially the fluid field is full of oxidizer. The wall for the fuel tube is assumed to be isothermal (temperature fixed at 300 K) because in this experiment this wall is stainless steel and conducts thermal energy rapidly. The outer wall is assumed to be adiabatic, as the quartz tube in the experiment is not highly thermally conductive. The simulation is able to predict some transient phenomena observed in the experiment. For example, the accumulation of CH_2O prior to autoignition is illustrated in Figure 58. At t = 0, the maximum temperature is only 831 K but a CH_2O region has been formed. 2 ms after, a hot spot is formed in the CH_2O region and the maximum temperature rises to 2068 K, consistent with the experimentally observed process shown in Figure 54.
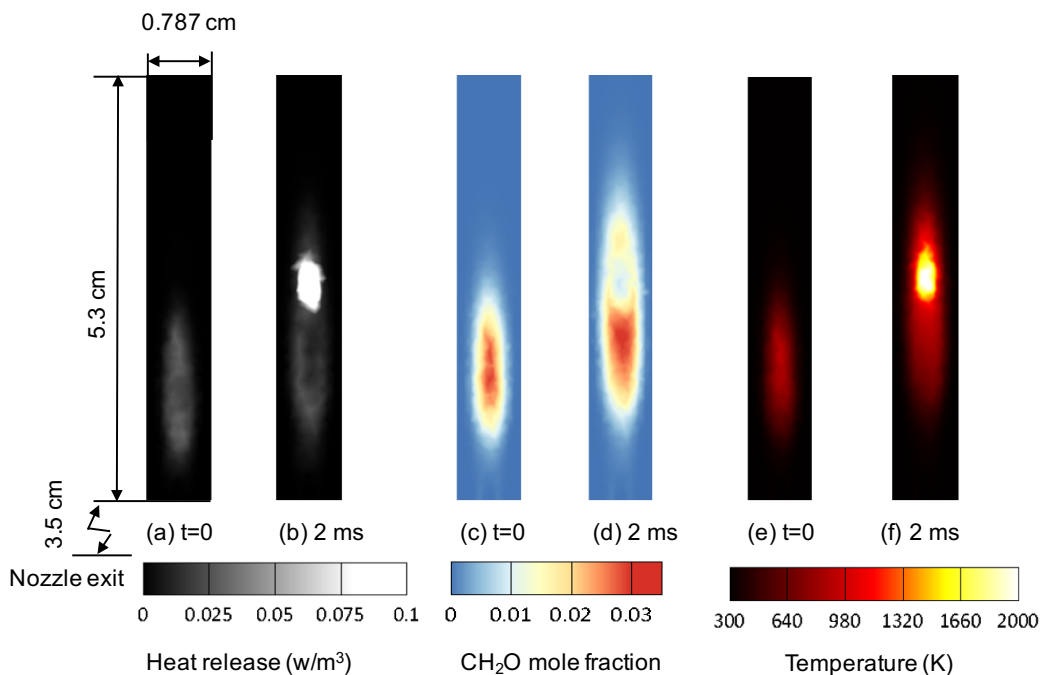
Figure 58. Simulation of the generation of autoignition kernels

6.3   Autoignition timescale

To analyze the effects of various processes (e.g., mixing, chemistry, and flow field) on autoignition quantitatively, the autoignition height, h_{ign}, is measured. This value is defined as the vertical distance between the nozzle exit and the center of the detected autoignition kernel. The autoignition timescale, τ_{ign}, is defined as

$$\tau_{ign} = \frac{h_{ign}}{U_0}$$

The dependence of τ_{ign} on O$_3$ concentration and flow conditions are discussed in the following sections. A jet exit Reynolds number Re is defined based on the velocity difference

$$Re = \frac{\left(U_{\text{jet}} - U_{\text{coflow}}\right)D_{\text{nozzle exit}}}{\nu}$$

where $D_{\text{nozzle exit}}$ is the inner diameter of the fuel tube, and ν is kinematic viscosity.

6.3.1   Uncertainty analysis

Before the measurements, several known sources of uncertainty should be controlled. Firstly, the O$_3$ concentration is not steady due to the uncertainty rooted in the O$_3$ generator. Based on the measurement from the O$_3$ monitor, the uncertainty in O$_3$ mole fraction, $[O_3]$, is estimated to be

$$\frac{\sigma_{[O_3]}}{[O_3]} \approx 2.5\%$$

This induces uncertainty in autoignition delay, which can be estimated using the difference between the simulated autoignition delay at two O$_3$ concentration: $[O_3] + \sigma_{[O_3]}$ and $[O_3] -$

$\sigma_{[O_3]}$, as illustrated in Figure 59. As the autoignition delay decreases rapidly as O_3 increases at low O_3 concentration, the uncertainty decreases with O_3 concentration, and becomes less dependent at high O_3 concentration. Therefore, a high O_3 concentration is expected to reduce uncertainty. For example, to constrain this uncertainty within 10%, at least 7.7 % O_3 should be converted to O_3, which corresponds to 3.7% overall O_3 concentration.
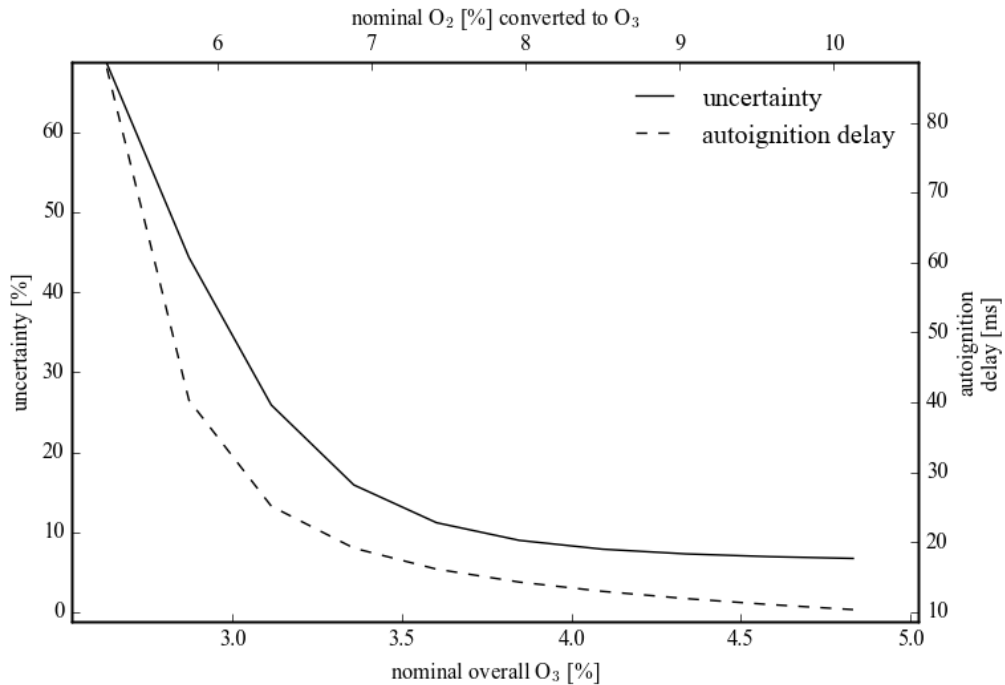
Figure 59. Simulated autoignition delay and its uncertainty due to 2.5% fluctuation in O_3 concentration, as a function of nominal O_3 concentration

Another source of uncertainty is the boundary temperature. For each run of the experiment, autoignition may occur repeatedly. This process may take several seconds. However, each autoignition releases a significant amount of heat, which heats the burner and the quartz tube. For example, an increase of up to 60 K in temperature of the quartz tube after the experiment may be detected. This makes the boundary condition less clear. Therefore, only the data for the autoignition occurs during the first second, since the first

detected autoignition, is recorded. The autoignition events afterwards are discarded, as the boundary temperature at later time may be too far away from the assumed initial temperature, which is 300 K. In addition, after fuel is turned on, the species field is developing before autoignition occurs. Therefore, the first autoignition event is also discarded to minimize such unsteadiness effects.

Uncertainty also exists in the flow velocity. It is estimated that

$$\frac{\sigma_{U_{\text{jet}}}}{U_{\text{jet}}} \approx \frac{\sigma_{U_{\text{coflow}}}}{U_{\text{coflow}}} \approx \frac{\sigma_{U_0}}{U_0} \approx 1\%$$

This uncertainty in flow velocity contributes to the uncertainty in Re and τ_{ign}. Based on the theory on error propagation, we have

$$\frac{\sigma_{Re}}{Re} = \frac{\sqrt{\sigma_{U_{\text{jet}}}^2 + \sigma_{U_{\text{coflow}}}^2}}{U_{\text{jet}} - U_{\text{coflow}}}$$

$$\frac{\sigma_{\tau_{ign}}}{\tau_{ign}} = \sqrt{\left(\frac{\sigma_{h_{ign}}}{h_{ign}}\right)^2 + \left(\frac{\sigma_{U_0}}{U_0}\right)^2}$$

where $\sigma_{h_{ign}}$ is estimated using the standard error of at least 10 measurements.

In the following discussion, error bar is used to represent the interval of $[\mu - \sigma, \mu + \sigma]$, where μ is the nominal value (for Re and $[O_3]$) or the sample mean of measurements (τ_{ign} or h_{ign}) .

6.3.2　Dependence on ozone concentration

The experimentally measured autoignition timescale, τ_{ign}, and autoignition delay simulated using 0D closed adiabatic reactor at different O_3 concentrations are illustrated in Figure 60. The trends for these two timescales are similar: both of them decrease with O_3 concentrations and this dependence is stronger at a lower O_3 concentration. Actually, when the overall O_3 concentration is below 3.4%, no autoignition events were observed. There is a significant difference between these two timescales. This may result from other components not considered yet, such as the mixing process. These factors are modeled and discussed in the following sections.
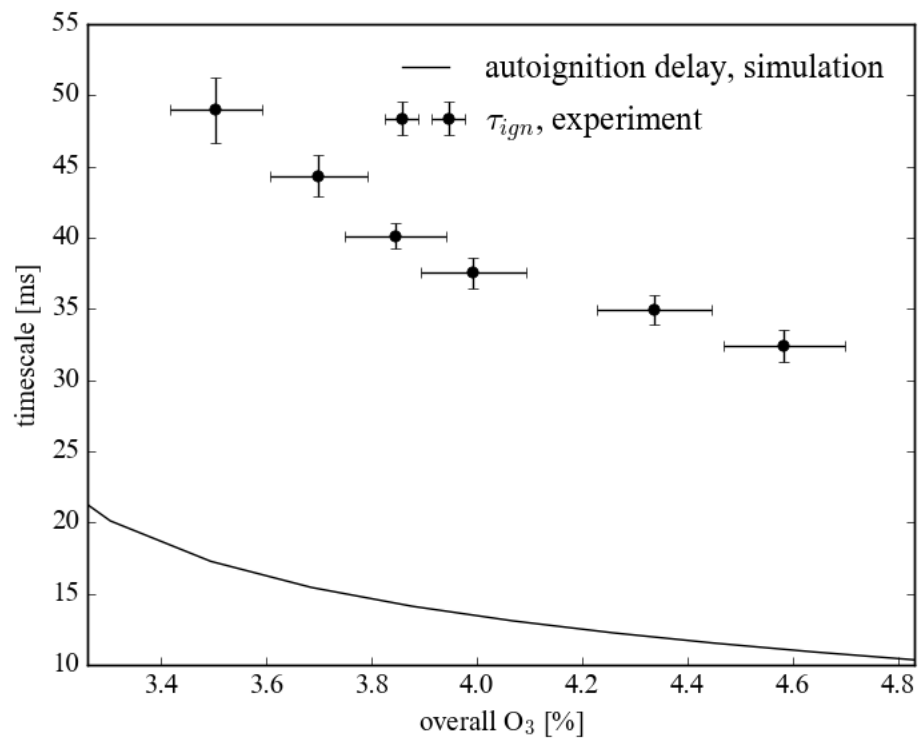
Figure 60. Experimentally measured τ_{ign} and simulated autoignition delay as a function of O_3 concentration

The uncertainty of the experimentally measured results are greater at lower O_3 concentrations, as indicated by the error bars in Figure 60. This is consistent with the trend shown in Figure 59. This supports the assumption that to reduce uncertainty of autoignition timescales from fluctuations in O_3 concentrations, the higher O_3 concentration should be used. However, the maximum measurable O_3 concentration is limited by the O_3 monitor, which can only measure a O_3 mass fraction that is up to 10%. The maximum O_3 concentration is also limited by the O_3 generator, whose capacity to convert O_2 to O_3 decreases as O_2 increases. Therefore, only a narrow window is available. Considering all of these constraints, an overall O_3 concentration of 3.7% is used in the following sections.

6.3.3 Dependence on Reynolds number

The experimentally measured h_{ign} at different Re is illustrated in Figure 61. It is observed that, for $Re < 3000$, h_{ign} increases monotonically with Re (and U_0), but then decreases slightly as Re further increases. Because of the limitations of O_3 generators, the highest Re reached is 3000 in the experiment. The initial increase of h_{ign} with Re is expected as a higher flow velocity implies the reactants need to travel a longer distance before being autoignited. The decrease of h_{ign} with Re when Re is above 3000, however, deserves further investigation on τ_{ign}.
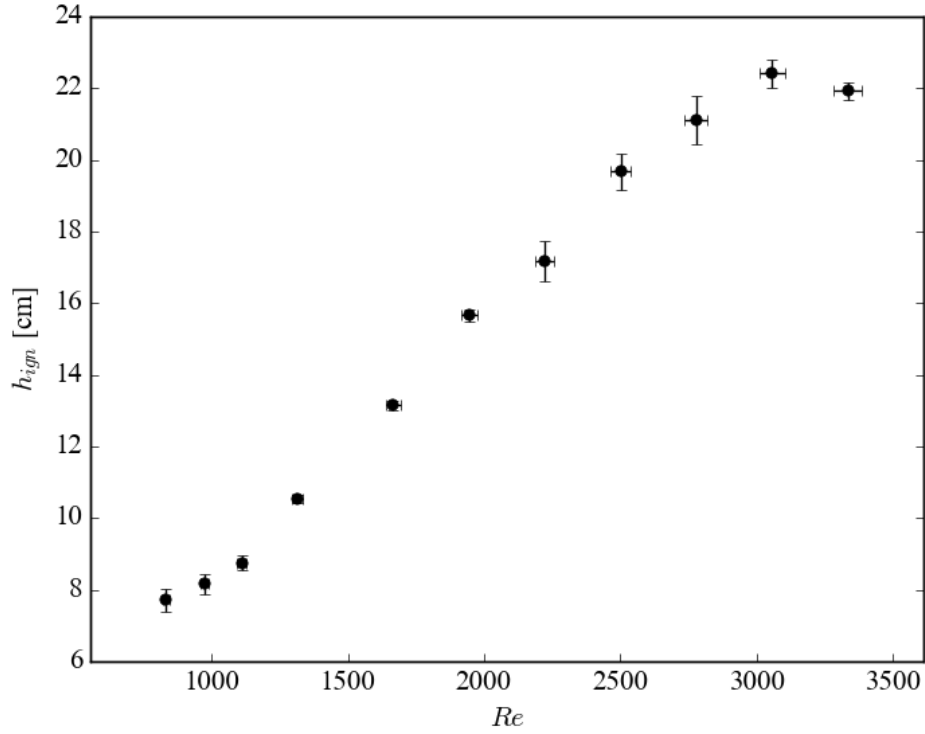
Figure 61. h_{ign} as a nonlinear function of *Re* and U_0

More details can be revealed if the autoignition timescale, instead of autoignition height, is considered. As shown in Figure 62, the autoignition timescale firstly decreases with U_0, then it becomes less dependent on U_0 (see the plateau for *Re* = 1250 ~ 2000). But as *Re* further increases to more than 2500, the autoignition timescale starts to decrease again. This nonlinear trend is discussed and modeled in the following sections.
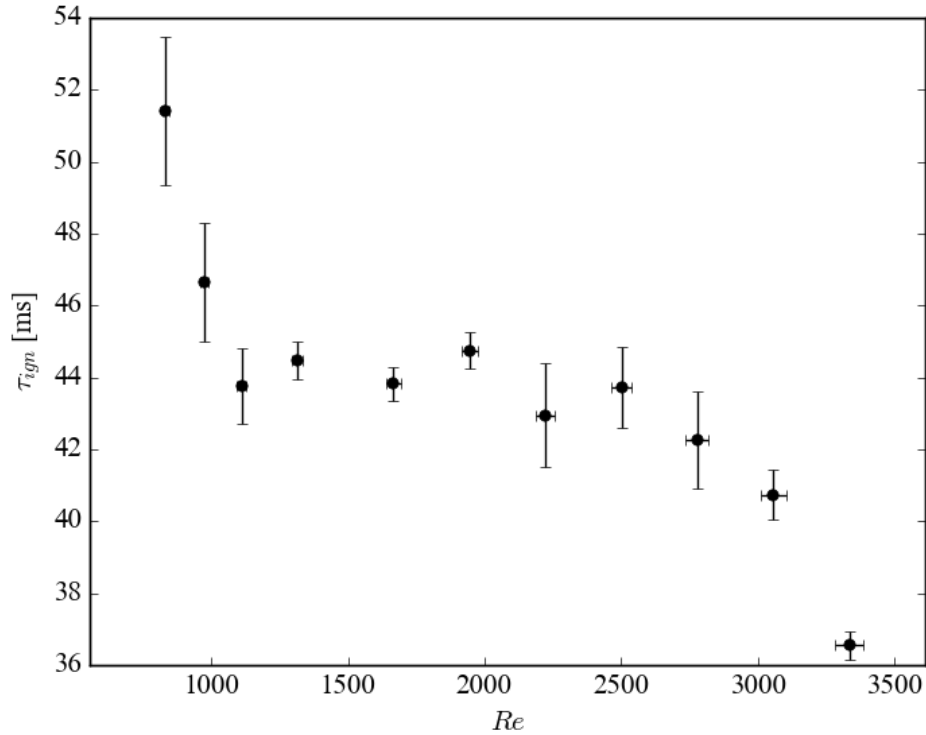
Figure 62. τ_{ign} as a nonlinear function of *Re* and U_0

6.3.4 A two-factor laminar model

This section discusses a simplified model to predict τ_{ign}. Only two factors, mixing and chemistry, are considered. To estimate the mixing timescale, a non-reacting model is built using FLUENT software [154]. The contour of the mixture fraction, *Z*, at the centerline slice is shown in Figure 63. The stoichiometric iso-surface (calculated based on all C, H, O atoms) is referred as $Z=Z_{st}$. If the reactants are well mixed, Z should be nearly homogenous at the corresponding cross section. Therefore, one possible definition (and the one chosen in this section) of the mixing distance, h_{mixing}, is the distance between the tip of this iso-surface and the nozzle exit. At the cross section where this tip point belongs, the

102

maximum difference in Z is Z_{st}, which is 0.19. This value is much lower than the maximum

difference in Z at the inlet, which is 1, indicating a significant level of mixing. So a mixing

timescale can be defined as $\tau_{mixing} = h_{mixing} / U_0$.
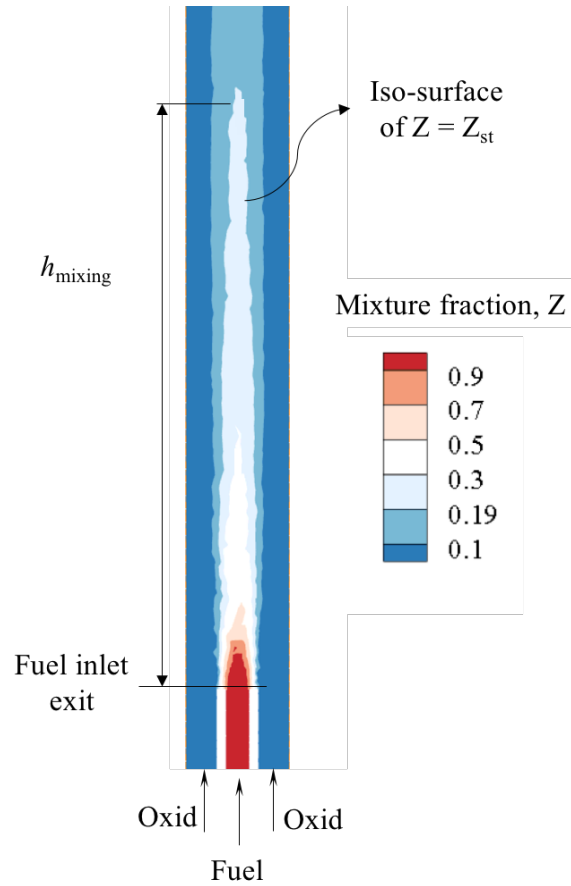
Figure 63. Contour of Z for non-reacting simulation results

For the chemistry timescale, a SENKIN reactor [152] is used for estimation. The

initial reactants are the mixture of fuel and oxidizer, mixed based on the flow rate of fuel

and oxidizer in the experiment. The initial temperature is 300K and the burner pressure is

1 atm and kept constant. The chemistry timescale, τ_{chem}, is approximated by the autoignition

delay, which is defined as the time corresponding to the temperature rise of 1000 K.

Based on these definitions, τ_{mixing} and τ_{chem} are compared with the experimentally measured autoignition timescale, as illustrated in Figure 64. The interesting trend is that, the mixing timescale decreases with U_0. The reason is that, unlike free jet, for the present setup, the width of the jet is constrained by the quartz tube. This does not allow the jet width to grow as quickly as the jet height. The constrained width actually allows mixing to be faster in the radial direction. For this reason, the mixing timescale is shortened at higher U_0. The chemistry time is computed using the homogenous reactor, as mentioned above; therefore, for this model, it is assumed to be independent of flow parameters, U_0 or Re. Therefore, it is a constant line as shown in Figure 64.
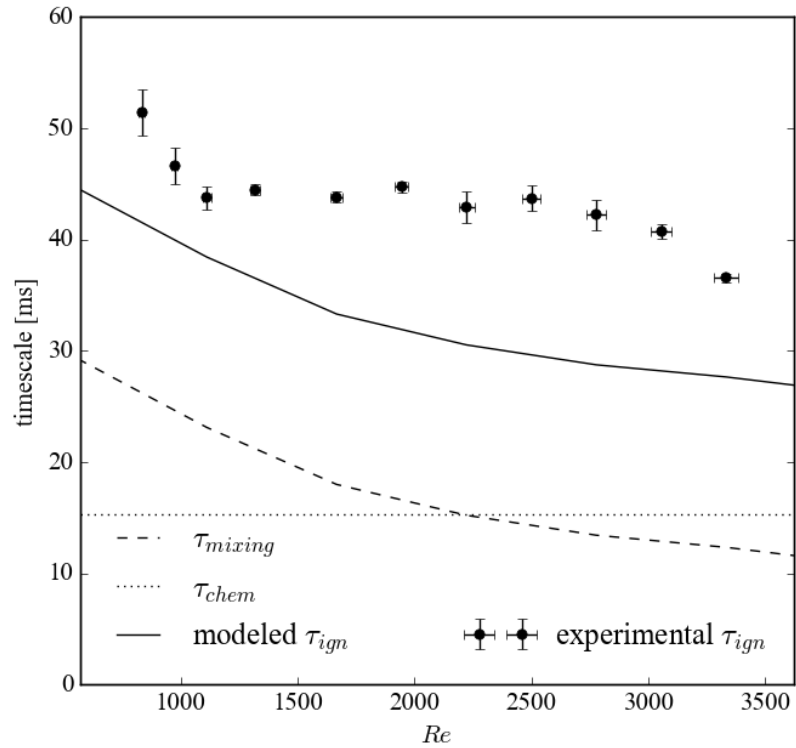
Figure 64. Timescales experimentally measured and predicted by the two-factor model

Assuming the autoignition process is only significant when the reactants are partially mixed, an estimation of the autoignition timescale is

$$\tau_{ign} = \tau_{chem} + \tau_{mixing}$$

as shown in solid line in Figure 64. This modeled autoignition timescale is of a similar magnitude. Furthermore, it captures the general negative relation between τ_{ign} and U_0. The two-factor model has suggested that, one contributor for this trend is the fact that the mixing timescale decreases with Re because of promoted mixing at higher U_0 utilizing at the present experimental setups. Such effects become less significant at higher U_0 as indicated by smaller slope at high U_0. This is consistent with the plateau observed in experimental results.

It is worthy to mention that, τ_{chem} and τ_{mixing} are of the similar order, which implies that the corresponding Damköhler number is on the order of 1. This suggests that the studied combustion process in autoignitive condition is controlled by autoignition. Previous simulation study of the jet-in-coflow configuration by Lu et al [119] obtained similar results and concluded that the important role of autoignition in stabilization of lifted jet flame.

6.3.5   3D model and the effects of turbulence

Homogenous distribution of species, temperature and other chemical-thermal properties were assumed when estimating the chemistry timescale in the two-factor model. However, inhomogeneity is the case for non-premixed jet flames. To take these factors into consideration, 3D model is built for laminar and turbulent cases, where fluid and chemistry are simulated simultaneously. The geometry model and grid are exactly the same with the

3D laminar model, but the k-ε turbulent model is used. This simplified simulation model provides an estimation of the limiting case when turbulence is well developed. The root-mean-square (RMS) velocity fluctuations calculated using this model is approximately 7% of the local velocity magnitude. As shown in Figure 65, the mixing timescale for the turbulent case is much shorter than that of the laminar case. This confirms that faster mixing at turbulent conditions, and provides an explanation for the decrease of τ_{ign} as Re increases.
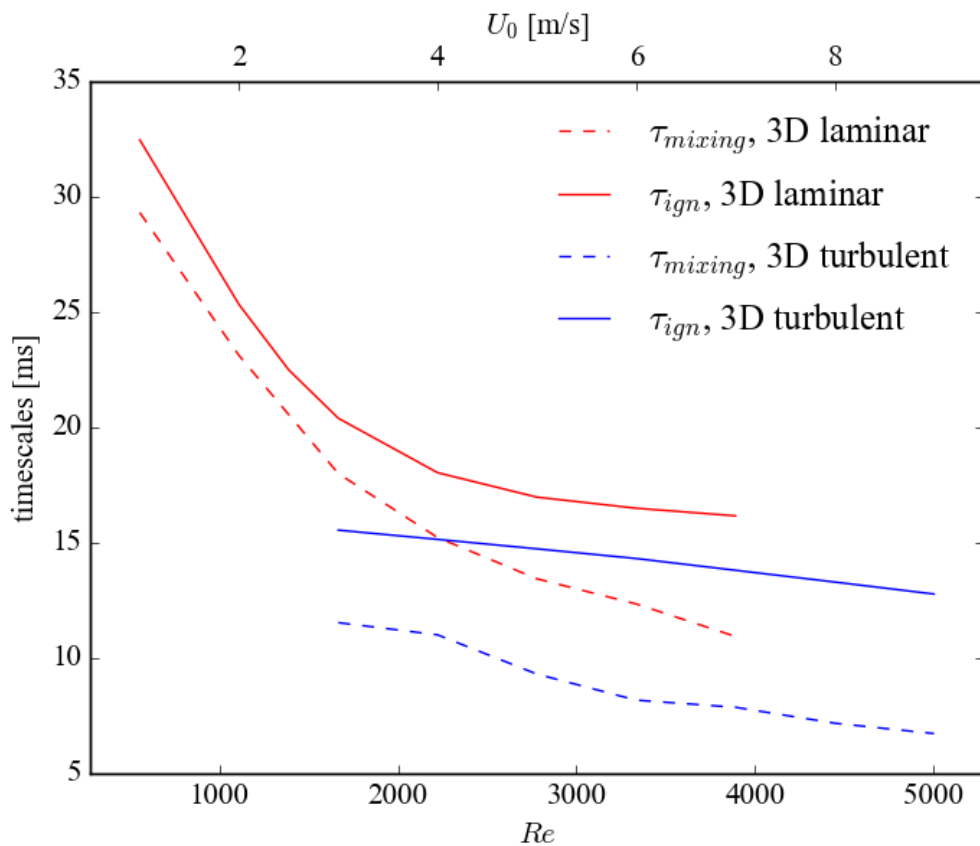
Figure 65. Timescales predicted by the 3D laminar and turbulent models

To further confirm the effects of turbulence, the experiments are repeated with two layers of mesh (from McMaster-Carr) to promote turbulent flow. This mesh is made of

stainless steel wire. The size of the holes on the mesh is approximately 0.6 mm. The open area is approximately 50%. It is placed between the outer wall of the center tube for fuel and the inner wall of the oxidizer coflow tube. The vertical distance between the mesh and the fuel tube exit is approximately 1 cm. Coflow (oxidizer) passes through this mesh before it mixes with the fuel. This mesh is expected to trigger turbulence earlier. The autoignition timescale is measured with this mesh employed and the results are shown in Figure 66. It is observed that, for large Re, adding this mesh significantly decreases the autoignition timescale. For example, at Re = 2750, the autoignition timescale is approximately 41 ms, but with mesh employed, this value is decreased to 35 ms. For lower Re, in contrast, the effect of mesh is less significant. For example, at Re = 1200, adding mesh essentially does not change the autoignition timescale. This is expected, as at low Re, turbulence should not be significant, even with mesh. The observation that autoignition timescale decreases at high *Re* when mesh is employed confirms that turbulence is responsible for faster autoignition.
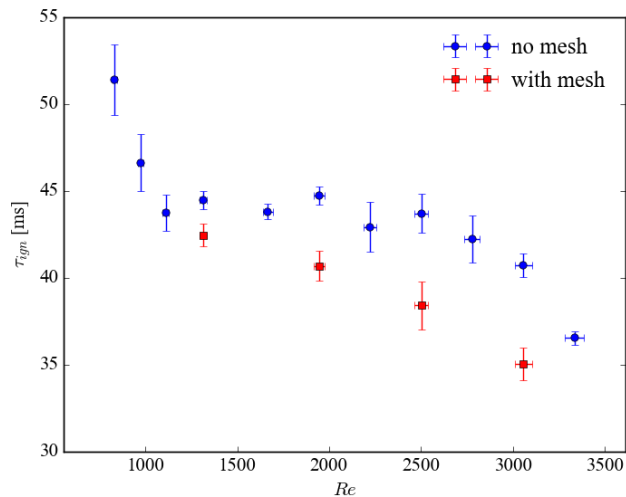
Figure 66. τ_{ign} experimentally measured and predicted by the two-factor model

CHAPTER 7 THE EFFECTS OF OZONOLYSIS ON FLAME STABILIZATION

7.1   Introduction

At proper conditions, ignition happens spontaneously at room temperature. It is expected that, at autoignitive conditions created by hot coflow, the flame dynamics may become different [117, 119, 129]. This may enhance flame stabilization. This possibility is explored in this chapter.

7.2   Experimental phenomenon and discussion

The autoignition and subsequent flame dynamics are investigated at the following flow conditions. The ratio of N atoms and O atoms (including these in O_2 and O_3) in the oxidizer jet is N/O = 0.28. This value is much lower than that in air to allow autoignition at room temperature. The overall equivalence ratio (calculated using the number of C, H, and atoms in the well-mixed reactants) is ϕ = 0.4. 7.7% of O_2 is converted to O_3 and this corresponds the mole fraction of O_3 in total reactants of 3.7%. The adiabatic 1D laminar flame speed, S_L, at such condition obtained using PREMIX [84] model is approximately 2 m/s when ozonolysis reactions are not included in the chemistry mechanism. A nominal velocity scale, U_0, is defined to quantify the flow field. It is the ratio of the total flow rate of the reactants to the cross-section area of the quartz tube.

A typical result is illustrated in Figure 67 at the condition of U_0 = 2.37 m/s. This chemiluminescence signal is recorded directly using the high-speed camera at 4000 frames

per second. At t = 0, the first detectable autoignition kernel (Kernel-1) is generated at approximately 11.5 cm downstream of the burner exit. This distance between the autoignition kernel and the nozzle exit is labeled as h_{ign}. 0.25 ms after that, a second autoignition (Kernel-2) is generated upstream of Kernel-1 (distance from Kernel-2 to the nozzle exit is approximately 7.0 cm). Both kernels start to grow and finally they merge. During t = 1.5 to 2 ms, the downstream part of this merged reacting zone burns out, while the upstream part evolves to a flame structure similar to a Bunsen flame. Finally, this flame propagates back to the nozzle exit.
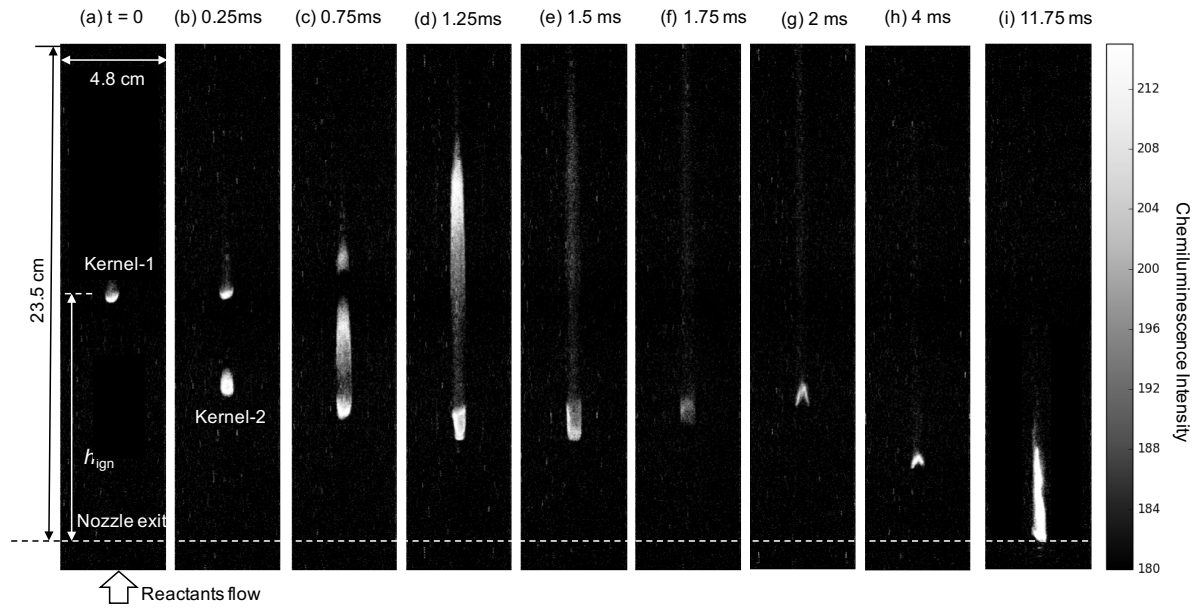
Figure 67. Direct chemiluminescence from a flashback process

The reactants at this condition do not autoignite if no O_2 is converted to O_3, or if the fuel is replaced by the species that has negligible ozonolysis reactions at room temperature such as CH_4. This confirmed that the autoignition kernel is activated by the explosive

109

ozonolysis reactions of C_2H_4. Besides the autoignition, ozonolysis may promote the flashback of the reacting zone in several ways: autoignition-assisted "propagation" and "jump" of flame front, which is discussed in the following sections.

7.2.1 Autoignition-assisted "propagation"

During t = 0.25~1.25 ms of the process shown in Figure 67, the propagation of the front of the reacting zone is also extremely fast (~20 m/s). It is not likely to be a conventional flame propagation. In fact, the upstream reactants are already reacting prior to the arrival of the flame front. Therefore, it's reasonable to expect that at the upstream, reactive species already exist and temperature already rises. So this propagation mechanism can be referred as "autoignition-assisted propagation." In contrast, the conventional flame propagation relies on the diffusion of the radicals and thermal energy.

To extract more details, the experiment is repeated with the intensifier and the bandpass filter centered at 430 nm. This filter allows the chemiluminescence from CH* and CH_2O* to pass through. Images are taken at a frame rate of 2500 Hz and gate exposure time of 0.2 ms, and illustrated in Figure 68. A weak emission zone is formed prior to the formation of the high-intensity zone. As discussed previously in Section 6.2.1, this zone indicates accumulation of CH_2O, which is a major product of ozonolysis. It is observed that, once the autoignition kernel is formed, the front propagates back at a very high speed (~12 m/s) during t = 2~3.6 ms. This fast propagation slows near the location of upstream boundary of the CH_2O emission zone. This implies that the high propagation speed is due

to the products and heat released from the ozonolysis reactions upstream. Once the flame propagates back to the location before ozonolysis happens, the propagation slows down.
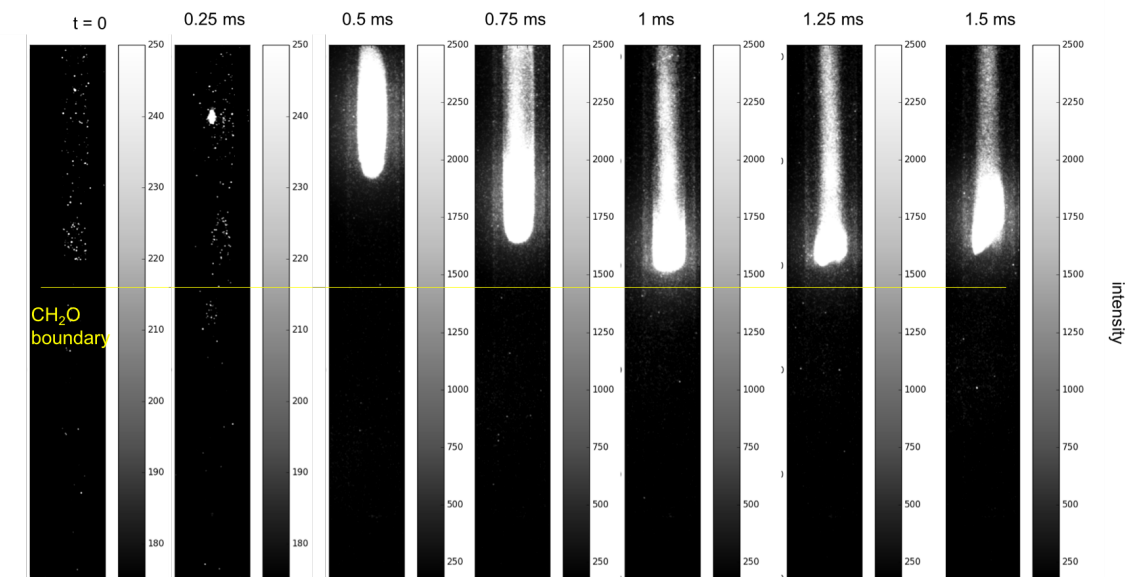
Figure 68. Chemiluminescence filtered at 430 nm from the autoignition-assisted "propagation" process

The reactions occurring upstream of the flame may enhance the propagation in two ways. Firstly, due to ozonolysis and subsequent reactions, fuel is "pre-processed" before entering the flame. This changes the reactivity of the reactants, and may increase the flame speed. A similar idea has been employed previously in the studies on the fuel preprocessing using O_3 addition to control the reactivity [42, 43].

A simple 1D simulation is conducted to study this fuel "preprocessing" effect due to ozonolysis reactions. A PLUG [153] flow reactor is used to calculate the composition and temperature of the reacting flow prior to the flame. The inlet velocity is fixed at 2.37 m/s. The length of the PLUG flow reactor is varied so that different amounts of fuel are "preprocessed." Then the reactivity of this thermal-chemical state is quantified by

calculating its mass burning rate using the PREMIX model [84]. That is, the exit of PLUG is the inlet of the PREMIX model. Both reactors are adiabatic. However, for PREMIX, the gradient should vanish near the inlet, as mentioned in Section 3.3.3. To avoid violating such requirements, ozonolysis reactions are not included in PREMIX, and PREMIX is not applied for the cases where the PLUG ending temperature is greater than 700 K. As shown in Figure 69(a), as the length of the PLUG flow reactor increases, a greater amount of fuel is consumed ("preprocessed"). The change in composition results in heat release, indicated by higher temperature. Due to such "pre-processing," the mass burning rate of the reactants become higher. This is illustrated in Figure 69(b). When 15% of the fuel is preprocessed, corresponding to the PLUG flow reactor length of 4 cm, the mass burning rate is increased by 115%. This confirms that the mass burning rate is increased due to fuel "preprocessing" due to ozonolysis.
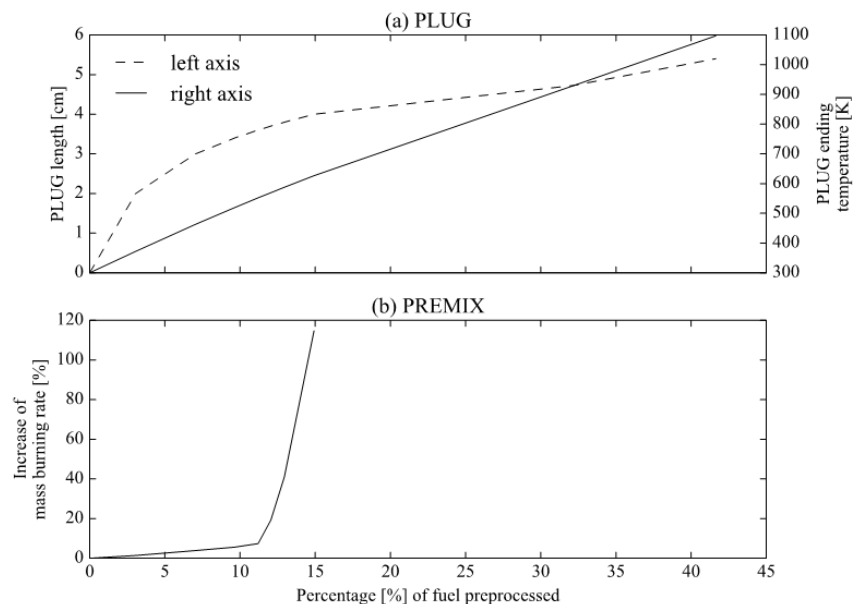
Figure 69. Effects of fuel preprocessing by ozonolysis estimated using 1D model. (a) PLUG flow reactor, and (b) PREMIX (exit of PLUG is used as inlet of PREMIX)

7.2.2   Jump of flame front

During t = 0~0.25 ms of the process shown in Figure 67, the co-existence of the multiple kernels shows a dynamic different from the conventional laminar jet flame theory. The generation of Kernel-2 effectively moved the height of the reacting zone front from 11.5 cm to 7.0 cm from t = 0 to 0.25 ms. This "jump" of flame front corresponds to a "propagation" speed of 180 m/s. This is on the order of 100 times S_L. This dynamic with such extremely high "propagation" speed is controlled by autoignition. In contrast, the conventional laminar jet flame is controlled by flame propagation and the propagation speed is on the order of S_L.

7.3   Semi-one-dimensional unsteady simulation

Simulations can provide insight by creating a simplified flow field, such as the 1D case. However, the conventional 1D model, PREMIX [84], is only applicable for steady simulation and cannot be applied for the current autoignitive conditions. Therefore, a semi-1D unsteady model is built using FLUENT software [154]. The geometry of this model is a tube of square cross-section, as illustrated in Figure 70. The side length of the cross-section square is 1 cm and the length of the tube is 15 cm. A velocity inlet boundary condition is used, which means the inlet velocity and composition are fixed. The second one is the mass flow inlet, which means the mass flow at the inlet is fixed. The boundary condition (BC) for the outlet is pressure out, meaning the pressure is fixed (at 1 atm). The four walls of the tube are assumed to have symmetric BC rather than wall BC. The purpose is to avoid the wall effects so that this 3D model can act similar to a 1D model.
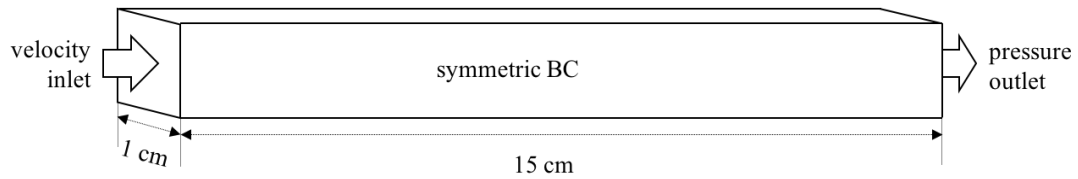
Figure 70. Geometry of the semi-1D model

To validate this semi-1D model, firstly, the simulation results are conducted without including ozonolysis reactions. The results are illustrated in Figure 71. It shows that the results are homogenous within the cross section, indicating this semi-1D model is close enough to a 1D model. S_L at the current condition is found by varying the inlet velocity. When the inlet velocity is greater than 2 m/s, the flame blows out, while the velocity is smaller than 2 m/s, the flame flashes back. This confirms that S_L found using this semi-1D model is similar to that found using PREMIX [84] model, which is 2 m/s.
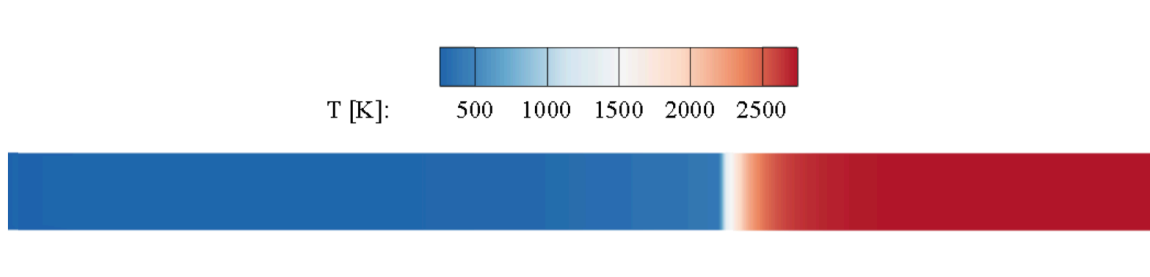
Figure 71. Temperature countour of the semi-1D model

After being validated, this semi-1D model is used to model the autoignition-assisted propagation. At t = 0, flame is established at approximately x = 5.4 cm (defined as the location of T = 1000 K) without including ozonolysis reactions. The corresponding temperature profile is shown by the solid line in Figure 72. Then, ozonolysis reactions are included. The heat released from and products produced by ozonolysis accumulate. After 8 ms, the temperature upstream of the original flame position has been raised to

114

approximately above 900 K, as shown in Figure 72(a). The temperature profile also changes. At t = 0, temperature suddenly increases near x = 5.4 cm. But with the ozonolysis reaction, at t = 8 ms, the temperature increases gradually before the flame. The ozonolysis products, such as CH_2O, also accumulate. As shown in Figure 72(b), the peak CH_2O mole fraction has increased from 0.2% to 1%. Then the flame suddenly propagates back. At t = 10 ms, the location of the flame front has moved from x = 5.3 cm to 3.3 cm. This implies that, due to ozonolysis reactions, the flame has moved by 2 cm within 2 ms, corresponding to a "propagation" speed of 10 m/s. This is consistent with the experiment observations.
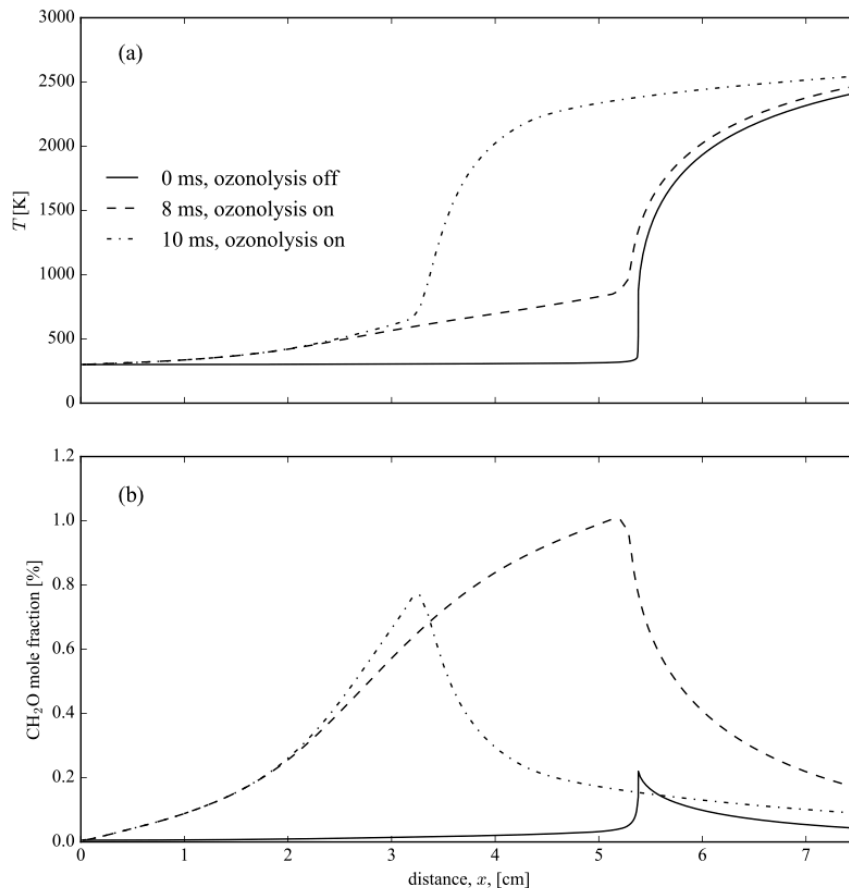
Figure 72. Semi-1D results corresponding to propagation-assisted propagation: Profiles of (a) temperature, and (b) CH₂O mole fracton

The propagation speed during t = 8~10 ms is on the scale of five times of the flame speed without ozonolysis reactions. This fast propagation is fundamentally different with the conventional flame. As shown by the above simulation results, at such autoignitive conditions, the reactants are reacting before they meet the flame sheet. In other words, this region is in the early stage of autoignition. Therefore, the reactive species and temperature rise in this region are not limited by the diffusion process as in a conventional flame. This allows the propagation to be much faster than the conventional flame. To summarize, as the controlling mechanism changes from diffusion to autoignition, the propagation speed of autoignition-assisted "propagation" is several times higher than that of a conventional flame.
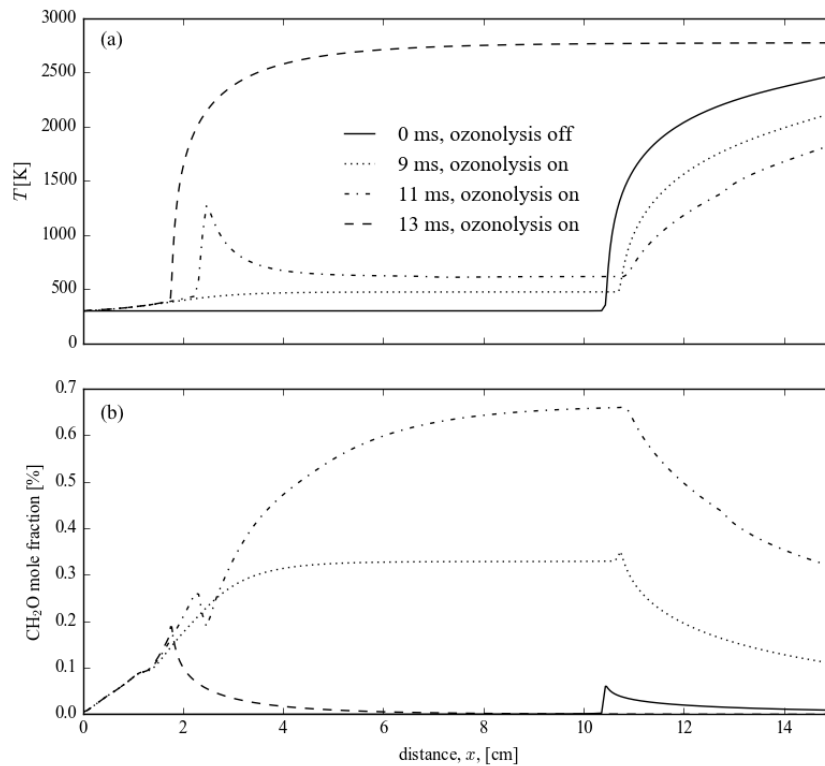
Figure 73. Semi-1D results corresponding to the "jump" of the flame front: Profiles of (a) temperature, and (b) CH₂O mole fraction

This semi-1D model is then used to mimic the "jump" of flame front. The simulation is repeated, as shown in Figure 73. The initial flame is set to a position that is farther away from the inlet compared to the previous case (from x = 5.4 cm in Figure 72 to x = 10.5 cm Figure 73). This allows the upstream autoignition before the original flame propagates back and mimics the jump of flame front. Similar to the previous case, ozonolysis reactions are only included for cases t > 0. As time passes, reactants at the upstream of flame starts to react, indicated by the rise in temperature shown in Figure 73(a), and the accumulation of intermediate species such as CH_2O, shown in Figure 73(b). This differs from the previous case shown in Figure 72, since as the distance between the original flame and the inlet is sufficiently long, an autoignition kernel is formed near x = 2.5 cm at t = 11 ms. Finally, this new burning zone merges with the original flame, and a single flame remains at t = 13 ms. The flame front "jumps" from x = 11.4 cm at t = 11 ms to x = 1.8 cm at t = 13 ms. This corresponds to a "propagation" speed of 48 m/s, and the jump of flame front phenomena observed.

CHAPTER 8 CONCLUSIONS

8.1   Contributions

This dissertation investigates the effects of O_3 addition on some fundamental combustion processes, to serve as a basis for future application of O_3 addition on practical combustion systems, such as engines operating at extreme conditions

For the effects of O_3 addition on premixed laminar flame propagation, the present results provide a more comprehensive understanding. Previously, the dependence on pressure, initial temperature, and fuel kinetics of flame propagation is not clear. This issue is addressed in this dissertation for small-molecule fuel species in this dissertation. Furthermore, there was conflicts in the previous studies regarding the effects of O_3 addition on C_2H_4 flame propagation. Such conflicts are revolved in this study by analyzing the ozonolysis reactions, which are absent in previous studies.

In addition, this dissertation demonstrates ozonolysis reactions as an alternative way to create a platform for fundamental research on flames in autoignitive environment. Previously, autoignitive conditions were primarily created using a jet in hot coflow. Compared to this method, ozonolysis reactions provide a more controlled way, as the O_3 concentration can be easily and rapidly adjusted. A non-premixed burner is presented as a demonstration, and the major conclusions are summarized in the following sections.

8.2   The effects of ozone addition on laminar premixed flame propagation

The effects of O_3 addition on the propagation speed are investigated with considerations on fuel kinetics, O_3 concentration, pressure and initial temperature. Regarding the pressure dependence, high-pressure Bunsen flame experiments in the present work showed that the alkane enhancement increases with pressure. The stoichiometric CH_4/air S_L for 6334 ppm O_3 addition was increased from 7.7% at atmospheric pressure to 11% at 2.5 atm. Simulations indicate that this is due to the O_3 decomposition becoming a faster and a more dominant step in O_3 concentration. Therefore, O atoms can be released faster to attack the fuels. This positive relationship between enhancement and pressure makes O_3 addition an attractive technique for high-pressure applications.

Regarding the dependence on initial temperature, simulation results show that adding O_3 at higher initial temperature is not as effective as that at lower initial temperature. If the initial temperature is further increased, O_3 may be decomposed before entering the flame, then O cannot be released in the flame to act as a chain initiation step. Consequently, adding O_3 can only slightly enhance the propagation. This suggests that, to enhance flame propagation with O_3 addition, one should either apply it with a low initial temperature, or restrict the residence time to minimize the decomposition of O_3 before it is transported to the flame.

To account for the fuel kinetics, unsaturated hydrocarbons are considered. While O_3 reacts very slowly with alkanes at room temperature, this is not true with C_2H_4. Instead, a large portion of the O_3 is consumed as it mixes with C_2H_4 through ozonolysis reaction. If the heat from this reaction is lost (and not available to the flame), S_L, reaction rates of fuel

oxidization, and flame temperature decreases. If such loss of energy is minimized by freezing the ozonolysis reactions, either by cooling the reactants to 200 K or decreasing the pressure to 0.53 atm, an increase in S_L was observed after O_3 addition.

8.3   The flame in autoignitive environment created by ozonolysis reactions

Ozonolysis reactions is proposed as an alternative way to create the platform for the fundamental research on flame in autoignitive environment. With this platform, ozonolysis activated autoignition is studied. Images of filtered chemiluminescence show that the ozonolysis product, CH_2O, always accumulates before autoignition happens, which confirms that ozonolysis reactions initiate autoignition. The autoignition timescale, τ_{ign}, is further investigated quantitatively. A jet exit Reynolds number Re is defined based on the difference of jet and coflow velocity and the jet nozzle exit inner diameter. Overall, τ_{ign} decreases with Re. At low Re, this trend is explained by the inverse relation between mixing timescale and flow velocity observed using a non-reacting 3D model. At higher Re, this trend is attributed to the promoted mixing due to turbulence, and confirmed experimentally. Similar to previous studies [116, 126] using jet-in-hot-coflow configuration, there exists a large uncertainty of the autoignition location.

Due to ozonolysis reactions, fuel can be "preprocessed" and reactivity is observed to be increased, in terms of increased mass burning velocity. Also the radicals are generated and thermal energy is released locally, so that the propagation is not solely controlled by the diffusion process. This enhances the propagation by more than 10 times. Similar to previous studies [126], it is possible to observe several autoignition kernels at the same time, which merged rapidly to a connected combustion zone. This effectively move the front of existing combustion upstream at a significant speed. The autoignition kernels and

propagation enhanced by fuel preprocessing are due to the autoignitive conditions created by ozonolysis reactions. It is the important difference with the classical jet flames at non-autoignitive conditions.

Chapter 9

FUTURE RECOMMENDATION

9.1   Detailed ozonolysis kinetics

As introduced in Chapter 1, the detailed pathways of ozonolysis reactions are still not clear. However, an accurate ozonolysis chemistry mechanism is important to analyze and simulate O_3 assisted combustion for unsaturated hydrocarbons. Previous studies suggest that several pathways may exist in parallel. It is not clear how different pathways affect the combustion process differently. It is possible that such effects are dependent on local conditions, including temperature, pressure and composition. Therefore, a study conducted under wide range of operating conditions relevant to practical combustion system is recommended.

9.2   Dependence on fuels

In the present work, only several fuels of small molecules are investigated (CH_4, C_3H_8, and C_2H_4). It is not clear just how conclusions changes if fuels of a larger molecule, or fuels of a different functional group such as aromatics, are applied. For large molecules, generally they break down into smaller molecules before entering into the strong burning state. However, when O_3 is added, ozonolysis reactions, if rapid enough, may fundamentally change this pattern. Such a possibility deserves further investigation. Furthermore, the effects of O_3 addition on the multi-component fuel are also not clear.

9.3   Experimental techniques

Regarding future studies on jet dynamics with O_3 addition, non-intrusive flame diagnostics techniques are recommended in future work to extract more details from experiments. These include, but are not limited to, planar laser-induced fluorescence (PLIF) and particle image velocimetry (PIV). Simultaneous measurements of temperature field, velocity field, species concentrations for a marker species for the hot flame (e.g., OH) and a marker for the ozonolysis-dominant zone (e.g., CH_2O) are expected to provide a more comprehensive picture.

As mentioned in Section 6.3.1, the temporal fluctuation in the O_3 concentration produced using an industrial O_3 generator can introduce uncertainty. In future work, efforts are recommended to reduce such uncertainty. One possible method is to store the generated well-mixed O_2/O_3 gas mixture in a vessel, such that the inlet O_3 concentration is not affected by the O_3 generator. However, safety issues must be carefully considered. High concentrations of O_3 may lead to an explosion due to O_3 decomposition.

Appendix. GLOBAL PATHWAY SELECTION ALGORITHM

A.1 Introduction

This chapter introduces an efficient algorithm for mechanism reduction. It is applied to generate reduced mechanism for 3D simulation of O_3-assisted combustion in Chapter 6 and 7. Before the detailed introduction of the algorithm, a review of previous works are presented.

A.1.1 State of the art

A great number of systematic methodologies have been proposed to alleviate the computational complexity while still retaining acceptable accuracy. The general rationale behind these approaches is to reduce the dimension of the system. This can be done with timescale decoupling, for example, using Computational Singular Perturbation (CSP) [163-165]. The dimension can also be reduced by mapping the complex chemical solution to states parameterized by a small set of state variables (tabulation, or "storage and retrieval" scheme), e.g., Intrinsic Low-Dimensional Manifolds (ILDM) [166-169], and progress variables with flamelet-based approaches [170-173]. Another kind of low-dimension representation of a chemical kinetic system is the skeletal mechanism. A set of species and elementary reactions is trimmed from the detailed mechanism if the removal does not induce significant error.

Different strategies are available to detect the redundant set for the generation of skeletal mechanisms. The first strategy is the sensitivity analysis. This method detects the potential redundant reaction/species by, for example, calculating the error after cutting the reaction rate [174], or removing species [175, 176]. Although this approach provides very

effective results, the process is extremely time consuming. Because of the coupling relationship between species, the redundancy does not satisfy additivity. For example, removal of species A and removal of species B is safe if done separately, but may be disastrous if done at the same time. Therefore, the sensitivity analysis needs to examine a great number of combinations and this usually is a brute-force method.

To explicitly calculate the error directly is time consuming; therefore, approaches have been proposed to estimate the importance of the species and/or elementary reactions. Strategies have been proposed to pick up species whose "score" is above some threshold. For example, methods are proposed to eliminate the reactions not contributing significantly to the heat production [177], or the total entropy production [178]. The score can also be defined by the relationship between species. One approach is to examine the element flux between species, a concept first proposed by Revel *et al*. [179] and then adapted in the studies [180-183] by Androulakis and coworkers. In these works [180-183], any pair of species is retained in the skeletal mechanisms if the element flux between them is greater than the threshold (hereafter "pair element flux method"). Another approach was developed by Zhao *et al*. [184] recently. It is based on the "betweenness centrality" (BC), a concept that originally emerged in social network research in the 1970s. BC is adapted in this work to measure the frequency of a species to serve as a hub between a given pair of species, based on identified shortest chemistry pathways. The species of highly ranked BC values are retained to generate the skeletal mechanism.

Besides selecting the important species simultaneously as introduced above, it is also possible to find this set of important species by identifying species that are closely related to the species already assumed to be important, e.g., fuel and oxidizer. A well-known

family of approaches is the Directed Relation Graph (DRG)-based methods [175, 176, 185-192], originally proposed by Lu and Law in 2005 [185]. The interaction coefficient between two species is defined to be high if most reactions that produce/consume one of them also involves another [185]. Sensitivity analysis can be integrated with DRG to further reduce the mechanism size (DRG aided sensitivity analysis, DRGASA [176]). Pepiot-Desjardins *et al.* [190] extended DRG by incorporating the error propagation (DRGEP). However the potential risks of DRGEP are discussed in [193, 194]. Another extension of DRG is the path flux analysis method (PFA) proposed by Sun *et al.* [193]. Unlike previous DRG-based methods which only consider the direct relation between species, the interaction coefficients from multiple generations between species are defined in this algorithm in order to improve the prediction of reaction fluxes.

Other approaches used to improve the simulation efficiency include adaptive chemistry reduction (on-the-fly reduction technique [182, 195-197]) and species/reactions lumping [198-202]. The afore-mentioned approaches can also be integrated together [165, 175, 182, 185, 196, 203-205].

A.1.2   Remaining challenges

Although numerous algorithms are proposed to generate skeletal mechanisms, there still exist some challenges. It is possible for some methods to underestimate the importance of certain species. For example, for the hypothesized chemistry mechanism shown in Figure 74, if the object is to reduce the size of a mechanism by approximately half, the appropriate set of species kept should be F, A_i (where $i = 1\sim12$), D and P, since 69% of the total atoms pass through these 15 species. However, every *single* flux connected with D is small, thus if the pair element flux method [180-183] is applied, D and A_i (where $i = 1\sim12$)

126

are neglected, but B_i (where $i = 1\sim13$), F and P are selected. The obtained skeletal mechanism ($B_{1\sim13}$, F and P) includes a total of 15 species but have two problems. Firstly, the pathway from F to P is broken because M_1 and M_2 are not selected (because the element flux to or from them are relatively small). Second, a significant portion of the reaction flux (through species D) is missed. The essential reason for missing species D is that only the first-generation relation between species (which is measured by the element flux for pair element method) is considered. One can find that 69% of the atoms from F passed D through three reaction steps, therefore F and D have a strong three-generation relation. Therefore, D could be kept if its multi-generation relation with F is properly considered. This example illustrates that the importance of considering the multi-generation relation between species. To address this issue, a Path Flux Analysis (PFA) [193] has been proposed to consider such a relation. PFA calculates the interaction coefficients of the $(m+1)$-th generation from the interaction coefficients of the mth generation. However the computation time for the reduction process of PFA increases rapidly with generations, as it is proportional to species number to the power of generations [193]. Thus usually only up to a two-generation relationship is considered by PFA. Therefore to develop a method that quantifies the relation between species from multi-generation efficiently and effectively is still challenging.
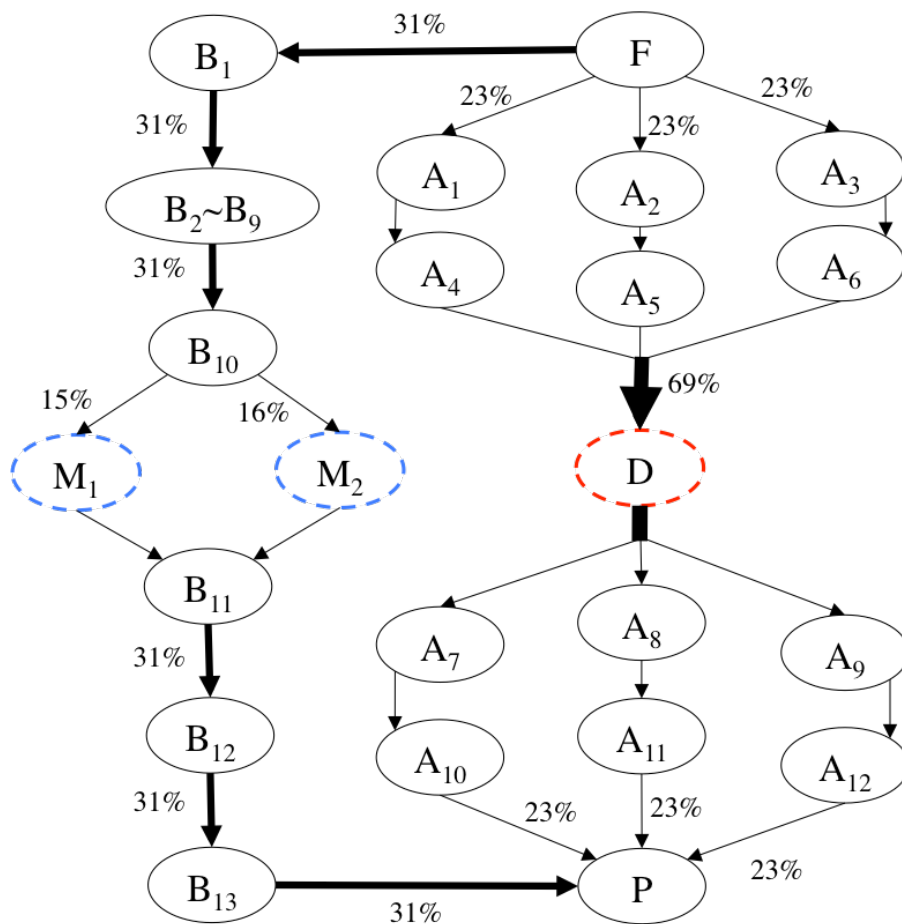
Figure 74 Schematic of a hypothesized flux relationship between different species.

(The percentage numbers denote the normalized flux. All arrows between A_i have the value of 23%; all arrows between B_i have the same value, 31%)

Another challenge is the application of reduction methods on multi-component fuels. When the reduction algorithm is applied to a mixture, it is possible that the reduction algorithm keeps the species related to the fuel component with simple reaction pathways or largest concentration. The pathways related to the fuel components with complex or multiple parallel pathways might be missed. A typical strategy is to generate a skeletal mechanism for each single component fuel and then combine the skeletal mechanisms

[206-208]. A potential drawback of this approach is that the chemical interactions between components cannot be fully captured. For example, Niemeyer and Sung [209] have shown that, for a three-component surrogate fuel, the skeletal mechanism achieved by performing the reduction on the mixture is smaller and more accurate than the combination of the skeletal mechanism for each component. However, performing reduction on mixtures introduces additional complexity. For example, in the work by Niemeyer and Sung [209], a conservative skeletal mechanism with a large number of species was produced by DRGEP first, then sensitivity analysis (SA) and unimportant reaction elimination (RE) based on CSP importance index [164, 210] were applied to further remove redundant species which cannot be identified by DRGEP (This three-step method is referred as DRGEPSARE in the present work). Still this technique requires time-consuming sensitivity analysis. Moreover, even after these steps, the error becomes significant as the mixture composition moves away from the composition used to generate the skeletal mechanism.

The early stage of analysis of chemical kinetics may start from timescale decoupling. One prominent example is Computational Singular Perturbation (CSP) [211], developed in the mid-1980s. CSP decouples fast and slow subspaces (modes) based on Jacobian analysis. The involvement of species and reactions in the fast processes can be identified by the radical pointer and the participation index [212], respectively. The wide applications of CSP include mechanism reduction [164, 213], analysis of flow-chemistry interactions [214], and biochemical systems [215]. Intrinsic low-dimensional manifold (ILDM) [166] is another approach in this category. The identified manifolds represent attractors for the chemical kinetics, thus separating the fast processes, which relax towards the attractors,

and the slow ones, which move within the manifolds [216]. This method is then extended to reaction–diffusion manifolds (REDIMs) to tackle the coupling of reaction and diffusion processes [217, 218]. A more recent method is Chemical Explosive Mode Analysis (CEMA) proposed by Lu *et al.* [119]. It quantifies the timescales related to chemical explosive modes (CEM) based on the eigenvalue analysis of the Jacobian matrix of the chemical source term. Methods to evaluate the contribution of each species or elementary reaction to CEM are provided [119, 219, 220]. Such diagnostic techniques provide insights into complex flame dynamics, such as turbulent lifted jet flames associated with auto-ignition [149, 220, 221]. Besides the methods based on eigenvalue analysis of the Jacobian matrix, approaches representing the results with basic physical quantities are available as well. In an investigation of diffusion flame extinction, Won *et al.* [222] introduced the concept of radical index, which is the normalized estimated OH radical formation rate, to quantify the impact of chemical kinetics, and a transport weighted enthalpy, to assess the mass transfer effect. For fuels with distinct chemical properties, a universal correlation between diffusion flame extinction strain rates and the product of radical index and transport-weighted enthalpy has been demonstrated in that work. Sensitivity analysis [223] is another method of analyzing the reacting system. However, this method is brute force and very time-consuming, especially when the number of variables is significant. Furthermore, the coupling relations between variables may not be discovered.

In this study, a Global Pathway Selection (GPS) algorithm is developed for the generation of skeletal mechanisms. The methodology of GPS is presented and analyzed first, and then simulations of ignition delay times, the extinction curves in a perfectly stirred

reactor (PSR), and 1-D flame propagation speeds are conducted to validate the present GPS method by comparison with PFA, DRGASA or DRGEPSARE.

Recently, a Global Pathway Selection algorithm (GPS) [120] is proposed to identify important Global Pathways for reacting systems, which are the chemical pathways that convert initial reactants to final products, based on atomic flux analysis. Different from the classical Path Flux Analysis algorithm (PFA) [193, 224], which typically considers one or two generations, GPS provides a way to consider the relation between species through all generations (reaction steps). GPS has been used for effective chemical kinetic mechanism reduction [120, 225]. In this study, Global Pathways is used to formulate an automatic and quantified framework to understand the complex chemical kinetics. Demonstrations are given using simulation results from zero-dimensional reactors.

A.2 Chemistry mechanism reduction algorithm

The GPS method is based on two assumptions. (i) If a significant portion of atoms passes a species, then this species should be kept in the skeletal mechanism. (ii) Other species important to building the chemical pathway to produce or consume this species should also be retained. To identify such species, element flux graphs are constructed and are discussed in the following section.

A.2.1 Construction of the element flux graph

For each element considered (usually C, H, and O for combustion of hydrocarbon fuels), an element flux graph is constructed individually. The nodes of these graphs are the

species, and the directed edge from the ith to jth node is the element flux from the ith to the jth species, whose physical meaning is the rate (mole/s-cm^3) of the atoms of the eth element transferring from the ith to the jth species from all possible elementary reactions. Mathematically, the edge has the value:

$$A_{e,i \to j} = \sum_r a_{e,r,i \to j} \tag{1}$$

where $a_{e,r,i \to j}$ is the element flux contributed by the rth elementary reaction to the conversion of the eth atoms from the ith to the jth species:

$$a_{e,r,i \to j} = \max\left(0, C_{e,r,i \to j} \dot{R}_r\right) \tag{2}$$

where $\dot{R}_r$ is the instantaneous net reaction rate (mole/s-cm^3) of the rth reaction (positive if the forward reaction is faster than the reverse reaction, otherwise negative). $C_{e,r,i \to j}$ is the number of the eth atoms transferred from the ith to the jth species in the rth elementary reaction.

$$C_{e,r,i \to j} = \begin{cases} n_{e,r,j} \dfrac{n_{e,r,i}}{n_{e,r}}, & v_{e,r,j} v_{e,r,i} < 0 \\ 0, & \text{otherwise} \end{cases}$$

(3)

where, $n_{e,r,i} = v_{r,i} N_{e,i}$ is the number of the eth atoms transferred into or out from the ith species in the rth elementary reaction. $v_{r,i}$ is the stoichiometric coefficient of the ith species in the rth reaction (positive for products, negative for reactants). $N_{e,i}$ is the number of the eth atoms in the molecule of the ith species. $n_{e,r}$ is the total number of the eth atoms involved in the rth elementary reaction, which can be calculated either by $\sum_{(k:n_{e,r,k}>0)} n_{e,r,k}$ or $\sum_{(k:n_{e,r,k}<0)} n_{e,r,k}$.

It is worthy to mention that, the formation and destruction of a species is separately considered. As shown in Eq. (1), the element flux going into the ith species, $A_{M \to i}$, and the element flux going out from it, $A_{i \to M}$, are measured individually. This should reduce the risk of underestimating the importance of quasi-steady-state (QSS) species, which have a small net generation rate but significant formation and destruction rate.

A.2.2 Selection of the hub species

With the element flux graph constructed in the previous section, the conversion relationship between the initial reactants (usually fuel and O_2) and any species from *all generations* (reaction steps) can be measured by introducing the concept of "hub species". It is defined as the species for which the normalized total element flux coming into, or out of, is greater than a prescribed threshold value α_{crit}

133

$$\frac{\max\left(\sum_k A_{e,i \to k}, \sum_k A_{e,k \to i}\right)}{\max_M \left[\max\left(\sum_k A_{e,M \to k}, \sum_k A_{e,k \to M}\right)\right]} \equiv \alpha_{e,i} > \alpha_{\text{crit}} \tag{4}$$

Then, for each element, a set of hub species is identified by Eq. (4), and all are kept in the skeletal mechanism.

Considering the total element flux of a species as defined in Eq. (4) essentially measures the conversion relationship between the initial reactants and this species from *all generations*. For example, for the combustion of hydrocarbon fuel in air, the carbon atoms of any species are from the fuel, through one or multiple steps. Therefore, if $\alpha_{C,i}$ is a large number, it can be concluded that a significant portion of the fuel is converted to the ith species, from any number of reaction steps. Therefore the all-generation relationship between the initial reactants and any species can be measured. Different from PFA, whose computational cost increases with the number of generation considered, that cost for GPS is independent of generations. Although the pair element flux method [180-183] also uses the element flux, species are kept by assessing the direct element flux between a pair of species. Therefore only the one-generation relation is explicitly considered in this method. Its potential risk has been discussed previously using the system shown in Figure 74 as example. Another difference is that the risk of broken pathways can be reduced in the present method, as discussed in the following section.

A.2.3 Identification of the global pathways

This step is designed to retain the species important to the production and consumption of the hub species identified in previous section. For this purpose, the concept of "global pathway" is introduced. A Global Pathway is defined for a given hub species, as the chemistry pathway that transfers atoms of considered element from the initial reactants to the final product through this hub species. There may exist many possible global pathways for each hub species. In the present study, only the fastest ones are considered. For this purpose, we define a reciprocal element flux graph, whose nodes are species, and edge value is the reciprocal of the element flux

$$
B_{e,i \to j} = \frac{1}{A_{e,i \to j}} \tag{5}
$$

As the quantity $A_{e,i \to j}$ measures the rate of atoms transfer, $B_{e,i \to j}$ is proportional to the time needed to transfer the atom from the ith to the jth nodes. Then, the top K fastest global pathways for a given hub species can be found by searching K shortest paths from the reciprocal element graph, by a graph algorithm proposed by Yen [226]. However for simplicity K is set as 1 for the cases tested in the present work. The species on these identified global pathways are kept in the skeletal mechanism. For example, if C_2H_5CO is identified as a hub species by Eq. (4) for the combustion of n-heptane (nC_7H_{16}), the fastest global pathways can be identified as these listed in Table 3. These species are kept in the skeletal mechanism.

Table 3 The global pathways of C_2H_5CO identified from nC_7H_{16}/air autoignition data

Element considered	Rank of the path	Global pathways
Carbon	1st	$nC_7H_{16} \rightarrow C_7H_{15} \rightarrow C_7H_{15}O_2 \rightarrow C_7H_{14}OOH \rightarrow C_7H_{14}OOHO_2 \rightarrow nC_7^{(Ket)} \rightarrow C_2H_5CHO \rightarrow C_2H_5CO \rightarrow CO \rightarrow CO_2$
	2nd	$nC_7H_{16} \rightarrow C_7H_{15} \rightarrow C_7H_{15}O_2 \rightarrow C_7H_{15}O \rightarrow C_2H_5CHO \rightarrow C_2H_5CO \rightarrow C_2H_5 \rightarrow C_2H_5O \rightarrow CH_2O \rightarrow HCO \rightarrow CO \rightarrow CO_2$
Hydrogen	1st	$nC_7H_{16} \rightarrow C_7H_{15} \rightarrow C_7H_{15}O_2 \rightarrow C_7H_{14}OOH \rightarrow C_7H_{14}OOHO_2 \rightarrow nC_7^{(Ket)} \rightarrow C_2H_5CHO \rightarrow C_2H_5CO \rightarrow C_2H_5 \rightarrow C_2H_5O \rightarrow CH_2O \rightarrow H_2O$
	2nd	$nC_7H_{16} \rightarrow C_7H_{15} \rightarrow C_7H_{15}O_2 \rightarrow C_7H_{15}O \rightarrow C_2H_5CHO \rightarrow C_2H_5CO \rightarrow C_2H_5 \rightarrow C_2H_4 \rightarrow H_2O$
Oxygen	1st, to CO_2	$O_2 \rightarrow OH \rightarrow C_2H_5CO \rightarrow CO \rightarrow CO_2$
	1st, to H_2O	$O_2 \rightarrow HO_2 \rightarrow OH \rightarrow C_2H_5CO \rightarrow CH_2O \rightarrow H_2O$

To the authors' best knowledge, the application of shortest path concept and K shortest paths search algorithm in chemistry analysis was first proposed by Egli in 2003 [227]. In that work, a digraph was built, whose nodes not only included species, but also reactions. The edge value between nodes in that work was the mass flow. Though that work was not aimed to provide a skeletal mechanism generation method, it provided a novel and useful idea to extract the main reaction pathways. The shortest path concept was also used in the BC method recently proposed [184]. Comparing to previous methods, the shortest paths identified in the present method could provide more information. For example, one path from nC_7H_{16} to CO identified in Fig. 8b in Ref. [184] is $nC_7H_{16} \rightarrow H_2O \rightarrow OH \rightarrow C_2H_5CO \rightarrow CO$. How carbon atoms were transferred to C_2H_5CO needs further investigation. In contrast, the shortest paths given by the present method, shown in Table 3, provide more complete details.

A global pathway is a combination of many conversion steps. For example, CO→CO_2 is one conversion step of the global pathway of C_2H_5CO listed in Table 3. One reaction usually contributing significantly to this conversion is CO+OH=CO_2+H, therefore OH and H should also be kept to achieve the conversion from CO to CO_2 in the skeletal mechanism. Similarly, the species important to the rest of conversion steps in identified global pathways should also be retained. This process can be formulated to keep the top n_r reactions whose total contribution (labeled as $\beta_{e,i \to j, r=1 \sim n_r}$) to the considered conversion step $i \to j$ is greater than a given threshold β_{crit}:

$$\frac{\sum_{r=1}^{n_r} a_{e,r,i \to j}}{A_{e,i \to j}} \equiv \beta_{e,i \to j, r=1 \sim n_r} > \beta_{crit} \tag{6}$$

where the reactions are assumed to be ranked in descending order according to $a_{e,r,i \to j}$. By searching the global pathways for hub species and keeping necessary species to these obtained global pathways, one can reduce the risk that the formation or consumption pathway of a hub species may be broken. For the example shown in Figure 74, if GPS already picked any B_i as a hub species (i = 1~13), then GPS searches for a global pathway of this B_i, and obtains F→B_1→…→B_{10}→M_2→B_{11}→,,,→B_{13}→P. Then the pathway from F to P is no longer broken, in contrast to the case with the broken pathway discussed in Section 1.2 (where neither M_1 nor M_2 is selected).
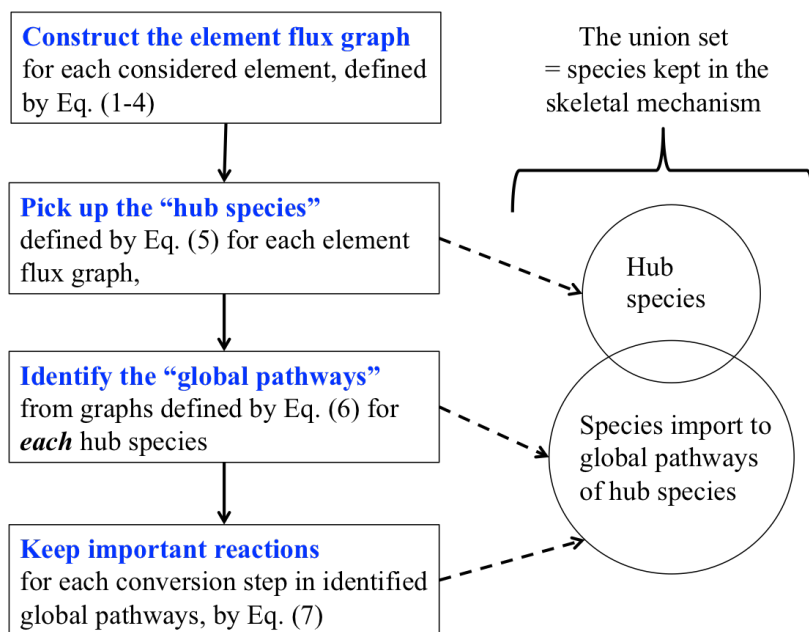
Figure 75 The procedure of GPS algorithm

To sum up, GPS identifies the important species in a sequential order, as shown in Figure 75. Species are ranked first by the normalized element flux passing through them, and the top-ranked ones are kept as hub species. Then global pathways for each of these hub species are searched and ranked, and the species appeared on the fastest ones are kept. Finally, reactions are ranked by their contribution to selected global pathways, and the species involved in the most contributing reactions are kept. The species kept in the skeletal mechanism is the union set of the species identified in the above steps. The major difference between GPS and the existing element flux methods [180-183] and other reaction rate based methods [176, 185, 190, 193] is that, all-generation relation is considered and measured in an efficient way, as analyzed at the end of Section 2.2. Furthermore, the risk of broken pathways for important species can be reduced, as discussed above.

A.2.4 A demonstration: n-dodecane/air combustion

This test is on the combustion of n-dodecane ($nC_{12}H_{26}$) in air using JetSurF 1.0-ll mechanism [228] as the detailed mechanism, which contains 123 species and 977 reactions. The simulation results of PSR at $T_0 = 500K$ and autoignition at $T_0 = 1000K$ at $\phi = 0.5\sim1.5$, and $p = 1\sim10$atm with the detailed mechanism are used as the raw database for the reduction algorithms. A series of skeletal mechanisms with different number of species are generated using this raw database by GPS with varying thresholds, as shown in Figure 76(a). The maximum error of these mechanisms over the predicted ignition delays over $T_0 = 1000\sim1800K$ at $\phi = 0.5\sim1.5$, and $p = 1\sim10$atm are calculated and shown in Figure 76(b). It is observed that the size of the skeletal mechanisms generated by GPS is a function of both α_{crit} and β_{crit}. However, as shown in Figure 76(b), for most cases, if the size of the mechanism is the same, the thresholds do not significantly affect the accuracy (of ignition delay prediction). Indeed, for these cases, different combinations of thresholds (α_{crit} and β_{crit}) essentially select the same set of species. In Figure 76(b), most skeletal mechanisms generated by GPS can be obtained by varying one parameter, α_{crit}, and keeping β_{crit} at a moderate level (e.g., 0.5). This should reduce the computational cost for thresholds selection. Furthermore, the maximum error shown in Figure 76(b) has an approximately monotonic relation with the number of species, which increases with α_{crit} for given β_{crit}. Therefore, the maximum error of the ignition delays of the skeletal mechanisms generated by GPS in Figure 76(b) decreases with the decrease of α_{crit}, showing an example to control the error of the skeletal mechanisms by α_{crit}.
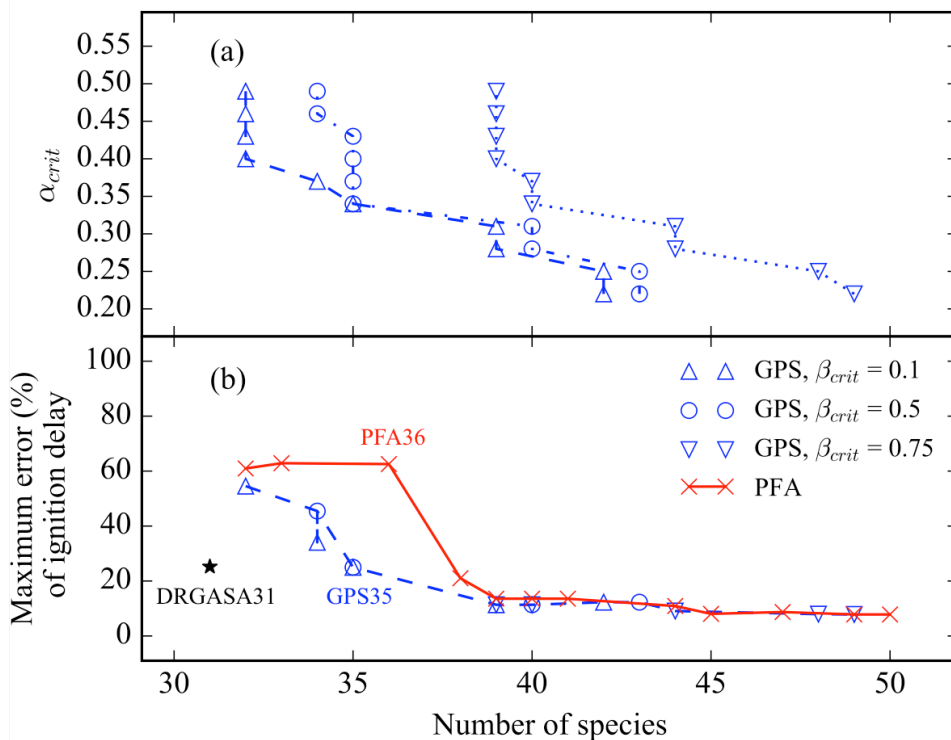
Figure 76 The number of species of obtained skeletal mechanisms and the corresponding (a) GPS thresholds values and (b) the maximum error of the predicted ignition delays over φ = 0.5–1.5, T0 = 1000–1800 K and p = 1–10 atm.

PFA is applied using the same raw database to generate another series of skeletal mechanisms for comparison, shown in Figure 77. For the larger ones, the accuracy is high and similar to that of the GPS-generated mechanisms. However, as the mechanism size decreases, the error of PFA-generated mechanisms starts to grow and becomes much higher than GPS, for the region where the number of species is between 32 and 38. For example, the error of the predicted ignition error is 25% for the 35-species mechanism obtained by

GPS (hereafter GPS35), but reaches 64% for a 36-species mechanism generated by PFA (hereafter PFA36). The prediction and error of these two mechanisms are further compared in Figure 77 as a function of T_0. One can observe that the error of PFA36 comes from the underestimated ignition delay. By comparing the species kept in PFA36 and larger PFA-generated mechanism (which gives accurate ignition delay), it is found that this error is primarily due to the removal of C_2H_6. If this species is added to PFA36, the maximum error of the predicted ignition delays is decreased to 24%. This is because the major production pathway of C_2H_6 is from CH_3. However, converting CH_3 to C_2H_6 is a chain termination reaction. Therefore neglecting C_2H_6 by PFA36 leads to overestimated system reactivity and thus under predicts ignition delay.
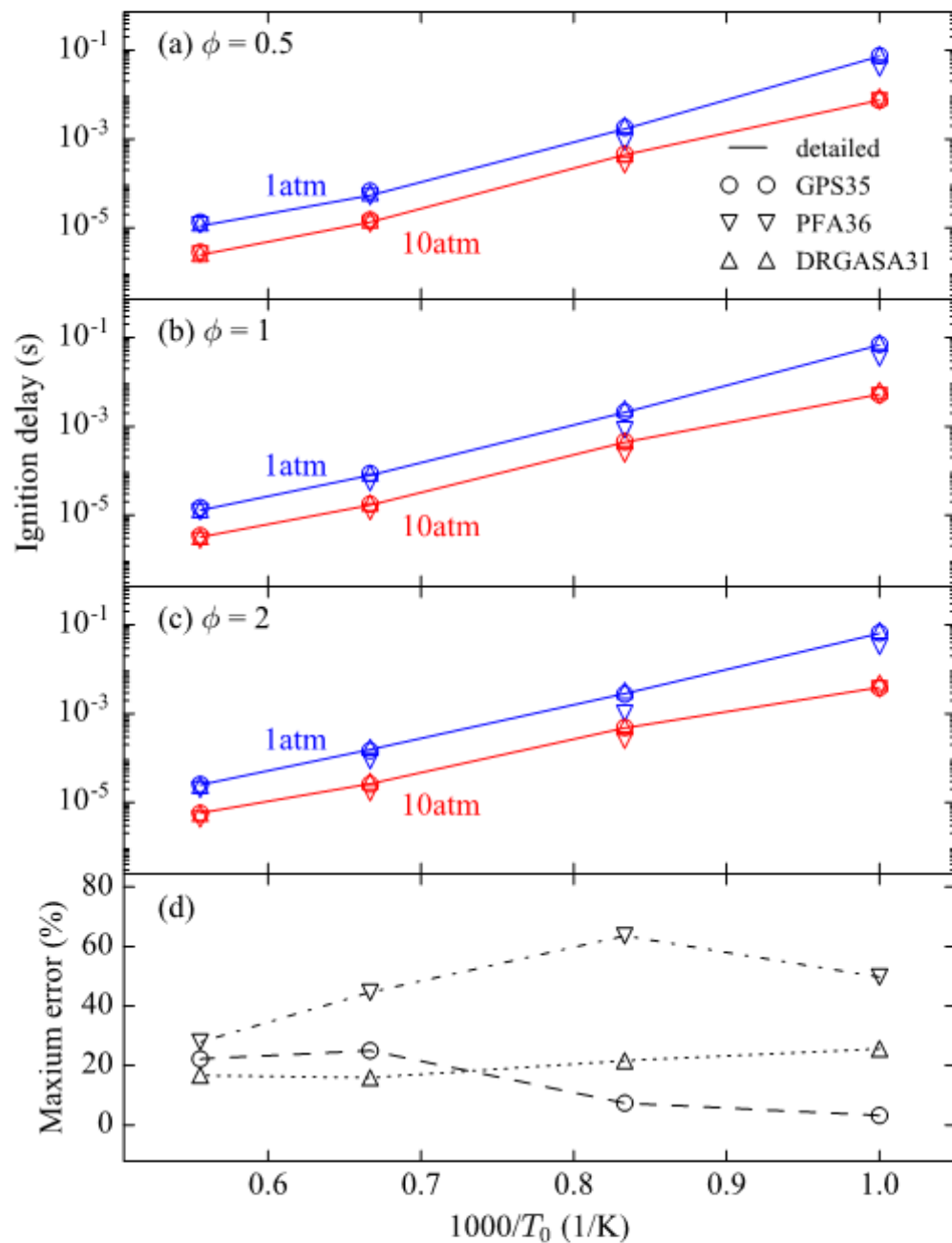
Figure 77 Comparison of the prediction on ignition delay of n-dodecane/air mixture by detailed and skeletal mechanisms: (a–c) ignition delays (d) the maximum error of the predicted ignition delays over φ = 0.5–2, and p = 1–10 atm as a function of T₀.
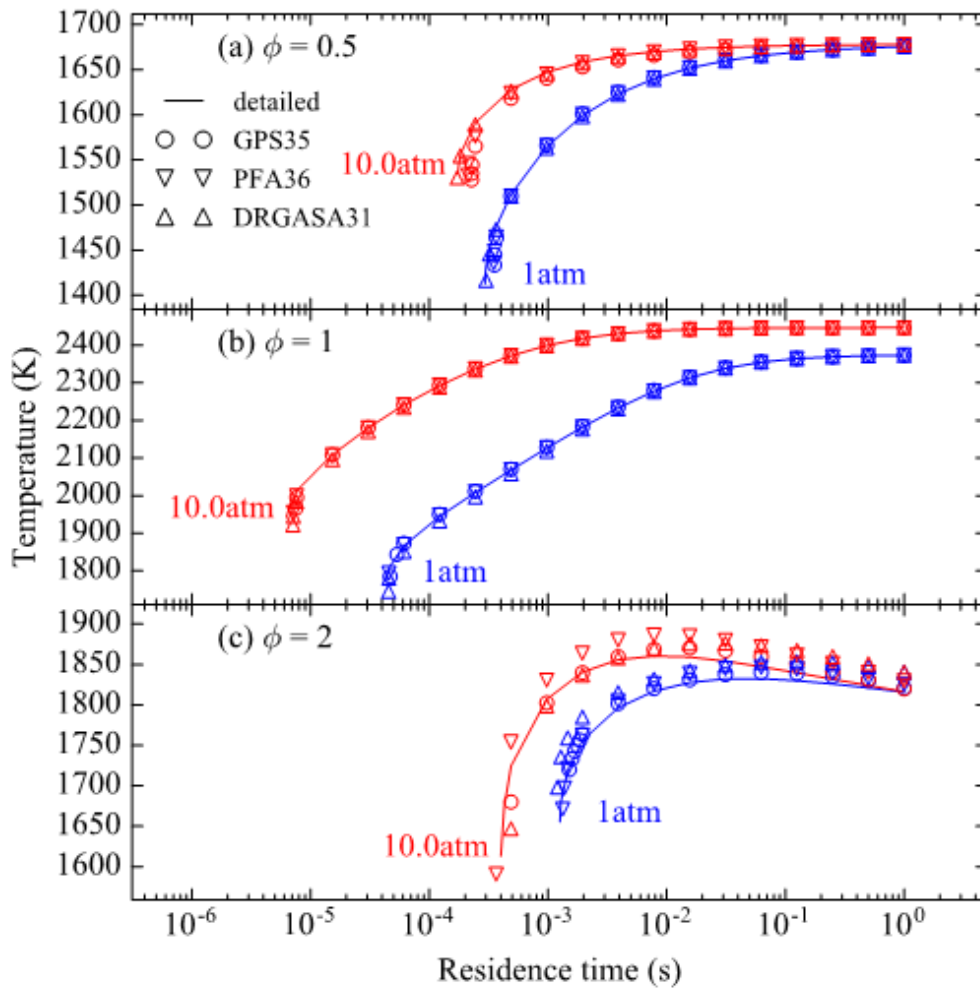
Figure 78 Comparison of the PSR curves of n-dodecane/air mixture at $T_0 = 500$ K pre- dicted by the detailed mechanism and the skeletal mechanisms.

143
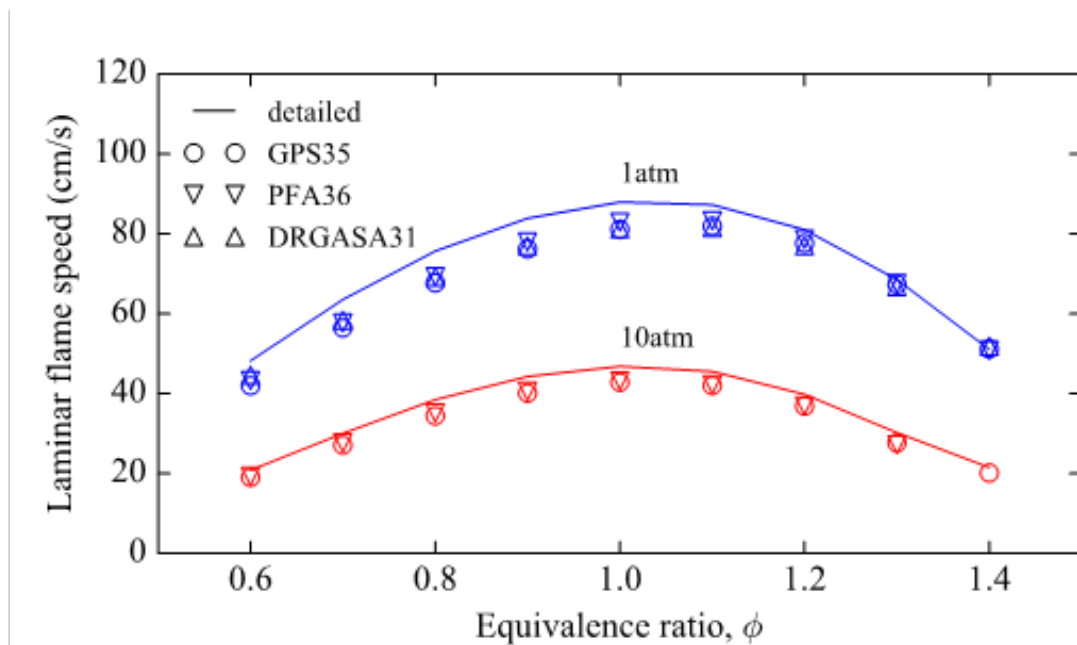
Figure 79 Comparison of the laminar flame speeds of n-dodecane/air mixture predicted by the detailed and skeletal mechanisms at T0 = 500 K and p = 1–10 atm.

DRGASA was applied on using the same detailed mechanism by Vié *et al*. [229] and obtained a 31-species mechanism (hereafter DRGASA31). As discussed in the introduction section, sensitivity analysis is usually a very effective method and performs better than other methods not using sensitivity analysis such as PFA and the original DRG. Therefore DRGASA31 is used as the benchmark of the optimal mechanism at its mechanism size level. However sensitivity analysis is a brute-force process and thus very time consuming. Therefore it is helpful if an algorithm can reach similar accuracy and mechanism size without the burden of sensitivity analysis. As shown in Figure 77, GPS is closer to this benchmark compared to PFA. GPS35 is further compared with DRGASA31 for the prediction of ignition delays (Figure 77), PSR curves (Figure 78), and laminar flame speeds (Figure 79). It is observed that these two skeletal mechanisms have similar accuracy for

144

autoignition simulation. The maximum error over tested conditions is approximately 25% for both mechanisms. For the predicted PSR curves, both skeletal mechanisms show reasonable accuracy as they match the results simulated with detailed mechanisms. GPS35 has a larger error of extinction residence time at the fuel-lean case (28% error for $\phi = 0.5$ case shown in Figure 78), however it gives a better temperature prediction at the fuel-rich case. For example, DRGASA31 overestimates the temperature at residence time of 1s by approximately 30K for both low (1atm) and high pressures (10atm). For the laminar flame speeds, GPS35 and DRGASA31 show similar accuracy, with the worst prediction at fuel lean side, but the error is within 15% for both of them. To sum up, GPS35 and DRGASA31 show similar overall accuracy for the tested conditions.

A.3   Reacting system analysis framework

A.3.1   Introduction

The Global Pathway Selection algorithm (GPS) [120] introduced previously is used to formulate an automatic and quantified framework to understand the complex chemical kinetics. After reviewing the related previous works, introducing the methodology, a demonstration is given using simulation results from zero-dimensional reactors.

A.3.2   The methodology

As illustrated in Figure 80, a hierarchical model to analyze chemical kinetics is proposed. Other aspects such as transport are not focused on in the present work (The software can be downloaded from http://sun.gatech.edu/download.htm). The objective is

to find the elementary reactions controlling the phenomena of interest in a complex reacting system and underlying connections among different species. Therefore, it is necessary to formulate an interface between the behavior of the system and the elementary reactions. For this purpose, Global Pathways are identified using GPS algorithm [120] for considered source/sink pairs of species. The source species are usually components of the fuel or the oxidizer which are providing C, H, and O atoms, and the sink species are usually final products which absorb C, H, and O atoms. For example, for H_2/air mixture, two possible Global Pathways from H_2 to H_2O are:

$$H_2 \rightarrow H \rightarrow HO_2 \rightarrow H_2O_2 \rightarrow OH \rightarrow H_2O \qquad \textbf{(GP-H}_2\textbf{-1)}$$

$$H_2 \rightarrow H \rightarrow OH \rightarrow H_2O \qquad \textbf{(GP-H}_2\textbf{-2)}$$

These Global Pathways provide a simplified representation of the reacting system, yet reflect the key chemical information of species conversion. Each arrow ($\rightarrow$) in a Global Pathway is called a conversion step.
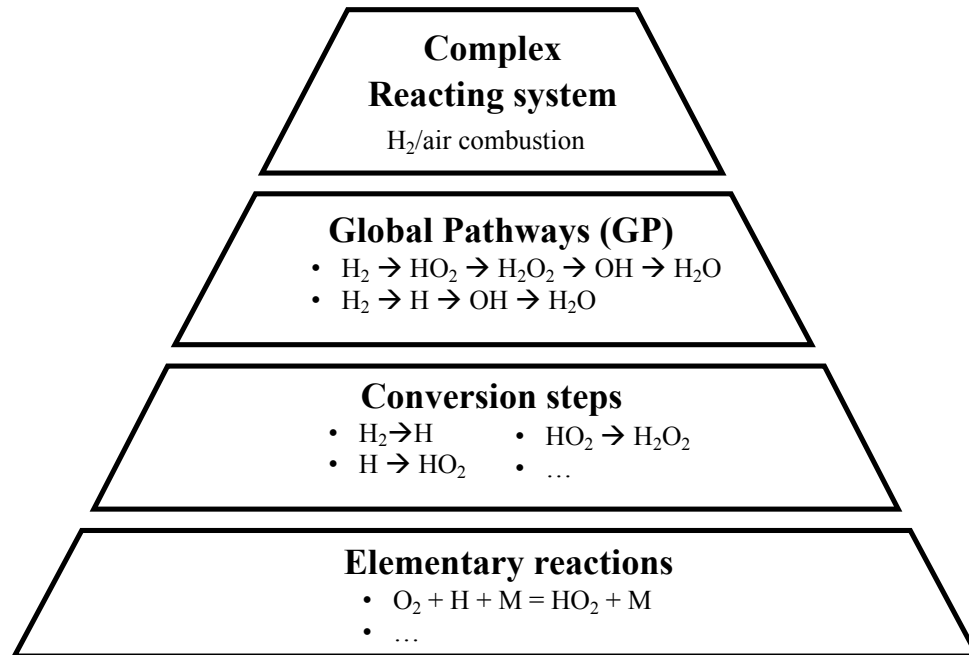
Figure 80. A hierarchical model to analyze complex chemical kinetics, using H$_2$/air combustion as a demonstration.

Then, for the identified Global Pathways, their dominancy and effects on radical production and consumption are quantified. The effects on other aspects such as heat release and entropy production can be quantified as well in a similar way but are not focuses of the present work. These quantities provide an overview of each Global Pathway and explain that how these Global Pathways compete with each other and affect the reacting system differently. The dominancy of a Global Pathway, $D_{GP,e}$, represents the fraction of the e-th atoms (e.g., C atoms) that are going through this Global Pathway. It ranges from 0 to 1, and is defined as

$$D_{GP,e} = D_{\text{source},e} D_{\text{GP/source},e}$$

where $D_{\text{source},e}$ is the ratio of the number of the e-th atoms from the source species of this Global Pathway to the total number of the e-th atoms,

$$D_{\text{source},e} = \frac{n_{\text{source,init}} N_{\text{source},e}}{\sum_i n_{\text{i,init}} N_{\text{i},e}}$$

The subscript "source" means the source species (the first species) of the considered Global Pathway. $N_{\text{i},e}$ is the number of the e-th atoms in one molecule of the i-th species. $n_{\text{i,init}}$ is the mole number of the i-th species in the initial reactants (fuel or oxidizer). $D_{\text{GP/source},e}$ is the fraction of the e-th atom that are going from the source species to sink species through this specific Global Pathway. It is the geometric mean of the fractions of the e-th atoms distributed to the conversion steps of this Global Pathway.

$$D_{\text{GP/source},e} = \left(\prod_{i,j \in GP} \frac{A_{e,i \to j}}{\sum_k A_{e,i \to k}} \right)^{\frac{1}{|GP|}}$$

where $|GP|$ is the number of conversion steps of this Global Pathway. $A_{e,i \to j}$ is the element flux of the e-th element from the i-th to the j-th species.

$$A_{e,i \to j} = \sum_r \max\left(0, C_{e,r,i \to j} \dot{\omega}_r\right)$$

where $\dot{\omega}_r$ is the instantaneous net reaction rate (mole/m^3-s) of the r-th reaction. $C_{e,r,i \to j}$ is the number of the e-th atoms transferred from the i-th to the j-th species in the r-th elementary reaction.

$$C_{e,r,i \to j} = \begin{cases} v_{r,j} N_{e,j} \dfrac{v_{r,i} N_{i,e}}{\sum_{k:v_{r,k}<0} \left(v_{r,k} N_{k,e}\right)}, & v_{r,j} v_{r,i} < 0 \\ 0, & \text{otherwise} \end{cases}$$

where $v_{r,i}$ is the stoichiometric coefficient of the i-th species in the r-th reaction (positive for products, negative for reactants)

The net radical production rate associated with a Global Pathway, R_{GP}, is defined as the sum of net radical production rates of all reactions involved in this global pathway scaled by its dominancy D_{GP}

$$R_{GP} = D_{GP,e} \sum_{r \in GP} \Omega_r$$

Ω_r is the net radical production rate of the r-th reaction:

$$\Omega_r = \dot{\omega}_r \sum_k \delta_k v_{r,k}$$

δ_k equals 1 if the k-th species is a prescribed radical, otherwise it is 0. Though special concern may be necessary to prescribe the radicals, for simplicity, O, H, and OH are chosen as the prescribed radicals for the present study. By defining R_{GP}, it is clear that which Global Pathways are consuming or producing radicals at a given spatial-temporal point.

The Global Pathways provide the interface with the reacting system. To bridge it with the elementary reactions, conversion steps are considered. The conversion step is labeled by arrow ($\rightarrow$) in the Global Pathway, such as H $\rightarrow$ HO$_2$. Similar to the definition of R_{GP}, the net radical production rate associated with the conversion step from the i-th species to the j-th species, $R_{i \rightarrow j}$, is defined as the sum of net radical production rate of all reactions involved in this conversion step:

$$R_{i \to j} = \sum_{r \in (i \to j)} \Omega_r$$

As this hierarchical framework is based on the analysis of Global Pathways, this methodology is hereafter referred as Global Pathway Analysis (GPA).

A.3.3 A demonstration: the explosion limit of hydrogen

The first demonstration is to analyze the auto-ignition of stoichiometric H_2/air mixture in a constant pressure adiabatic reactor at different reactor pressures (P) using GRI-Mech 3.0 [230]. The initial temperature (T_0) is 1000 K. As shown in Figure 81, the variation of auto-ignition delay (τ_{ign}) of the mixture is non-monotonic with the change of P. This phenomenon represents the well-known second explosion limit of H_2.
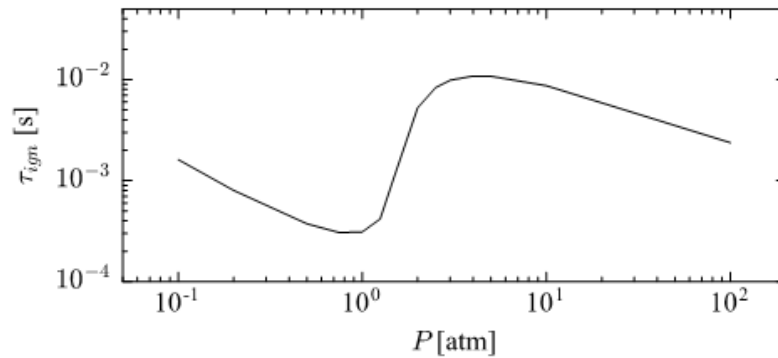
Figure 81. τ_{ign} of stoichiometric H_2/air at different P with T_0 = 1000 K.

Different Global Pathways can be identified from simulations at different conditions. This section focuses on the second limit, so the simulation results at 1 atm and 10 atm are further investigated. Considering hydrogen element flux graphs, the most dominant Global Pathway identified at 10 atm is GP-H_2-1, and the one at 1 atm is GP-H_2-2. The evolution of the dominant Global Pathways is also illustrated by D_{GP} in Figure 82(a). At 1 atm, the dominant Global Pathway during the temperature jump is GP-H_2-2, as indicated by its

higher D_{GP} than GP-H$_2$-1. However, as P increases from 1 atm to 10 atm, GP-H$_2$-1 becomes the dominant Global Pathway as shown in Figure 82(b). The net radical (H, O, and OH in this study) production rates R_{GP} of the two Global Pathways are illustrated in Figure 82 as well. Generally, GP-H$_2$-1 consumes radicals when temperature is below 1100 K while GP-H$_2$-2 produces radicals. The radical destruction associated with GP-H$_2$-1 becomes more dominant as P increases from 1 atm to 10 atm. This decreases the system reactivity and explains the increase of τ_{ign} as P increases in Figure 81.
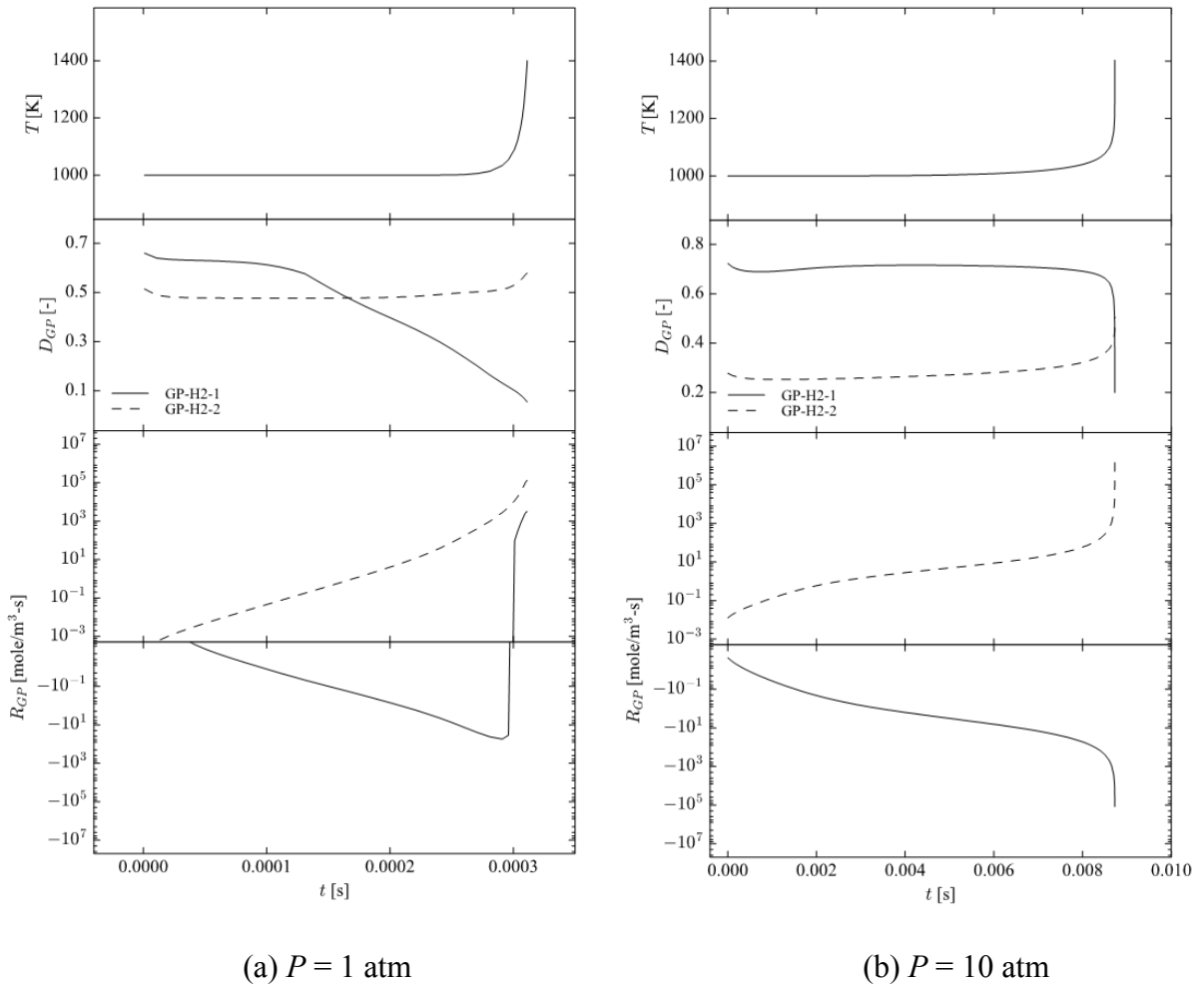
(a) $P = 1$ atm   (b) $P = 10$ atm

Figure 82. H$_2$ Global Pathways at (a) $P = 1$ atm and (b) $P = 10$ atm.

The net radical production rate of conversion steps, $R_{i \rightarrow j}$, for GP-H$_2$-1 and GP-H$_2$-2 during the auto-ignition at 10 atm is then investigated to extract more details at temperature $T = 1200$ K (i.e., temperature rise of 200 K), and shown in Figure 83. The value of $R_{i \rightarrow j}$ is illustrated by black bars, and the major reactions contributing to $R_{i \rightarrow j}$ are listed in gray color. It should be noted that, some bars have zero value but it does not necessarily mean the corresponding conversion step is frozen. For example, the reaction 2HO$_2$ = H$_2$O$_2$ + O$_2$ is neither producing nor consuming radicals (in this study HO$_2$ is not prescribed as a radical as it is relatively inactive [83]). Therefore $R_{i \rightarrow j}$ is zero (analogy to chain propagation reactions) for its corresponding conversion step, HO$_2$→H$_2$O$_2$, although the element flux through this conversion step is not necessarily zero. The comparison between $R_{i \rightarrow j}$ of these two Global Pathways implies that the conversion step H → HO$_2$ controls radical destruction, indicated by the negative $R_{i \rightarrow j}$ shown in Figure 83(a). This is due to reaction H+O$_2$+M=HO$_2$+M. This reaction favors higher pressure, which explains the higher dominancy of GP-H$_2$-1 as pressure is increased from 1 to 10 atm, illustrated in Figure 82(b). This observation agrees with the classical understanding of the second explosion limit [83]. That is, the system changes from explosive to non-explosive because of the increased radical destruction with the formation of HO$_2$ at elevated pressure conditions.
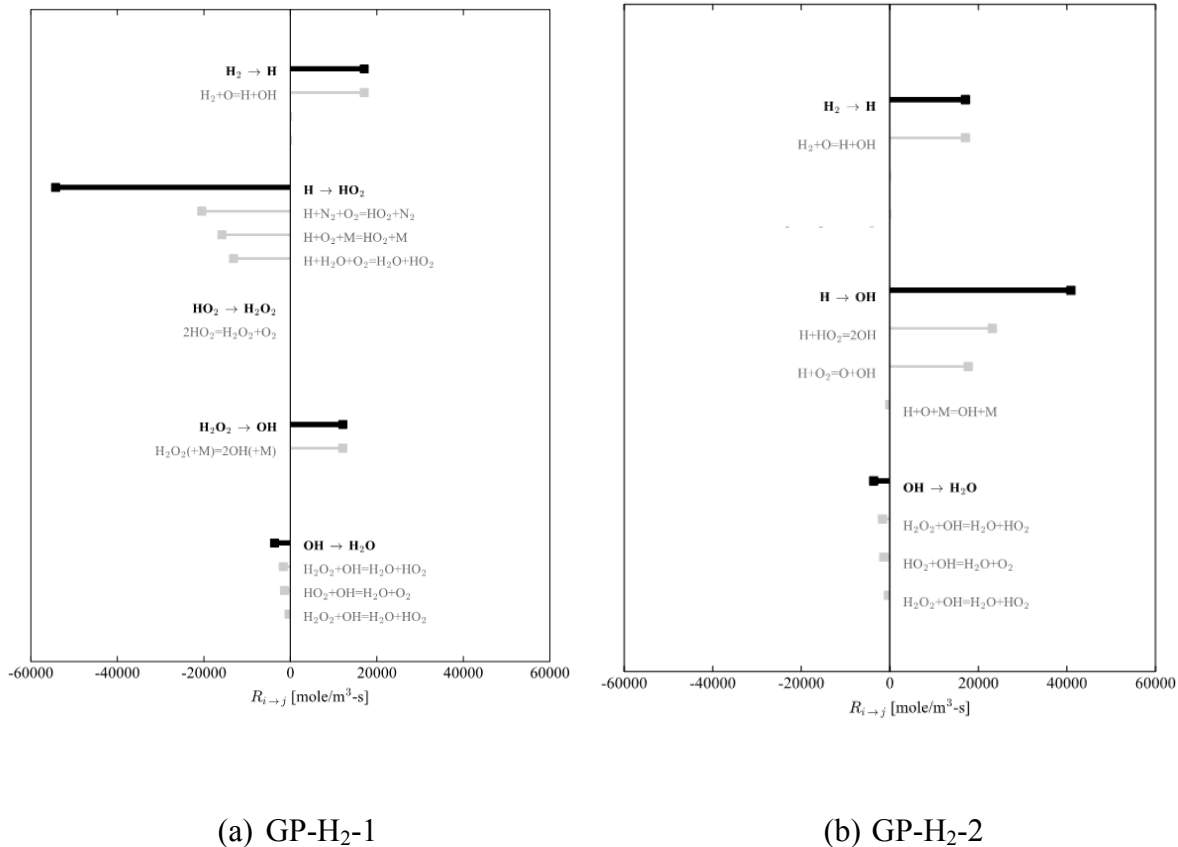
(a) GP-H$_2$-1   (b) GP-H$_2$-2

Figure 83. Net radical production rates for conversion steps for (a) GP-H$_2$-1 and (b) GP-H$_2$-2

A.4 Conclusions

A global pathway selection (GPS) algorithm is proposed and validated in this work for the systematic generation of skeletal mechanisms. GPS considers all-generation relations between species and initial reactants when quantifying the importance of species. The risk of having broken or dead-end chemistry pathway for important species can be reduced using this method. Validations are performed on a single-component fuel, n-dodecane. A series of skeletal mechanisms are obtained with various threshold values by GPS. It is observed that the maximum error of ignition delays has an approximate monotonic relation with the threshold α_{crit}, giving an example of feasible error control with

153

threshold value for these specific testing cases. Another threshold β_{crit} can be fixed at a moderate level, which does not significantly affect the results. A series of skeletal mechanisms is generated using Path Flux Analysis (PFA, [193]) for comparison. It is observed that GPS-generated mechanisms show a smaller maximum error of ignition delays compared to these generated by PFA with similar number of species. When the mixture of toluene, iso-octane, and n-heptane is used as the fuel, for mechanism with 280~340 species, the error of PFA-generated mechanisms reaches 100%, while GPS can control error within 40%. Methods using sensitivity analysis are also compared with GPS. For n-dodecane case, a 35-species mechanism generated by GPS shows similar overall accuracy comparing to a 31-species mechanism generated using Direct Relation Graph Aided Sensitivity Analysis (DRGASA, [190, 229]). The accuracy is measured by comparing the results of ignition delay, PSR temperatures, and laminar flame speed over a wide range of operating conditions.

GPS is then extended to a hierarchical framework, Global Pathway Analysis (GPA), to understand the proposed chemical kinetics. The behavior of the reacting system at macro level is bridged to elementary reactions by Global Pathways. The analysis is conducted by investigating the effects of radical production and consumptions, and the dominancy of these Global Pathways. The number of variables to be investigated is significantly reduced. This feature becomes advantageous when a reacting system involves complex chemistry kinetics. The second hydrogen explosion limit is discussed as a demonstration of GPA. GPA concludes that this is caused by a radical-consuming Global Pathway (GP-H_2-1) which becomes dominant as P increases, due to the pressure-dependent reaction $H+O_2+M=HO_2+M$. This is consistent with the classical explanation.

REFERENCES

[1] Sun, W., and Ju, Y., "Nonequilibrium Plasma-Assisted Combustion: A Review of Recent Progress," *J. Plasma Fusion Res* Vol. 89, No. 4, 2013, pp. 208-219.

[2] Ju, Y., and Sun, W., "Plasma assisted combustion: Dynamics and chemistry," *Progress in Energy and Combustion Science,* 2014.

[3] Sun, W., "Non-equilibrium Plasma-Assisted Combustion." Princeton University, 2013.

[4] Ombrello, T., Won, S. H., Ju, Y., and Williams, S., "Flame propagation enhancement by plasma excitation of oxygen. Part II: Effects of O2(a1Δg)," *Combustion and Flame* Vol. 157, No. 10, 2010, pp. 1916-1928.

[5] Rubin, M. B., "The history of ozone. The Schönbein period, 1839–1868," *Bull. Hist. Chem* Vol. 26, No. 1, 2001, pp. 40-56.

[6] Schönbein, C., "On the Odour Accompanying Electricity, and on the Probability of Its Dependence on the Presence of a New Substrate," *Proceedings of the Royal Society of London Series I* Vol. 4, 1837, p. 226.

[7] PAUL, O. M., "TUBULAR OZONE-GENERATOR." US Patent App. 1/163,768, 1913.

[8] Sandri, R., "On the decomposition flame of liquid ozone-oxygen mixtures in a tube," *Combustion and Flame* Vol. 2, No. 4, 1958, pp. 348-352.

[9] Streng, A., and Grosse, A., "The quenching diameter of ozone flames," *Combustion and Flame* Vol. 5, 1961, pp. 81-86.

[10] Cramarossa, F., and Dixon-Lewis, G., "Ozone decomposition in relation to the problem of the existence of steady-state flames," *Combustion and Flame* Vol. 16, No. 3, 1971, pp. 243-251.

[11] Heimerl, J., and Coffee, T., "The detailed modeling of premixed, laminar steady-state flames. I. Ozone," *Combustion and Flame* Vol. 39, No. 3, 1980, pp. 301-315.

[12] Rogg, B., Linan, A., and Williams, F., "Deflagration regimes of laminar flames modeled after the ozone decomposition flame," *Combustion and flame* Vol. 65, No. 1, 1986, pp. 79-101.

[13] Lunin, B., Kuricheva, O., and Zhitnev, Y. N., "Determination of the Arrhenius parameters of the ozone thermal decomposition reaction initiated by pulsed infrared laser radiation," *Zh. Fiz. Khim* Vol. 60, 1986, p. 2050.

[14] Schönbein, C. F., "Recherches sur la nature de l'odeur, qui se manifeste dans certaines actions chimiques," *C. R. Hebd. Seances Acad. Sci., Ser. C,* , 1840, pp. 10, 706-10.

[15] Schoene, E., "Spectrum of ozone, and the presence of ozone in the atmosphere," *Jour. Russ. Chem. Soc* Vol. 2, 1884, pp. 250-252.

[16] Seinfeld, J. H., "Urban air pollution: state of the science," *Science* Vol. 243, No. 4892, 1989, pp. 745-752.

[17] Council, N. R. *Rethinking the ozone problem in urban and regional air pollution*: National Academies Press, 1992.

[18] Greene, C. R., and Atkinson, R., "Rate constants for the gas-phase reactions of O3 with a series of alkenes at 296±2 K," *International Journal of Chemical Kinetics* Vol. 24, No. 9, 1992, pp. 803-811.

[19] Atkinson, R., and Carter, W. P., "Kinetics and mechanisms of the gas-phase reactions of ozone with organic compounds under atmospheric conditions," *Chemical Reviews* Vol. 84, No. 5, 1984, pp. 437-470.

[20] Drugman, J., "The oxidation of hydrocarbons by ozone at low temperatures," *Journal of the Chemical Society, Transactions* Vol. 89, 1906, pp. 939-945.

[21] Schubert, C. C., Schubert, S., and Pease, R. N., "The Oxidation of Lower Paraffin Hydrocarbons. I. Room Temperature Reaction of Methane, Propane, n-Butane and Isobutane with Ozonized Oxygen1," *Journal of the American Chemical Society* Vol. 78, No. 10, 1956, pp. 2044-2048.

[22] Atkinson, R., Baulch, D., Cox, R., Crowley, J., Hampson Jr, R., Kerr, J., Rossi, M., and Troe, J., "Summary of evaluated kinetic and photochemical data for atmospheric chemistry," 2001, pp. 1-56.

[23] DeMore, W. B., Sander, S. P., Golden, D. M., Hampson, R. F., Kurylo, M. J., Howard, C. J., Ravishankara, A. R., Kolb, C. J., and Molina, M. J., "Chemical Kinetic and Photochemical Data for Use in Stratospheric Modeling: Evaluation No. 11 of the NASA Panel for Data Evaluation," *JPL Publication 94-26*, 1994.

[24] Morrissey, R. J., and Schubert, C., "The reactions of ozone with propane and ethane," *Combustion and Flame* Vol. 7, 1963, pp. 263-268.

[25] Atkinson, R., Baulch, D. L., Cox, R. A., Crowley, J. N., Hampson, R. F., Jr., Kerr, J. A., Rossi, M. J., and Troe, J., "Summary of Evaluated Kinetic and Photochemical Data for Atmospheric Chemistry," *IUPAC Subcommittee on Gas Kinetic Data Evaluation for Atmospheric Chemistry* Vol. Web Version December 2001, 2001.

[26] Shi, Y., Xu, Y., and Jia, L., "Arrhenius parameters for the gas-phase reactions of O3 with two butenes and two methyl-substituted butenes over the temperature range of 295–351 K," *International Journal of Chemical Kinetics* Vol. 43, No. 5, 2011, pp. 238-246.

[27] Criegee, R., "Mechanism of ozonolysis," *Angewandte Chemie International Edition* Vol. 14, No. 11, 1975, pp. 745-752.

[28] Olzmann, M., Kraka, E., Cremer, D., Gutbrod, R., and Andersson, S., "Energetics, kinetics, and product distributions of the reactions of ozone with ethene and 2, 3-dimethyl-2-butene," *The Journal of Physical Chemistry A* Vol. 101, No. 49, 1997, pp. 9421-9429.

[29] Anglada, J. M., Crehuet, R., and Bofill, J. M., "The Ozonolysis of Ethylene: A Theoretical Study of the Gas-Phase Reaction Mechanism," *Chemistry-A European Journal* Vol. 5, No. 6, 1999, pp. 1809-1822.

[30] Berndt, T., Herrmann, H., and Kurtén, T., "Direct probing of Criegee intermediates from gas-phase ozonolysis using chemical ionization mass spectrometry," *Journal of the American Chemical Society*, 2017.

[31] Anglada, J. M., Bofill, J. M., Olivella, S., and Solé, A., "Unimolecular isomerizations and oxygen atom loss in formaldehyde and acetaldehyde carbonyl oxides. A theoretical investigation," *Journal of the American Chemical Society* Vol. 118, No. 19, 1996, pp. 4636-4647.

[32] Phillips, L., and Schiff, H., "Mass spectrometric studies of atomic reactions. III. Reactions of hydrogen atoms with nitrogen dioxide and with ozone," *The Journal of Chemical Physics* Vol. 37, No. 6, 1962, pp. 1233-1238.

[33] DeMore, W. B., Sander, S. P., Golden, D., Hampson, R. F., Kurylo, M. J., Howard, C. J., Ravishankara, A., Kolb, C., and Molina, M., "Chemical Kinetics and Photochemical Data for Use in Stratospheric Modeling. Evaluation No. 12," 1997.

[34] Howard, C. J., and Finlayson-Pitts, B. J., "Yields of HO2 in the reaction of hydrogen atoms with ozone," *The Journal of Chemical Physics* Vol. 72, No. 6, 1980, pp. 3842-3843.

[35] Atkinson, R., Baulch, D., Cox, R., Crowley, J., Hampson, R., Hynes, R., Jenkin, M., Rossi, M., and Troe, J., "Evaluated kinetic and photochemical data for atmospheric chemistry: Part 1? gas phase reactions of O x, HO x, NO x and SO x species," *Atmospheric Chemistry and Physics Discussions* Vol. 3, No. 6, 2003, pp. 6179-6699.

[36] Steinberg, M., Yang, R. T., Hom, T. K., and Berlad, A. L., "Desulphurization of coal with ozone: an attempt," *Fuel* Vol. 56, No. 2, 1977, pp. 227-228.

[37] Razumovskii, S., and Zaikov, G. E. *Ozone and its reactions with organic compounds*: Elsevier, 1984.

[38] Sharypov, V., Kuznetsov, B., Baryshnikov, S., Beregovtsova, N., Selyutin, G., Chumakov, V., and Kamianov, V., "Some features of chemical composition, structure and reactive ability of Kansk-Achinsk lignite modified by ozone treatment," *Fuel* Vol. 78, No. 6, 1999, pp. 663-666.

[39] Gao, Y., Külaots, I., Chen, X., Aggarwal, R., Mehta, A., Suuberg, E., and Hurt, R., "Ozonation for the chemical modification of carbon surfaces in fly ash," *Fuel* Vol. 80, No. 5, 2001, pp. 765-768.

[40] Patrakov, Y. F., Fedyaeva, O., Semenova, S., Fedorova, N., and Gorbunova, L., "Influence of ozone treatment on change of structural–chemical parameters of coal vitrinites and their reactivity during the thermal liquefaction process," *Fuel* Vol. 85, No. 9, 2006, pp. 1264-1272.

[41] Soriano, N. U., Migo, V. P., and Matsumura, M., "Ozonized vegetable oil as pour point depressant for neat biodiesel," *Fuel* Vol. 85, No. 1, 2006, pp. 25-31.

[42] Schönborn, A., Hellier, P., Aliev, A. E., and Ladommatos, N., "Ignition control of homogeneous-charge compression ignition (HCCI) combustion through adaptation of the fuel molecular structure by reaction with ozone," *Fuel* Vol. 89, No. 11, 2010, pp. 3178-3184.

[43] Schönborn, A., Hellier, P., Ladommatos, N., Hulteberg, C. P., Carlström, G., Sayad, P., Klingmann, J., and Konnov, A. A., "1-hexene autoignition control by prior reaction with ozone," *Fuel Processing Technology* Vol. 145, 2016, pp. 90-95.

[44] Slater, S. M., and Rizzone, M. S., "Simultaneous oxidation of SO2 and NO in flue gas by ozone injection," *Fuel* Vol. 59, No. 12, 1980, pp. 897-899.

[45] Tachibana, T., Hirata, K., Nishida, H., and Osada, H., "Effect of ozone on combustion of compression ignition engines," *Combustion and flame* Vol. 85, No. 3-4, 1991, pp. 515-519.

[46] Wilk, M., and Magdziarz, A., "Ozone effects on the emission of pollutants coming from natural gas combustion," *Polish J. Environ. Stud* Vol. 19, 2010, pp. 1331-1336.

[47] Jarvis, J. B., Day, A., and Suchak, N., "LoTOxTM process flexibility and multi-pollutant control capability," *Proc. Combined Power Plant Air Pollution Control Mega Symposium, Washington, USA*. 2003, pp. 19-22.

[48] Fu, Y., Diwekar, U., Suchak, N., and Rohrer, W., "Modeling the Best Available Control Technology: Numerical Difficulties and the Optimization Framework," *Proceedings of the AIChE Annual Meeting*. 1999.

[49] Fu, Y., and Diwekar, U. M., "Cost effective environmental control technology for utilities," *Advances in Environmental Research* Vol. 8, No. 2, 2004, pp. 173-196.

[50] Mok, Y. S., and Lee, H.-J., "Removal of sulfur dioxide and nitrogen oxides by using ozone injection and absorption–reduction technique," *Fuel Processing Technology* Vol. 87, No. 7, 2006, pp. 591-597.

[51] Wang, Z., Zhou, J., Zhu, Y., Wen, Z., Liu, J., and Cen, K., "Simultaneous removal of NOx, SO 2 and Hg in nitrogen flow in a narrow reactor by ozone injection: Experimental results," *Fuel Processing Technology* Vol. 88, No. 8, 2007, pp. 817-823.

[52] Sun, W.-y., Ding, S.-l., Zeng, S.-s., Su, S.-j., and Jiang, W.-j., "Simultaneous absorption of NO x and SO 2 from flue gas with pyrolusite slurry combined with gas-phase oxidation of NO using ozone," *Journal of hazardous materials* Vol. 192, No. 1, 2011, pp. 124-130.

[53] Nomaguchi, T., and Koda, S., "Spark ignition of methane and methanol in ozonized air," *Symposium (International) on Combustion*. Vol. 22, 1989, pp. 1677-1682.

[54] Tachibana, T., Hirata, K., Nishida, H., and Osada, H., "Effect of ozone on combustion of compression ignition engines," *Combustion and Flame* Vol. 85, No. 3, 1991, pp. 515-519.

[55] Flynn, P. F., Hunter, G. L., Loye, A. O., Akinyemi, O. C., Durrett, R. P., Moore, G. A., Mudd, J. M., Muntean, G. G., Wagner, J. A., and Wright, J. F., "Premixed charge compression ignition engine with optimal combustion control." Google Patents, 2001.

[56] Nishida, H., and Tachibana, T., "Homogeneous charge compression ignition of natural gas/air mixture with ozone addition," *Journal of propulsion and power* Vol. 22, No. 1, 2006, pp. 151-157.

[57] Foucher, F., Higelin, P., Mounaïm-Rousselle, C., and Dagaut, P., "Influence of ozone on the combustion of n-heptane in a HCCI engine," *Proceedings of the Combustion Institute* Vol. 34, No. 2, 2013, pp. 3005-3012.

[58] Masurier, J.-B., Foucher, F., Dayma, G., and Dagaut, P., "Homogeneous Charge Compression Ignition Combustion of Primary Reference Fuels Influenced by Ozone Addition," *Energy & Fuels* Vol. 27, No. 9, 2013, pp. 5495-5505.

[59] Masurier, J.-B., Foucher, F., Dayma, G., and Dagaut, P., "Investigation of iso-octane combustion in a homogeneous charge compression ignition engine seeded by ozone, nitric oxide and nitrogen dioxide," *Proceedings of the Combustion Institute* Vol. 35, No. 3, 2015, pp. 3125-3132.

[60] Masurier, J.-B., Foucher, F., Dayma, G., and Dagaut, P., "Ozone applied to the homogeneous charge compression ignition engine to control alcohol fuels combustion," *Applied Energy* Vol. 160, 2015, pp. 566-580.

[61] Ombrello, T., Won, S. H., Ju, Y., and Williams, S., "Flame propagation enhancement by plasma excitation of oxygen. Part I: Effects of O3," *Combustion and Flame* Vol. 157, No. 10, 2010, pp. 1906-1915.

[62] Halter, F., Higelin, P., and Dagaut, P., "Experimental and detailed kinetic modeling study of the effect of ozone on the combustion of methane," *Energy & Fuels* Vol. 25, No. 7, 2011, pp. 2909-2916.

[63] Wang, Z. H., Yang, L., Li, B., Li, Z. S., Sun, Z. W., Aldén, M., Cen, K. F., and Konnov, A. A., "Investigation of combustion enhancement by ozone additive in CH4/air flames using direct laminar burning velocity measurements and kinetic simulations," *Combustion and Flame* Vol. 159, No. 1, 2012, pp. 120-129.

[64] Liang, X., Wang, Z., Weng, W., Zhou, Z., Huang, Z., Zhou, J., and Cen, K., "Study of ozone-enhanced combustion in H2/CO/N2/air premixed flames by laminar burning velocity measurements and kinetic modeling," *International Journal of Hydrogen Energy* Vol. 38, No. 2, 2013, pp. 1177-1188.

[65] Vu, T. M., Won, S. H., Ombrello, T., and Cha, M. S., "Stability enhancement of ozone-assisted laminar premixed Bunsen flames in nitrogen co-flow," *Combustion and Flame* Vol. 161, No. 4, 2014, pp. 917–926.

[66] Zhang, Y., Zhu, M., Zhang, Z., Shang, R., and Zhang, D., "Ozone effect on the flammability limit and near-limit combustion of syngas/air flames with N 2, CO 2, and H 2 O dilutions," *Fuel* Vol. 186, 2016, pp. 414-421.

[67] Weng, W., Nilsson, E., Ehn, A., Zhu, J., Zhou, Y., Wang, Z., Li, Z., Aldén, M., and Kefa Cen. "Investigation of formaldehyde enhancement by ozone addition in CH4/air premixed flames," *Combustion and Flame* Vol. 162, No. 4, 2015, pp. 1284-1293.

[68] Ehn, A., Zhu, J., Petersson, P., Li, Z., Aldén, M., Fureby, C., Hurtig, T., Zettervall, N., Larsson, A., and Larfeldt, J., "Plasma assisted combustion: Effects of O 3 on large scale turbulent combustion studied with laser diagnostics and Large Eddy Simulations," *Proceedings of the Combustion Institute* Vol. 35, No. 3, 2015, pp. 3487-3495.

[69] Pinchak, M., Ombrello, T., Carter, C., Gutmark, E., and Katta, V., "The Effect of Hydrodynamic Stretch on the Flame Propagation Enhancement of Ethylene by Addition of Ozone," *Philosophical Transactions of the Royal Society A* Vol. 373, No. 2048, 2015, p. 20140339.

[70] Gluckstein, M. E., Morrison, R. B., and Khammash, T. B., "Combustion with ozone-modification of flame speeds C2 hydrocarbon-air mixtures." University of Michigan, 1955.

[71] Fenske, J. D., Hasson, A. S., Paulson, S. E., Kuwata, K. T., Ho, A., and Houk, K., "The pressure dependence of the OH radical yield from ozone-alkene reactions," *The Journal of Physical Chemistry A* Vol. 104, No. 33, 2000, pp. 7821-7833.

[72] Paulson, S. E., Fenske, J. D., Sen, A. D., and Callahan, T. W., "A novel small-ratio relative-rate technique for measuring OH formation yields from the reactions of O3 with alkenes in the gas phase, and its application to the reactions of ethene and propene," *The Journal of Physical Chemistry A* Vol. 103, No. 13, 1999, pp. 2050-2059.

[73] Ju, Y., Reuter, C. B., and Won, S. H., "Numerical simulations of premixed cool flames of dimethyl ether/oxygen mixtures," *Combustion and Flame* Vol. 162, No. 10, 2015, pp. 3580-3588.

[74] Reuter, C. B., Won, S. H., and Ju, Y., "Experimental study of the dynamics and structure of self-sustaining premixed cool flames using a counterflow burner," *Combustion and Flame* Vol. 166, 2016, pp. 125-132.

[75] Hajilou, M., Ombrello, T., Won, S. H., and Belmont, E., "Experimental and numerical characterization of freely propagating ozone-activated dimethyl ether cool flames," *Combustion and Flame* Vol. 176, 2017, pp. 326-333.

[76] Won, S. H., Jiang, B., Diévart, P., Sohn, C. H., and Ju, Y., "Self-sustaining n-heptane cool diffusion flames activated by ozone," *Proceedings of the Combustion Institute*, 2015.

[77] Reuter, C. B., Lee, M., Won, S. H., and Ju, Y., "Study of the low-temperature reactivity of large n-alkanes through cool diffusion flame extinction," *Combustion and Flame* Vol. 179, 2017, pp. 23-32.

[78] Perkin, W., "LVII.—Some observations on the luminous incomplete combustion of ether and other organic bodies," *Journal of the Chemical Society, Transactions* Vol. 41, 1882, pp. 363-367.

[79] Ombrello, T., Carter, C., and Katta, V., "Burner platform for sub-atmospheric pressure flame studies," *Combustion and Flame* Vol. 159, No. 7, 2012, pp. 2363-2373.

[80] Mallard, E., and Le Chatelier, H., "Thermal model for flame propagation," *Annales des Mines*. Vol. 4, 1883, pp. 379-568.

[81] Semenov, N., "Theory of Flame Propagation," *NACA TM* Vol. 1282, 1951.

[82] Tanford, C., "Theory of burning velocity. I. Temperature and free radical concentrations near the flame front, relative importance of heat conduction and diffusion," *The Journal of Chemical Physics* Vol. 15, No. 7, 1947, pp. 433-439.

[83] Law, C. K. *Combustion physics*: Cambridge university press, 2010.

[84] Kee, R. J., Grcar, J. F., Smooke, M., Miller, J., and Meeks, E., "PREMIX: a Fortran program for modeling steady laminar one-dimensional premixed flames." 1985.

[85] Glassman, I., Yetter, R. A., and Glumac, N. G. *Combustion*: Academic press, 2014.

[86] Westbrook, C. K., and Dryer, F. L., "Chemical kinetic modeling of hydrocarbon combustion," *Progress in Energy and Combustion Science* Vol. 10, No. 1, 1984, pp. 1-57.

[87] Lewis, B., and Von Elbe, G., "Determination of the speed of flames and the temperature distribution in a spherical bomb from time-pressure explosion records," *The Journal of Chemical Physics* Vol. 2, No. 5, 1934, pp. 283-290.

[88] Kelley, A., and Law, C., "Nonlinear effects in the extraction of laminar flame speeds from expanding spherical flames," *Combustion and Flame* Vol. 156, No. 9, 2009, pp. 1844-1851.

[89] Powling, J., "A new burner method for the determination of low burning velocities and limits of inflammability," *Fuel* Vol. 28, No. 2, 1949, pp. 25-28.

[90] Botha, J., and Spalding, D., "The laminar flame speed of propane/air mixtures with heat extraction from the flame," *Proceedings of the Royal Society of London A: Mathematical, Physical and Engineering Sciences*. Vol. 225, The Royal Society, 1954, pp. 71-96.

[91] Phillips, H., "Flame in a buoyant methane layer," *Symposium (International) on Combustion*. Vol. 10, Elsevier, 1965, pp. 1277-1283.

[92] Chung, S., and Lee, B., "On the characteristics of laminar lifted flames in a nonpremixed jet," *Combustion and Flame* Vol. 86, No. 1-2, 1991, pp. 62-72.

[93] Lee, B., and Chung, S., "Stabilization of lifted tribrachial flames in a laminar nonpremixed jet," *Combustion and Flame* Vol. 109, No. 1-2, 1997, pp. 163-172.

[94] Ruetsch, G., Vervisch, L., and Liñán, A., "Effects of heat release on triple flames," *Physics of Fluids* Vol. 7, No. 6, 1995, pp. 1447-1454.

[95] Boulanger, J., Vervisch, L., Reveillon, J., and Ghosal, S., "Effects of heat release in laminar diffusion flames lifted on round jets," *Combustion and Flame* Vol. 134, No. 4, 2003, pp. 355-368.

[96] Lee, B., Kim, J., and Chung, S., "Effect of dilution on the liftoff of non-premixed jet flames," *Symposium (International) on Combustion*. Vol. 25, Elsevier, 1994, pp. 1175-1181.

[97] Lee, J., Won, S.-H., Jin, S.-H., and Chung, S.-H., "Lifted flames in laminar jets of propane in coflow air," *Combustion and Flame* Vol. 135, No. 4, 2003, pp. 449-462.

[98] Pitts, W. M., "Assessment of theories for the behavior and blowout of lifted turbulent jet diffusion flames," *Symposium (international) on combustion*. Vol. 22, Elsevier, 1989, pp. 809-816.

[99] Lyons, K. M., "Toward an understanding of the stabilization mechanisms of lifted turbulent jet flames: experiments," *Progress in Energy and Combustion Science* Vol. 33, No. 2, 2007, pp. 211-231.

[100] Lawn, C., "Lifted flames on fuel jets in co-flowing air," *Progress in Energy and Combustion Science* Vol. 35, No. 1, 2009, pp. 1-30.

[101] Vanquickenborne, L., and Van Tiggelen, A., "The stabilization mechanism of lifted diffusion flames," *Combustion and Flame* Vol. 10, No. 1, 1966, pp. 59-69.

[102] Burgess, C., and Lawn, C., "The premixture model of turbulent burning to describe lifted jet flames," *Combustion and Flame* Vol. 119, No. 1, 1999, pp. 95-108.

[103] Kalghatgi, G. T., "Blow-out stability of gaseous jet diffusion flames. Part I: in still air," *Combustion Science and Technology* Vol. 26, No. 5-6, 1981, pp. 233-239.

[104] Buckmaster, J., and Weber, R., "Edge-flame-holding," *Symposium (International) on Combustion*. Vol. 26, Elsevier, 1996, pp. 1143-1149.

[105] Buckmaster, J., "Edge-flames," *Progress in Energy and Combustion Science* Vol. 28, No. 5, 2002, pp. 435-475.

[106] Upatnieks, A., Driscoll, J. F., Rasmussen, C. C., and Ceccio, S. L., "Liftoff of turbulent jet flames—assessment of edge flame and other concepts using cinema-PIV," *Combustion and Flame* Vol. 138, No. 3, 2004, pp. 259-272.

[107] Peters, N., and Williams, F. A., "Liftoff characteristics of turbulent jet diffusion flames," *AIAA journal* Vol. 21, No. 3, 1983, pp. 423-429.

[108] Bray, K., and Peters, N., "Laminar flamelets in turbulent flames," *Turbulent reacting flows*, 1994, pp. 63-113.

[109] Schefer, R., Namazian, M., and Kelly, J., "Stabilization of lifted turbulent-jet flames," *Combustion and Flame* Vol. 99, No. 1, 1994, pp. 75IN979-78IN1086.

[110] Broadwell, J. E., Dahm, W. J., and Mungal, M. G., "Blowout of turbulent diffusion flames," *Symposium (international) on combustion*. Vol. 20, Elsevier, 1985, pp. 303-310.

[111] Miake-Lye, R. C., and Hammer, J. A., "Lifted turbulent jet flames: a stability criterion based on the jet large-scale structure," *Symposium (International) on Combustion*. Vol. 22, Elsevier, 1989, pp. 817-824.

[112] Kelman, J., Eltobaji, A., and Masri, A., "Laser imaging in the stabilisation region of turbulent lifted flames," *Combustion science and technology* Vol. 135, No. 1-6, 1998, pp. 117-134.

[113] Su, L., Sun, O., and Mungal, M., "Experimental investigation of stabilization mechanisms in turbulent, lifted jet diffusion flames," *Combustion and Flame* Vol. 144, No. 3, 2006, pp. 494-512.

[114] Dally, B. B., Karpetis, A., and Barlow, R., "Structure of turbulent non-premixed jet flames in a diluted hot coflow," *Proceedings of the combustion institute* Vol. 29, No. 1, 2002, pp. 1147-1154.

[115] Cabra, R., Myhrvold, T., Chen, J., Dibble, R., Karpetis, A., and Barlow, R., "Simultaneous laser raman-rayleigh-lif measurements and numerical modeling results of a lifted turbulent H 2/N 2 jet flame in a vitiated coflow," *Proceedings of the Combustion Institute* Vol. 29, No. 2, 2002, pp. 1881-1888.

[116] Markides, C., and Mastorakos, E., "An experimental study of hydrogen autoignition in a turbulent co-flow of heated air," *Proceedings of The Combustion Institute* Vol. 30, No. 1, 2005, pp. 883-891.

[117] Oldenhof, E., Tummers, M., Van Veen, E., and Roekaerts, D., "Ignition kernel formation and lift-off behaviour of jet-in-hot-coflow flames," *Combustion and Flame* Vol. 157, No. 6, 2010, pp. 1167-1178.

[118] Oldenhof, E., Tummers, M., Van Veen, E., and Roekaerts, D., "Role of entrainment in the stabilisation of jet-in-hot-coflow flames," *Combustion and Flame* Vol. 158, No. 8, 2011, pp. 1553-1563.

[119] Lu, T., Yoo, C. S., Chen, J., and Law, C. K., "Three-dimensional direct numerical simulation of a turbulent lifted hydrogen jet flame in heated coflow: a chemical explosive mode analysis," *Journal of Fluid Mechanics* Vol. 652, 2010, pp. 45-64.

[120] Gao, X., Yang, S., and Sun, W., "A global pathway selection algorithm for the reduction of detailed chemical kinetic mechanisms," *Combustion and Flame* Vol. 167, 2016, pp. 238-247.

[121] Gao, X., and Sun, W., "Using Global Pathway Selection Method to Understand Chemical Kinetics," *55th AIAA Aerospace Sciences Meeting*, Gaylord Texan, Grapevine, Texas, 2017.

[122] Yang, S., Gao, X., and Sun, W., "Global Pathway Analysis of the Extinction and Re-ignition of a Turbulent Non-Premixed Flame," *53rd AIAA/SAE/ASEE Joint Propulsion Conference*, Atlanta, Georgia, 2017.

[123] Gao, X., Yang, S., and Sun, W., "Using Global Pathway to Understand Chemical Kinetics," *6th International Workshop on Model Reduction in Reacting Flow*, Princeton, NJ, 2017.

[124] Gao, X., and Sun, W., "Global Pathway Analysis of the Autoignition and Extinction of Aromatic/Alkane mixture," *53rd AIAA/SAE/ASEE Joint Propulsion Conference*, Atlanta, Georgia, 2017.

[125] Meier, W., Boxx, I., Arndt, C., Gamba, M., and Clemens, N., "Investigation of auto-ignition of a pulsed methane jet in vitiated air using high-speed imaging techniques," *Journal of Engineering for Gas Turbines and Power* Vol. 133, No. 2, 2011, p. 021504.

[126] Arndt, C. M., Gounder, J. D., Meier, W., and Aigner, M., "Auto-ignition and flame stabilization of pulsed methane jets in a hot vitiated coflow studied with high-speed laser and imaging techniques," *Applied Physics B* Vol. 108, No. 2, 2012, pp. 407-417.

[127] Arndt, C. M., Schießl, R., Gounder, J. D., Meier, W., and Aigner, M., "Flame stabilization and auto-ignition of pulsed methane jets in a hot coflow: Influence of temperature," *Proceedings of the Combustion Institute* Vol. 34, No. 1, 2013, pp. 1483-1490.

[128] Choi, B., Kim, K., and Chung, S., "Autoignited laminar lifted flames of propane in coflow jets with tribrachial edge and mild combustion," *Combustion and Flame* Vol. 156, No. 2, 2009, pp. 396-404.

[129] Choi, B., and Chung, S.-H., "Autoignited laminar lifted flames of methane, ethylene, ethane, and n-butane jets in coflow air with elevated temperature," *Combustion and Flame* Vol. 157, No. 12, 2010, pp. 2348-2356.

[130] Deng, S., Zhao, P., Mueller, M. E., and Law, C. K., "Autoignition-affected stabilization of laminar nonpremixed DME/air coflow flames," *Combustion and Flame* Vol. 162, No. 9, 2015, pp. 3437-3445.

[131] Deng, S., Zhao, P., Mueller, M. E., and Law, C. K., "Stabilization of laminar nonpremixed DME/air coflow flames at elevated temperatures and pressures," *Combustion and Flame* Vol. 162, No. 12, 2015, pp. 4471-4478.

[132] Ko, Y., and Chung, S., "Propagation of unsteady tribrachial flames in laminar non-premixed jets," *Combustion and Flame* Vol. 118, No. 1, 1999, pp. 151-163.

[133] Ahmed, S., and Mastorakos, E., "Spark ignition of lifted turbulent jet flames," *Combustion and Flame* Vol. 146, No. 1, 2006, pp. 215-231.

[134] Markides, C. N., and Mastorakos, E., "Flame propagation following the autoignition of axisymmetric hydrogen, acetylene, and normal-heptane plumes in turbulent coflows of hot air," *Journal of Engineering for Gas Turbines and Power* Vol. 130, No. 1, 2008, p. 011502.

[135] Mastorakos, E., "Ignition of turbulent non-premixed flames," *Progress in Energy and Combustion Science* Vol. 35, No. 1, 2009, pp. 57-97.

[136] Kojima, J., Ikeda, Y., and Nakajima, T., "Spatially resolved measurement of OH*, CH*, and C2* chemiluminescence in the reaction zone of laminar methane/air premixed flames," *Proceedings of the Combustion institute* Vol. 28, No. 2, 2000, pp. 1757-1764.

[137] Najm, H. N., Paul, P. H., Mueller, C. J., and Wyckoff, P. S., "On the adequacy of certain experimental observables as measurements of flame burning rate," *Combustion and flame* Vol. 113, No. 3, 1998, pp. 312-332.

[138] Muruganandam, T., Kim, B.-H., Morrell, M., Nori, V., Patel, M., Romig, B., and Seitzman, J., "Optical equivalence ratio sensors for gas turbine combustors," *Proceedings of the Combustion Institute* Vol. 30, No. 1, 2005, pp. 1601-1609.

[139] Guiberti, T., Durox, D., and Schuller, T., "Flame chemiluminescence from CO2- and N2-diluted laminar CH4/air premixed flames," *Combustion and Flame* Vol. 181, 2017, pp. 110-122.

[140] Lindstedt, P., "Modeling of the chemical complexities of flames," *Symposium (International) on Combustion*. Vol. 27, Elsevier, 1998, pp. 269-285.

[141] Luque, J., Jeffries, J., Smith, G., Crosley, D., Walsh, K., Long, M., and Smooke, M., "CH (AX) and OH (AX) optical emission in an axisymmetric laminar diffusion flame," *Combustion and Flame* Vol. 122, No. 1, 2000, pp. 172-175.

[142] Sheinson, R. S., and Williams, F. W., "Chemiluminescence spectra from cool and blue flames: electronically excited formaldehyde," *Combustion and Flame* Vol. 21, No. 2, 1973, pp. 221-230.

[143] Toby, S., "Chemiluminescence in the gas-phase reaction between ozone and allene," *Journal of Luminescence* Vol. 8, No. 1, 1973, pp. 94-96.

[144] Bogan, D. J., Sheinson, R. S., Gann, R. G., and Williams, F. W., "Formaldehyde (A1A2. far. X1A1) chemiluminescence in the gas phase reaction of molecular oxygen

(A1. DELTA. g) plus ethyl vinyl ether," *Journal of the American Chemical Society* Vol. 97, No. 9, 1975, pp. 2560-2562.

[145] Deng, S., Zhao, P., Zhu, D., and Law, C. K., "NTC-affected ignition and low-temperature flames in nonpremixed DME/air counterflow," *Combustion and Flame* Vol. 161, No. 8, 2014, pp. 1993-1997.

[146] Kochar, Y. N., Vaden, S. N., Lieuwen, T. C., and Seitzman, J. M., "Laminar flame speed of hydrocarbon fuels with preheat and low oxygen content," *48th AIAA Aerospace Sciences Meeting and Exhibit AIAA Paper*. 2010.

[147] Natarajan, J., Lieuwen, T., and Seitzman, J., "Laminar flame speeds of H2/CO mixtures: Effect of CO2 dilution, preheat temperature, and pressure," *Combustion and Flame* Vol. 151, No. 1, 2007, pp. 104-119.

[148] Gao, X., Zhang, Y., Adusumilli, S., Seitzman, J., Sun, W., Ombrello, T., and Carter, C., "The effect of ozone addition on laminar flame speed," *Combustion and Flame* Vol. 162, No. 10, 2015, pp. 3914-3924.

[149] Gao, X., Sun, W., Ombrello, T., and Carter, C., "The Effect of Ozonolysis Activated Autoignition on Jet Flame Dynamics," *55th AIAA Aerospace Sciences Meeting*, Gaylord Texan, Grapevine, Texas, 2017.

[150] "CHEMKIN 10131," *Reaction Design: San Diego*, 2013.

[151] Wang, H., You, X., Joshi, A. V., Davis, S. G., Laskin, A., Egolfopoulos, F., and Law, C. K., "USC Mech Version II. High-Temperature Combustion Reaction Model of H2/CO/C1-C4 Compounds," 2007. http://ignis.usc.edu/USC_Mech_II.htm

[152] Lutz, A. E., Kee, R. J., and Miller, J. A., "SENKIN: A FORTRAN program for predicting homogeneous gas phase chemical kinetics with sensitivity analysis." Sandia National Labs., Livermore, CA (USA), 1988.

[153] Larson, R. S., "PLUG: A Fortran program for the analysis of plug flow reactors with gas-phase and surface chemistry." Sandia Labs., Livermore, CA (United States), 1996.

[154] "FLUENT release 17.1," *ANSYS, Inc.*, 2016.

[155] Launder, B. E., and Spalding, D. B. *Mathematical models of turbulence*: Academic press, 1972.

[156] Morrissey, R. J., and Schubert, C. C., "The reactions of ozone with propane and ethane," *Combustion and Flame* Vol. 7, 1963, pp. 263 - 268.

[157] Stedman, D., and Niki, H., "Ozonolysis rates of some atmospheric gases," *Environmental letters* Vol. 4, No. 4, 1973, pp. 303-310.

[158] Bosschaart, K. J., and De Goey, L., "The laminar burning velocity of flames propagating in mixtures of hydrocarbons and air measured with the heat flux method," *Combustion and Flame* Vol. 136, No. 3, 2004, pp. 261-269.

[159] Vagelopoulos, C. M., and Egolfopoulos, F. N., "Direct experimental determination of laminar flame speeds," *Symposium (international) on combustion*. Vol. 27, Elsevier, 1998, pp. 513-519.

[160] Gu, X., Haq, M., Lawes, M., and Woolley, R., "Laminar burning velocity and Markstein lengths of methane–air mixtures," *Combustion and flame* Vol. 121, No. 1, 2000, pp. 41-58.

[161] Egolfopoulos, F., Cho, P., and Law, C., "Laminar flame speeds of methane-air mixtures under reduced and elevated pressures," *Combustion and flame* Vol. 76, No. 3, 1989, pp. 375-391.

[162] Dugger, G. L., "Effect of initial mixture temperature on flame speed of methane-air, propane-air and ethylene-air mixtures." National Advisory Committee for Aeronautics, 1951.

[163] Lam, S., and Goussis, D., "Understanding complex chemical kinetics with computational singular perturbation," *Symposium (International) on Combustion*. Vol. 22, Elsevier, 1989, pp. 931-941.

[164] Lu, T., Ju, Y., and Law, C. K., "Complex CSP for chemistry reduction and analysis," *Combustion and Flame* Vol. 126, No. 1, 2001, pp. 1445-1455.

[165] Lu, T., and Law, C. K., "A criterion based on computational singular perturbation for the identification of quasi steady state species: A reduced mechanism for methane oxidation with NO chemistry," *Combustion and Flame* Vol. 154, No. 4, 2008, pp. 761-774.

[166] Maas, U., and Pope, S. B., "Simplifying chemical kinetics: intrinsic low-dimensional manifolds in composition space," *Combustion and flame* Vol. 88, No. 3, 1992, pp. 239-264.

[167] Maas, U., and Pope, S. B., "Implementation of simplified chemical kinetics based on intrinsic low-dimensional manifolds," *Symposium (International) on Combustion*. Vol. 24, Elsevier, 1992, pp. 103-112.

[168] Maas, U., and Pope, S., "Laminar flame calculations using simplified chemical kinetics based on intrinsic low-dimensional manifolds," *Symposium (International) on Combustion*. Vol. 25, Elsevier, 1994, pp. 1349-1356.

[169] Gicquel, O., Thevenin, D., Hilka, M., and Darabiha, N., "Direct numerical simulation of turbulent premixed flames using intrinsic low-dimensional manifolds," *Combustion Theory and Modelling* Vol. 3, No. 3, 1999, pp. 479-502.

[170] Gicquel, O., Darabiha, N., and Thévenin, D., "Liminar premixed hydrogen/air counterflow flame simulations using flame prolongation of ILDM with differential diffusion," *Proceedings of the Combustion Institute* Vol. 28, No. 2, 2000, pp. 1901-1908.

[171] Oijen, J. v., and Goey, L. D., "Modelling of premixed laminar flames using flamelet-generated manifolds," *Combustion Science and Technology* Vol. 161, No. 1, 2000, pp. 113-137.

[172] Pierce, C. D., and Moin, P., "Progress-variable approach for large-eddy simulation of non-premixed turbulent combustion," *Journal of Fluid Mechanics* Vol. 504, 2004, pp. 73-97.

[173] Najafi-Yazdi, A., Cuenot, B., and Mongeau, L., "Systematic definition of progress variables and Intrinsically Low-Dimensional, Flamelet Generated Manifolds for chemistry tabulation," *Combustion and Flame* Vol. 159, No. 3, 2012, pp. 1197-1204.

[174] Ju, Y., and Niioka, T., "Reduced kinetic mechanism of ignition for nonpremixed hydrogen/air in a supersonic mixing layer," *Combustion and flame* Vol. 99, No. 2, 1994, pp. 240-246.

[175] Niemeyer, K. E., Sung, C.-J., and Raju, M. P., "Skeletal mechanism generation for surrogate fuels using directed relation graph with error propagation and sensitivity analysis," *Combustion and flame* Vol. 157, No. 9, 2010, pp. 1760-1770.

[176] Zheng, X., Lu, T., and Law, C., "Experimental counterflow ignition temperatures and reaction mechanisms of 1, 3-butadiene," *Proceedings of the Combustion Institute* Vol. 31, No. 1, 2007, pp. 367-375.

[177] Turányi, T., and Tomlin, A. S. *Analysis of Kinetic Reaction Mechanisms*: Springer, 2014.

[178] Kooshkbaghi, M., Frouzakis, C. E., Boulouchos, K., and Karlin, I. V., "Entropy production analysis for mechanism reduction," *Combustion and Flame* Vol. 161, No. 6, 2014, pp. 1507-1515.

[179] Revel, J., Boettner, J., Cathonnet, M., and Bachman, J., "Derivation of a global chemical kinetic mechanism for methane ignition and combustion," *Journal de chimie physique* Vol. 91, No. 4, 1994, pp. 365-382.

[180] Androulakis, I. P., Grenda, J. M., and Bozzelli, J. W., "Time-integrated pointers for enabling the analysis of detailed reaction mechanisms," *AIChE journal* Vol. 50, No. 11, 2004, pp. 2956-2970.

[181] He, K., Ierapetritou, M. G., and Androulakis, I. P., "A graph-based approach to developing adaptive representations of complex reaction mechanisms," *Combustion and Flame* Vol. 155, No. 4, 2008, pp. 585-604.

[182] He, K., Androulakis, I. P., and Ierapetritou, M. G., "On-the-fly reduction of kinetic mechanisms using element flux analysis," *Chemical Engineering Science* Vol. 65, No. 3, 2010, pp. 1173-1184.

[183] He, K., Androulakis, I. P., and Ierapetritou, M. G., "Multi-element flux analysis for the incorporation of detailed kinetic mechanisms in reactive simulations," *Energy & Fuels* Vol. 24, No. 1, 2009, pp. 309-317.

[184] Zhao, P., Nackman, S. M., and Law, C. K., "On the application of betweenness centrality in chemical network analysis: Computational diagnostics and model reduction," *Combustion and Flame* Vol. 162, No. 8, 2015, pp. 2991-2998.

[185] Lu, T., and Law, C. K., "A directed relation graph method for mechanism reduction," *Proceedings of the Combustion Institute* Vol. 30, No. 1, 2005, pp. 1333-1341.

[186] Lu, T., and Law, C. K., "Linear time reduction of large kinetic mechanisms with directed relation graph: n-Heptane and iso-octane," *Combustion and Flame* Vol. 144, No. 1, 2006, pp. 24-36.

[187] Lu, T., Plomer, M., Luo, Z., Sarathy, S., Pitz, W., Som, S., and Longman, D. E., "Directed relation graph with expert knowledge for skeletal mechanism reduction," *7th US National Combustion Meeting*. 2011.

[188] Lu, T., and Law, C. K., "On the applicability of directed relation graphs to the reduction of reaction mechanisms," *Combustion and Flame* Vol. 146, No. 3, 2006, pp. 472-483.

[189] Luo, Z., Lu, T., Maciaszek, M. J., Som, S., and Longman, D. E., "A reduced mechanism for high-temperature oxidation of biodiesel surrogates," *Energy & Fuels* Vol. 24, No. 12, 2010, pp. 6283-6293.

[190] Pepiot-Desjardins, P., and Pitsch, H., "An efficient error-propagation-based reduction method for large chemical kinetic mechanisms," *Combustion and Flame* Vol. 154, No. 1, 2008, pp. 67-81.

[191] Tosatto, L., Bennett, B., and Smooke, M., "A transport-flux-based directed relation graph method for the spatially inhomogeneous instantaneous reduction of chemical kinetic mechanisms," *Combustion and Flame* Vol. 158, No. 5, 2011, pp. 820-835.

[192] Sankaran, R., Hawkes, E. R., Chen, J. H., Lu, T., and Law, C. K., "Structure of a spatially developing turbulent lean methane–air Bunsen flame," *Proceedings of the combustion institute* Vol. 31, No. 1, 2007, pp. 1291-1298.

[193] Sun, W., Chen, Z., Gou, X., and Ju, Y., "A path flux analysis method for the reduction of detailed chemical kinetic mechanisms," *Combustion and Flame* Vol. 157, No. 7, 2010, pp. 1298-1307.

[194] Xin, Y., Law, C., and Lu, T., "A reduced mechanism for iso-octane oxidation."

[195] Liang, L., Stevens, J. G., and Farrell, J. T., "A dynamic adaptive chemistry scheme for reactive flow computations," *Proceedings of the Combustion Institute* Vol. 32, No. 1, 2009, pp. 527-534.

[196] Lu, T., Law, C. K., Yoo, C. S., and Chen, J. H., "Dynamic stiffness removal for direct numerical simulations," *Combustion and Flame* Vol. 156, No. 8, 2009, pp. 1542-1551.

[197] Schwer, D. A., Lu, P., and Green, W. H., "An adaptive chemistry approach to modeling complex kinetics in reacting flows," *Combustion and Flame* Vol. 133, No. 4, 2003, pp. 451-465.

[198] Wei, J., and Kuo, J. C., "Lumping analysis in monomolecular reaction systems. Analysis of the exactly lumpable system," *Industrial & Engineering chemistry fundamentals* Vol. 8, No. 1, 1969, pp. 114-123.

[199] Stagni, A., Cuoci, A., Frassoldati, A., Faravelli, T., and Ranzi, E., "Lumping and reduction of detailed kinetic schemes: an effective coupling," *Industrial & Engineering Chemistry Research* Vol. 53, No. 22, 2013, pp. 9004-9016.

[200] Gery, M. W., Whitten, G. Z., Killus, J. P., and Dodge, M. C., "A photochemical kinetics mechanism for urban and regional scale computer modeling," *Journal of Geophysical Research: Atmospheres (1984–2012)* Vol. 94, No. D10, 1989, pp. 12925-12956.

[201] Peters, N., Paczko, G., Seiser, R., and Seshadri, K., "Temperature cross-over and non-thermal runaway at two-stage ignition of n-heptane," *Combustion and Flame* Vol. 128, No. 1, 2002, pp. 38-59.

[202] Gao, Y., Shan, R., Lyra, S., Li, C., Wang, H., Chen, J. H., and Lu, T., "On lumped-reduced reaction model for combustion of liquid fuels," *Combustion and Flame*, 2015.

[203] Oluwole, O. O., Ren, Z., Petre, C., and Goldin, G., "Decoupled Species and Reaction Reduction: An error-controlled method for Dynamic Adaptive Chemistry simulations," *Combustion and Flame*, 2015.

[204] Pope, S. B., "Computationally efficient implementation of combustion chemistry using in situ adaptive tabulation," *Combustion Theory Modelling* Vol. 1, 1997, pp. 41-63.

[205] Contino, F., Jeanmart, H., Lucchini, T., and D'Errico, G., "Coupling of in situ adaptive tabulation and dynamic adaptive chemistry: An effective method for solving combustion in engine simulations," *Proceedings of the Combustion Institute* Vol. 33, No. 2, 2011, pp. 3057-3064.

[206] Andrae, J. C., Brinck, T., and Kalghatgi, G., "HCCI experiments with toluene reference fuels modeled by a semidetailed chemical kinetic model," *Combustion and Flame* Vol. 155, No. 4, 2008, pp. 696-712.

[207] Blanquart, G., Pepiot-Desjardins, P., and Pitsch, H., "Chemical mechanism for high temperature combustion of engine relevant fuels with emphasis on soot precursors," *Combustion and Flame* Vol. 156, No. 3, 2009, pp. 588-607.

[208] Ra, Y., and Reitz, R. D., "A combustion model for IC engine combustion simulations with multi-component fuels," *Combustion and flame* Vol. 158, No. 1, 2011, pp. 69-90.

[209] Niemeyer, K. E., and Sung, C.-J., "Mechanism reduction for multicomponent surrogates: A case study using toluene reference fuels," *Combustion and Flame* Vol. 161, No. 11, 2014, pp. 2752-2764.

[210] Lu, T., and Law, C. K., "Strategies for mechanism reduction for large hydrocarbons: n-heptane," *Combustion and flame* Vol. 154, No. 1, 2008, pp. 153-163.

[211] Lam, S., and Goussis, D., "Understanding complex chemical kinetics with computational singular perturbation," *Symposium (International) on Combustion*, Vol. 22, Elsevier, 1989, 1.

[212] Lam, S., and Goussis, D., "The CSP method for simplifying kinetics," *International Journal of Chemical Kinetics* Vol. 26, No. 4, 1994, pp. 461-486.

[213] Valorani, M., Creta, F., Goussis, D. A., Lee, J. C., and Najm, H. N., "An automatic procedure for the simplification of chemical kinetic mechanisms based on CSP," *Combustion and Flame* Vol. 146, No. 1, 2006, pp. 29-51.

[214] Valorani, M., Najm, H. N., and Goussis, D. A., "CSP analysis of a transient flame-vortex interaction: time scales and manifolds," *Combustion and Flame* Vol. 134, No. 1, 2003, pp. 35-53.

[215] Goussis, D. A., and Najm, H. N., "Model reduction and physical understanding of slowly oscillating processes: the circadian cycle," *Multiscale Modeling & Simulation* Vol. 5, No. 4, 2006, pp. 1297-1332.

[216] Maas, U., "Efficient calculation of intrinsic low-dimensional manifolds for the simplification of chemical kinetics," *Computing and Visualization in Science* Vol. 1, No. 2, 1998, pp. 69-81.

[217] Bykov, V., and Maas, U., "The extension of the ILDM concept to reaction–diffusion manifolds," *Combustion Theory and Modelling* Vol. 11, No. 6, 2007, pp. 839-862.

[218] Bykov, V., and Maas, U., "Problem adapted reduced models based on Reaction–Diffusion Manifolds (REDIMs)," *Proceedings of the Combustion Institute* Vol. 32, No. 1, 2009, pp. 561-568.

[219] Luo, Z., Yoo, C. S., Richardson, E. S., Chen, J. H., Law, C. K., and Lu, T., "Chemical explosive mode analysis for a turbulent lifted ethylene jet flame in highly-heated coflow," *Combustion and Flame* Vol. 159, No. 1, 2012, pp. 265-274.

[220] Shan, R., Yoo, C. S., Chen, J. H., and Lu, T., "Computational diagnostics for n-heptane flames with chemical explosive mode analysis," *Combustion and Flame* Vol. 159, No. 10, 2012, pp. 3119-3127.

[221] Gao, X., Zhai, J., Sun, W., Ombrello, T., and Carter, C., "The Effect of Ozone Addition on Autoignition and Flame Stabilization," *54th AIAA Aerospace Sciences Meeting*. 2016, pp. AIAA 2016-0960.

[222] Won, S. H., Dooley, S., Dryer, F. L., and Ju, Y., "A radical index for the determination of the chemical kinetic contribution to diffusion flame extinction of large hydrocarbon fuels," *Combustion and Flame* Vol. 159, No. 2, 2012, pp. 541-551.

[223] Turányi, T., "Sensitivity analysis of complex kinetic systems. Tools and applications," *Journal of Mathematical Chemistry* Vol. 5, No. 3, 1990, pp. 203-248.

[224] Yang, S., Ranjan, R., Yang, V., Menon, S., and Sun, W., "Parallel On-the-fly Adaptive Kinetics in Direct Numerical Simulation of Turbulent Premixed Flame," *Proceedings of the Combustion Institute*, 2016. doi:10.1016/j.proci.2016.07.021

[225] Coogan, S., Gao, X., McClung, A., and Sun, W., "Evaluation of Kinetic Mechanisms for Direct Fired Supercritical Oxy-Combustion of Natural Gas," *ASME Turbo Expo 2016: Turbomachinery Technical Conference and Exposition*. 2016, pp. GT2016-56658.

[226] Yen, J. Y., "Finding the k shortest loopless paths in a network," *management Science* Vol. 17, No. 11, 1971, pp. 712-716.

[227] Egli, W., and Kraus, M., "Shortest paths in chemical kinetic applications," *Physical Chemistry Chemical Physics* Vol. 5, No. 18, 2003, pp. 3916-3920.

[228] B. Sirjean, E. Dames, D.A. Sheen, and Wang, H., "Paper 23F1," *6th US National Combustion Meeting*, Ann, Arbor, Michigan, 2009.

[229] Vié, A., Franzelli, B., Gao, Y., Lu, T., Wang, H., and Ihme, M., "Analysis of segregation and bifurcation in turbulent spray flames: A 3D counterflow configuration," *Proceedings of the Combustion Institute* Vol. 35, No. 2, 2015, pp. 1675-1683.

[230] Smith, G. P., Golden, D. M., Frenklach, M., Moriarty, N. W., Eiteneer, B., Goldenberg, M., Bowman, C. T., Hanson, R. K., Song, S., and Gardiner Jr, W. C., "GRI-Mech 3.0," *URL:* http://www.me.berkeley.edu/gri_mech Vol. 51, 1999, p. 55.